Mémoire

Auteur : Delsupexhe, Lionel
Promoteur(s) : Pozuelos Romero, Francisco José
Faculté : Faculté des Sciences
Diplôme : Master en sciences spatiales, à finalité approfondie
Année académique : 2020-2021
URI/URL : http://hdl.handle.net/2268.2/12326

University of Liège
Faculty of Sciences
Master in Space Sciences

Detection of habitable terrestrial exoplanets orbiting K dwarf stars

A thesis carried out for the obtention of the Master's degree in Space Sciences

Author:
Lionel Delsupexhe

Supervisor:
Francisco Pozuelos

Board of Examiners:
Michaël Gillon
Emmanuel Jehin
Christian Delacroix

Academic year 2020 - 2021

Acknowledgements

First of all, I would like to address a special thank you to my supervisor, Francisco Pozuelos, for proposing me this very interesting exoplanet-related topic, as well as for all the time he accorded to me, both carefully reading and discussing my work during many online sessions, and for his useful advice that helped me a lot when I was struggling the most with this work. I also extend my special thanks to the members of the Board of Examiners, Michaël Gillon, Emmanuel Jehin and Christian Delacroix for the time they will spend reading my Master thesis.

Then, I would like to express all my gratitude to Dominique for the help she offered me checking and enhancing the language in my whole work.

Finally, I would like to thank as much as possible my family and friends for the exceptional support they provided me all along this Master's degree when I needed it the most, and especially during these hard, peculiar times of COVID-19 pandemics.

It would probably have been much more difficult to carry out this Master thesis without the help of all the people mentioned above, so thank you, to all of you.

Contents

Introduction

There is an old question one may ask: "*Are we alone in the Universe?*".

Since the beginning of astronomy, this question has been recurring in minds, but the tools available at that time were not evolved enough to allow astronomers to detect life elsewhere, or even to discover planets outer the Solar System, i.e. *extrasolar planets* or *exoplanets*. However, the advent of bigger and better ground-based and space-based telescopes has enable such discoveries to be done, thus even more emphasizing the old question mentioned above.

Now, a few thousands exoplanets[1] have been discovered, and with them an enormous variety of physical and orbital characteristics. Indeed, from Earth-sized planets or smaller to Jupiter-sized ones or bigger, orbiting their host stars on more or less wide orbits, with masses that can go from less than the Earth's mass to tens of Jupiter's mass, the number of different planetary systems one can imagine and find is gigantic.

Considering all of this, finding exoplanets that could have suitable conditions to sustain life may seem as a puzzling task. So, first of all, we need to know what we are looking for. In that sense, to detect life on a planet, which means to discover an inhabited planet, therefore a habitable planet, we need to make the difference between "habitable" planets and "uninhabitable" ones. In a further extent, we can also define the concept of "superhabitability" for which the best stellar candidates are thought to be K dwarf stars, i.e. main-sequence K-type stars. Some physical parameters of the host stars of superhabitable exoplanets will also be given. This will be done in chapter one.

In chapter two, we will discuss about methods to detect exoplanets. We will evaluate the potential detection of these superhabitable planets by means of different observation techniques.

In chapter three, we will discuss about a list of future space-based and ground-based missions having as a goal, among others, to find new exoplanets and to study their atmospheres.

Chapter four will be dedicated to give an overview about the TESS mission, and to explain how and where to retrieve relevant stars in order to analyze their light curves to find signals corresponding to superhabitable exoplanets.

[1] According to the Extrasolar Planet Encyclopaedia website (`http://exoplanet.eu/`), 4753 confirmed exoplanets have been detected (consulted on the 29th of May 2021)

Chapter 1

Habitability and superhabitability of planets

In the present chapter, we will first compare "habitable" and "uninhabitable" planets to determine which conditions are necessary for a planet to harbour life.
Then, knowing what we mean about "habitable" planets, we will emphasize the fact that Earth and its conditions may not represent the best cradle for life. This will lead us to the concept of "superhabitability" of planets, which will be interesting for us all along this work.

1.1 "Habitable" vs "uninhabitable" planets

The Earth being so far the only inhabited planet we know about, let us start the discussion from a geocentric point of view.

From that point of view, an inhabited planet should be a rocky planet that has an atmosphere not too thick nor too thin, and which is located in a certain distance range from its host star, called the habitable zone (HZ), to allow the presence of liquid water on its surface. This distance should include the greenhouse effect of the atmosphere.

We could also think of other parameters such as its tilt angle (to have seasons), the presence of a moon, plate tectonics, etc. However, this would need a much more complex approach. So we will assume in the frame of this work, that a habitable planet is simply a rocky planet with an atmosphere and which resides within the habitable zone of its host star.

Let us now take a look at the concept of habitable zone. As explained in [Kopparapu et al., 2013], the boundaries of this region may be defined following different ways. For the inner boundary of the habitable zone, there are three main definitions:

- **Moist greenhouse effect**: When the temperature increases too much, liquid water at the surface of a planet (if there is some) evaporates and the amount of atmospheric H_2O increases. Water vapor being a strong greenhouse gas, this will further increase the temperature at the surface of the planet. This limit is said to be conservative in [Kopparapu et al., 2013].
- **Runaway greenhouse effect**: This inner boundary can be seen as an extension of the moist greenhouse limit. Indeed, this corresponds to the situation where the temperature at the surface of the planet is so high that all water of the oceans evaporated. The planetary surface is dry (as for Venus), over this limit. It is interesting

to note that for stars characterized by $T_{eff} < 5000$ K, this limit is pretty close to the moist greenhouse limit. Indeed, as explained in [Kopparapu et al., 2013], such stars are emitting a lot in the infrared (where H_2O absorbs the most), so for a planet with an atmosphere dominated with H_2O, the runaway greenhouse effect arrives quickly after the moist greenhouse effect.

- **Recent Venus**: The recent Venus limit is based on radio observations of the surface of Venus, which tell us that Venus may not had liquid water on its surface for at least one billion years, but it probably had some before that. So, the recent Venus limit is defined as the distance (in the Solar system), where Venus was 1 Gyr ago. Therefore, based on the luminosity of the Sun at that epoch (obtained thanks to stellar evolution theories), [Kopparapu et al., 2013] have determined an inner limit for the habitable zone, which is said to be optimistic, in the sense that it allows the region around a star where we may find habitable planets to be larger, so it is more optimistic about the habitable characteristics of a planet.

There are also three main definitions used for the outer boundary:

- **Maximum greenhouse effect**: [Kopparapu et al., 2013] thought that, due to the negative feedback loop from the carbonate-silicate cycle, atmospheric CO_2 accumulates when the planet gets colder. As explained in the paper cited above and in [Ramirez, 2014], the increase of the CO_2 partial pressure will cause an increase of the planetary albedo that will at some point overcome the greenhouse effect. This will therefore cause the atmospheric CO_2 to condensate, and the surface temperature of the planet will become too cold to hold liquid water.[1]

- **First CO_2 condensation**: This limit is not supported by [Kopparapu et al., 2013], but papers such as [Cuntz and Guinan, 2016] still use it, so it is worth mentioning it. This corresponds to the distance from a star where the surface temperature of a planet becomes low enough for atmospheric CO_2 of that planet to start condensing and falling on the surface.

- **Early Mars**: Mars is thought, by some scientists including [Kopparapu et al., 2013] to have been warm enough to have liquid water in the past. Based on the same reasoning than for the recent Venus inner boundary, they therefore computed an outer boundary that corresponds to the distance at which early Mars was, when it had liquid water. As for the recent Venus limit, this one is also said to be optimistic.

Usually two habitable zones are defined:

- **Conservative habitable zone**: This one is delimited by the runaway (or moist) greenhouse effect for the inner limit and by the maximum greenhouse effect for the outer boundary.

- **Optimistic habitable zone**: Here, the inner and outer boundaries are respectively the recent Venus and the early Mars limits.

These two definitions of the habitable zone of a star, are represented in Figure 1.1:

[1] Source: `https://www.centauri-dreams.org/2013/01/31/habitable-zones-a-moving-target/`

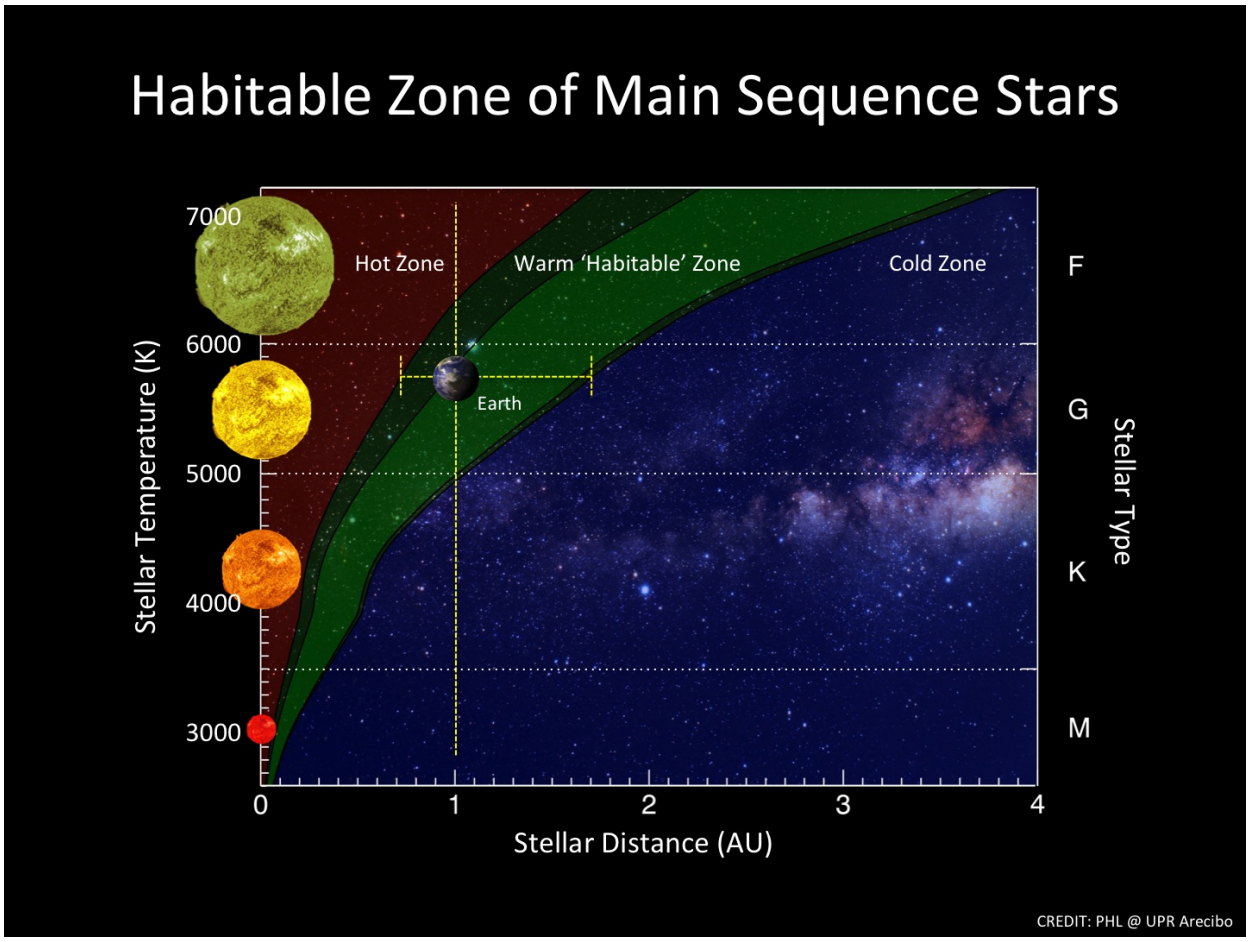

Figure 1.1: Representation of the habitable zone for different spectral types of main-sequence stars. The red and blue regions are respectively too hot and cold for a planet to have liquid water on its surface. The light green region delimits the conservative habitable zone, and the wider, dark green, one is the optimistic habitable zone. Taken from the website `http://phl.upr.edu/library/notes/summarylimitsofthenewhabitablezone`.

As we can see, the early Mars outer limit is quite close to the maximum greenhouse boundary, but the recent Venus inner limit is much closer to the star.

In the following chapter, we will work with the optimistic habitable zone, to be sure not to miss any (super)habitable exoplanets.

In addition to these inner and outer habitable zone boundaries, we may also discuss about another interesting concept, that is the continuous habitable zone (CHZ), as explained in [Cuntz and Guinan, 2016]. During its main-sequence lifetime, a star evolves. Its effective temperature and luminosity both increase. As a result, the habitable zone of that star, whatever the chosen inner and outer boundaries, will go outward. However, the planets orbiting that star will stay roughly on their orbits. So, they may at some point enter or exit the habitable zone of their host star. Therefore, the CHZ is defined as the habitable zone in which a planet will "continuously" be, i.e. until it exits, over time.
Cooler stars than the Sun evolving slower, their habitable zones will also recess slower than the Sun's HZ, and planets orbiting such stars will therefore be within the habitable zones of their host stars for a longer amount of time. They will therefore stay "habitable" longer than a planet orbiting a Sun-like star.

Another interesting distance, as far as the habitability of a planet is concerned, is the so-called homeothermic distance (HTD) as described in [Cuntz and Guinan, 2016]. This corresponds to the distance at which an exoplanet may be from its host star (not necessarily a Sun-like star) to have the same equilibrium temperature as the Earth around the Sun (this distance is also named Earth-equivalent distance).

Finally, although the concept of habitable zone is widely used in exoplanetology, it is important to realize that it can easily be misleading and therefore deserves a bit of attention. Indeed, the word "habitable" seems to indicate that a planet located in this region around its host star must be habitable. However, this is not always the case. As it is clearly said by [Schulze-Makuch et al., 2020], a planet said to be habitable is not necessarily inhabited. This to say that, even if a planet would fulfil all the requirements we set in our habitability models, it doesn't mean that this planet is inhabited (or really habitable). Take for instance planet Mars which is located inside of the Sun's optimistic habitable zone but is not really habitable. To some extent, it could even be possible for a planet said to be uninhabitable based on our models, to be habitable and maybe inhabited in reality. It is even possible to find worlds (planets or moons, as explained in [Heller and Armstrong, 2014] and [Schulze-Makuch et al., 2020]), outside of the habitable zone of a star, which fulfil the habitability conditions. This is notably thought to be the case of the Galilean moon Europa, beneath the surface of which scientists think that lies an ocean of liquid water[2] (staying liquid notably thanks to the tidal heating exerted by Jupiter).

1.2 Superhabitable planets

As said at the beginning of this chapter, planet Earth may not be the best cradle for life, even though it is the only inhabited planet we know so far.

While talking about superhabitability, we discuss about the conditions that allow an inhabited planet to have more biomass and biodiversity than planet Earth.

As argued by [Heller and Armstrong, 2014], [Heller, 2015] and refined by [Schulze-Makuch et al., 2020] there are some planetary parameters that could be fine-tuned for a planet to become even more life-friendly than the Earth. Here is a list of these parameters, as given in the papers cited above:

- **Planetary radius and mass**: The larger the radius of a planet, the larger the habitable surface. So, in principle, a planet slightly bigger than the Earth may be better in the sense that it would be able to have more biomass, because there would be more space to live on it. Concerning the mass, a planet heavier than the Earth would have more internal heat. This internal heat, as it is explained below in this section, will be in part responsible for the given surface temperature of the planet, among other things. However, too large a radius would also probably be inhibiting for life, since the increase of radius implies an increase of mass (to keep the same density, that of a rocky planet), hence an increase of the gravitational attraction. So, if the planet is too large and too massive, i.e. a radius greater than 1.1 $R_\oplus$ and a mass larger than 1.5 - 1.6 $M_\oplus$, as said in [Schulze-Makuch et al., 2020], the gravity of the planet could

[2] As seen on the website `https://europa.nasa.gov/europa/ocean/`

thus be strong enough to retain more gas and the planet could therefore transform into a mini-Neptune or a gas giant. It is also interesting to remark that a too massive planet, due to its stronger gravity, will be less porous, it will have less living space beneath the ground for potential subsurface-living species.

- **Land/ocean distribution**: The land-over-ocean ratio is also important. In the case of the Earth, about 70% of its surface is covered with oceans, but once again, the larger the land-over-ocean ratio, the larger the living space at the surface. This is, however, to take carefully, being the fact that complex water-living species do exist. An archipelagos should therefore provide a larger biodiversity than one single big continent, like it was the case in the early days of the Earth.

- **Type of oceans**: On Earth, we mainly have profound oceans, but as explained in [Schulze-Makuch et al., 2020] shallow waters yield a higher biodiversity than deep oceans. So, a planet with shallow waters may harbour more biomass and living species than a planet with deep oceans.

- **Temperature and moisture**: Temperature and moisture in the atmosphere of a planet are also important parameters. Indeed, living species may survive in some ranges of temperatures. These ranges depend on the biochemistry of the considered living beings (carbon-based and water for life on Earth), and may also vary with the complexity of the species. On Earth, living species are more represented in warmer and wetter environments, such as tropical rainforests. Evidence of that is the amount of biomass that was present on Earth during the Carboniferous period, and that we find beneath the surface today. On the opposite, less complex beings are found in the cold polar regions. Water vapor (hence moisture), among other compounds, also plays an important shield role against the harmful UV photons coming from the Sun. [Schulze-Makuch et al., 2020] therefore proposed a planetary temperature a bit higher than now on Earth (about 5°C more, as during the Carboniferous period).

- **Planetary age and atmospheric O_2**: The age of the planet considered is quite a critical factor for habitability considerations.

  On the one hand, if the planet is too young, based on the history of early Earth, its rocks may not had enough time to be oxidized, and a lesser amount of O_2 may be present in its atmosphere. As said in [Schulze-Makuch et al., 2020], the apparition of animals (fast-moving macro-organisms) on Earth would be unthinkable without O_2 in the atmosphere. Moreover, early Earth had more atmospheric O_2 than now, and complex living beings were much bigger at that time, as suggested by the sizes of some fossils discovered. So, the amount of O_2 in the atmosphere of a superhabitable exoplanet may be slightly larger than on actual Earth (21%), let's say 25-30%.

  On the other hand, if the planet is too old, it may have lost most of its internal heat, which would result in a global cooling, although some external effects such as tidal locking from the host star may counterbalance that cooling. The cooling, however, may be a problem for the development of life as living species (complex or not) may be shifted outward of their required temperature ranges. Nevertheless, it is quite complicated to give an estimate of what age for a planet is too old, since the amount

of internal heat, as well as the time for which it will last, may depend on the mass and on the size of the planet, as explained above in this section.

Considering all of that, [Schulze-Makuch et al., 2020] proposed for a superhabitable exoplanet an age of about 5 - 8 billion years old (Earth is ∼4.5 billion years old).

- **Plate tectonics**: The plate tectonics is also thought to have played a crucial role in the development of life on Earth. The early Earth had a single supercontinent called Pangaea, and the plate tectonics have driven the continental drift which has lead to the multiple continents we are living on today, therefore, likely leading to a better development of life. Indeed, as said above, an archipelagos yields a higher biodiversity, thus biomass, than a single big continent. Moreover, it is also partly responsible for the nutrient recycling process at the surface. Life needs such nutrients to survive and develop. Therefore, as stated in [Schulze-Makuch et al., 2020], if there are no plate tectonics or other geochemical processes to recycle the nutrients at the surface, they will be rapidly used by the living forms, and be lacking, which will not be advantageous for life on the planet.

- **Presence of a moon**: The presence of the Moon is also thought by some scientists to be a relevant element for the apparition and stability of life on Earth, although it is still highly discussed. It is thought to be a stabilizer of the tilt angle of about 23.5° of the Earth equatorial plane with respect to the ecliptic plane. Without the Moon, this tilt angle may have a large oscillation amplitude, which could be a disaster for life since there would no more be stable seasons (the conditions on the planet may not be stable enough to sustain life). However, according to the results of [Lissauer et al., 2012] and [Armstrong et al., 2014], this hypothesis may not be true. They think that the presence of a moon may not be mandatory for the tilt angle of a planet to remain stable, and even that large variations over time of this angle may not be as disastrous as it was initially thought for the habitability of the planet.

- **Magnetic field**: A planetary magnetic field may also be an important feature as far as the habitability of a planet is concerned. Indeed, the magnetic field of the Earth plays a protective role for its atmosphere against the solar wind. Therefore, if an exoplanet has an atmosphere, but no (or a weak, crustal) magnetic field to shield it from the harmful charged particles coming from its host star's wind (as it is the case for Mars), the atmosphere will get eroded progressively and could be, at some point, too thin to efficiently protect potential living beings on the surface.

Let us already note that, as explained in [Schulze-Makuch et al., 2020], most of these parameters are not yet observable, and we will need a lot of time before having technologies able to measure them.

In addition to the planetary parameters listed above, some host stars also propose better conditions for life to evolve. In fact, as said in [Schulze-Makuch et al., 2020] it took on Earth several billion years for complex life (meaning multi-cellular species) to develop. This stresses the fact that the emergence of complex life takes a lot of time, although this may not necessarily take the same amount of time to develop on another planet. Therefore, some

spectral types of stars would be preferable to host inhabited planets.

A Sun-like star (G-type star) spends about 10 billion years in its core-hydrogen burning phase, the so-called main sequence[3], while this lifetime will be shorter for a hotter star, and longer for a cooler star. Hence, since complex living species on Earth have been common on a timescale nearly of the same order of magnitude (4 billion years) as the Sun's main-sequence lifetime (10 billion years), there are good reasons to think that cooler stars (K or M spectral types) should yield better conditions than a Sun-like star for complex life to develop (K-type stars have a main-sequence lifetime between 15 and 45 billions of years, for K0V and K7V stars respectively[4], and this is even more for M dwarfs). At the opposite, hotter stars (O, B, A and F spectral types) will have too short main-sequence lifetimes, thus not giving life enough time to develop, in addition to their increased high-energy photon fluxes.

However, we can restrict the list of "suitable" spectral types even more, by arguing that the HZ of a cool star is closer than that of a hotter star. Therefore, the HZ of a M-type star should be too close, and the planets inside of it would likely be tidally locked. Moreover, due to that proximity with the host star, the planets would also undergo stronger effects by the stellar wind. This could cause a massive erosion of the planetary atmospheres. Therefore, if a planet is tidally locked and if its atmosphere has been massively removed by the wind, the heat accumulated on the dayside would not be well distributed over the entire planetary surface, thus leaving a hot, molten dayside and a cold, frozen nightside. In that case, it is easy to think that the chances for life to develop on such a planet drop to nothing. However, M dwarf stars may not be simply rejected from habitable exoplanets investigations for these reasons. Indeed, as for instance in [Pozuelos et al., 2020], M dwarfs are thought to be well suited to host habitable exoplanets and are therefore largely investigated. Nevertheless, in the frame of this work, we will still consider K dwarf stars to be the ideal stellar candidates for superhabitable exoplanets.

Even if we consider that a planet is not tidally locked and that it has a consistent atmosphere, one problem still remains: the high-energy radiation of the host star. Indeed, cold stars have a pretty strong early magnetic activity leading to high X-ray and FUV fluxes. This is shown in Figure 1.2:

[3]We focus on the main sequence only and neglect the following phases of the stellar evolution because we assume that life needs stable conditions to develop. Therefore, this is the case during the main sequence, while the radius, temperature and luminosity of a star do not change much, but not anymore when this sequence comes to an end, thus starting the giant phase.

[4]Source: `https://exoplanets.nasa.gov/what-is-an-exoplanet/stars/`

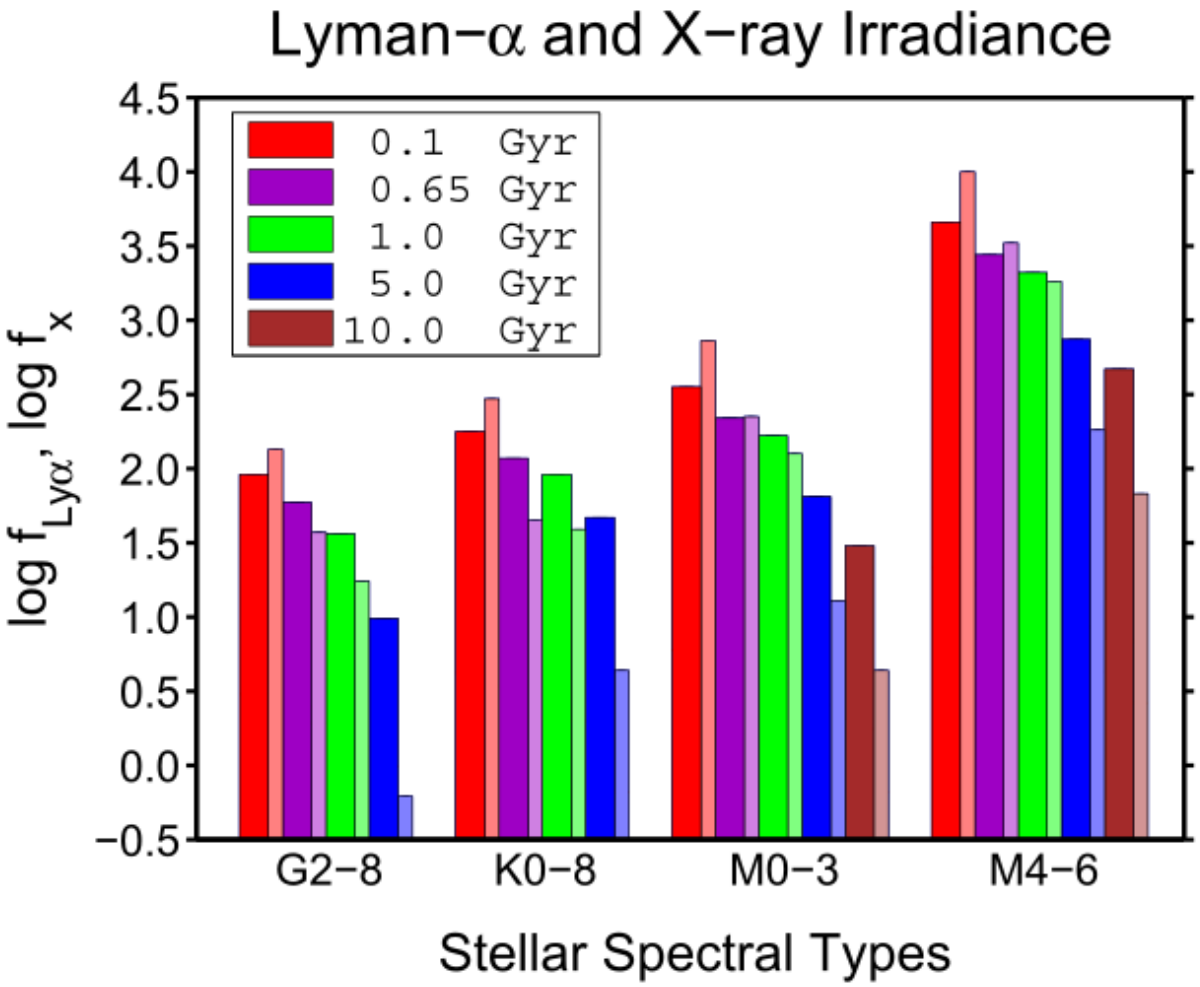

Figure 1.2: Ly-α, i.e. FUV, (wide bars) and X-ray (tight bars) irradiance for different spectral types of stars at different ages. Taken from [Cuntz and Guinan, 2016].

We can effectively notice that for a given age, mid to late M-type stars present much higher X-ray (tight bars) and FUV (wide bars) fluxes than G or even K-type stars. We can also see that these fluxes drop quicker for G stars than for M stars.

Furthermore, the close distance of the habitable zone planets from the stars is also responsible for a heavier high-energy bombardment of the planetary surfaces. By comparing the X-ray and FUV fluxes of K and M-type stars, it once again suggests that K stars may be better suited than M stars to host the so-called superhabitable exoplanets. This is illustrated in Figure 1.3:

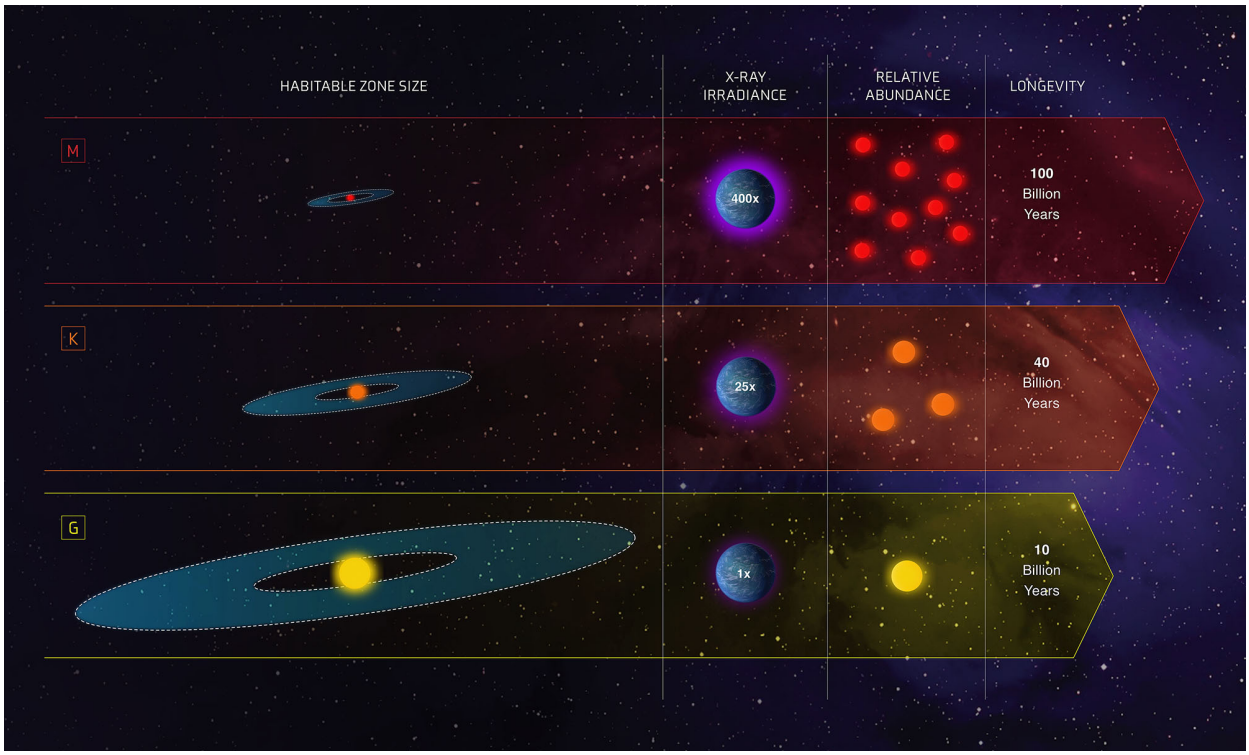

Figure 1.3: Representation of the habitable zones, the X-ray fluxes, the relative abundances and the main-sequence lifetimes of G, K and M dwarf stars. Taken from the website `https://exoplanets.nasa.gov/what-is-an-exoplanet/stars/`.

For all the reasons mentioned above, [Heller and Armstrong, 2014] came to the conclusion that K dwarf stars may be the most convenient stars to host superhabitable exoplanets. This discussion is the reason why we will focus on planets orbiting K dwarf stars in this work. [Heller and Armstrong, 2014] also tried to determine some ranges of values for planetary parameters in which a hypothetical superhabitable exoplanet should be. These values have been adjusted by [Schulze-Makuch et al., 2020]. Here are presented these hypothetical characteristics a superhabitable exoplanet may have:

- In orbit around a K dwarf star
- Age: 5 - 8 Gyr
- Mass: 1 $M_\oplus < m_p < 1.5\ M_\oplus$
- Radius: Up to 10% larger than Earth
- Mean surface temperature: about 5°C higher than on Earth
- Moist atmosphere with 25-30% O_2 levels, the rest mostly inert gases (*e.g.*, N_2)
- Type of oceans: archipelagos and shallow waters preferred to deep oceans
- Plate tectonics or similar geological/geochemical recycling mechanisms, as well as a strong protective magnetic field

[Schulze-Makuch et al., 2020] also provided a list of 24 actual best candidates for the status of superhabitable planets, including K-type stars. However, as they explained, only two of them, Kepler 1126b (KOI 2162) and Kepler-69c (KOI 172.02), are statistically confirmed exoplanets, the others being KOIs (Kepler Objects of Interest) and therefore possibly false positives, since they are still not confirmed. The entries corresponding to K-type stars among the 24 candidates are displayed in Table 1.1:

KOI	G-mag	Bp-Rp	dist (kpc)	T_{eff} (K)	Sp Tp.	$L/L_\odot$	$M/M_\odot$	Age (Gyr)	P_{orb} (d)	$R/R_\oplus$	a (AU)	T_p (°C)	T'_p (°C)
5878.01	15.797	1.090	3.157	4876	**K3V-IV**	4.409	0.76	**8.0 +/-2.0**	211.54	1.75-2.31	0.634	224.9	249.3
5135.01	15.525	1.161	1.302	4973	**K2.5V**	0.864	0.76	**5.9 +/-1.3**	314.77	1.85-2.46	0.826	17.11	31.33
5819.01	14.159	1.004	0.828	5306	**K0V**	1.158	0.87	4.3 +1.5/-1.0	381.38	1.16-1.65	0.983	13.27	**27.31**
5715.01	15.757	1.113	0.909	5018	**K3V**	0.337	0.76	**5.5 +/-2.0**	189.96	1.80-2.39	0.59	1.71	**11.59**
5276.01	15.838	1.175	0.996	4935	**K2.8V**	0.383	0.75	**6.0 +/-2.5**	220.72	1.84-2.59	0.649	5.98	7.12
5389.01	12.917	1.022	0.312	5146	**K1.5V**	0.529	0.82	2.9 +/-1.2	365.74	1.48-2.64	0.937	32.0	20.18
5130.01	15.618	1.171	0.943	4925	**K2.5V**	0.421	0.76	**6.0 +/-2.5**	370.06	1.75-2.34	0.921	43.3	32.12
5978.01	14.933	1.250	-	4900	**K3V**	0.39	0.75	-	364.20	1.62-2.58	0.907	46.17	-35.05
8047.01	15.202	1.326	0.59	4849	**K3V**	0.246	0.75	0.76 +/-0.3	302.34	1.85-2.09	0.801	-57.78	-47.23

Table 1.1: Stellar and planetary parameters of superhabitable candidate worlds. Bp-Rp is the blue-minus-red color index of the star, T_p and T'_p are the planetary surface temperatures estimated from a grey atmosphere model ([Heller et al., 2020]) (computed with different values of the optical depth, respectively $\tau = 0.35$, as observed on Earth, and $\tau = 0.705$ to reproduce the Earth's global mean surface temperature of 14°C). Adapted from [Schulze-Makuch et al., 2020].

In Table 1.1, the values in bold characters are those which correspond to the expected superhabitable parameters as listed above. Therefore, as seen from the point of view of [Schulze-Makuch et al., 2020], the best candidate to be a superhabitable planet out of this list is the object KOI 5715.01 which is orbiting a K3V star. As they said, this list is not given for a priority study from the next generation of telescopes (most of the planets listed are simply too far from the Earth), but mainly to put stress on the fact that, if such superhabitable planets do exist, some may already be present in the list of all the exoplanets we know about so far.

1.3 K dwarfs and their habitable zones

Before discussing about the detection methods, we first need to determine the ranges of physical parameters (effective temperature, mass, radius, luminosity) that characterize the K dwarf stars.

For typical effective temperatures of main-sequence K-type stars, we have Table 1.2:

Sp. type	T_{eff} **(K)**
K0	5240
K1	5110
K2	4960
K3	4800
K4	4600
K5	4400
K7	4000

Table 1.2: Effective temperatures of main-sequence K-type stars. Taken from `https://sites.uni.edu/morgans/astro/course/Notes/section2/spectralmasses.html`.

In order to study habitable zone rocky exoplanets, we need to determine the habitable zone boundaries of their host stars. For this, we will make use of the results in [Kopparapu et al., 2013]. In this paper is given the equation to obtain the distance of the habitable zone boundaries (in astronomical units AU):

$$d = \sqrt{\frac{L/L_{\odot}}{S_{\text{eff}}}} \tag{1.1}$$

where L is the stellar luminosity expressed in solar luminosity units, and where the effective stellar flux S_{eff} is given by:

$$S_{\text{eff}} = S_{\text{eff},\odot} + aT_* + bT_*^2 + cT_*^3 + dT_*^4 \tag{1.2}$$

Here, $T_* = T_{\text{eff}} - 5780$ K and the parameters $S_{\text{eff},\odot}$, a, b, c and d are also computed in [Kopparapu et al., 2013]:

Constant	**Recent Venus**	**Runaway greenhouse**	**Moist greenhouse**	**Maximum greenhouse**	**Early Mars**
$S_{eff\odot}$	1.7753	1.0512	1.0140	0.3438	0.3179
a	1.4316×10^{-4}	1.3242×10^{-4}	8.1774×10^{-5}	5.8942×10^{-5}	5.4513×10^{-5}
b	2.9875×10^{-9}	1.5418×10^{-8}	1.7063×10^{-9}	1.6558×10^{-9}	1.5313×10^{-9}
c	-7.5702×10^{-12}	-7.9895×10^{-12}	-4.3241×10^{-12}	-3.0045×10^{-12}	-2.7786×10^{-12}
d	-1.1635×10^{-15}	-1.8328×10^{-15}	-6.6462×10^{-16}	-5.2983×10^{-16}	-4.8997×10^{-16}

Table 1.3: Parameters to compute S_{eff}. Taken from [Kopparapu et al., 2013].

For the inner boundary, we will use both the runaway greenhouse and the recent Venus limits, and for the outer boundary, we will use the maximum greenhouse and the early Mars limits. In that way, we will compute both the conservative and optimistic habitable zones, and show the difference between these.

To compute the boundaries of a habitable zone, we cannot simply use the values for the temperature and luminosity from the website given in the caption of Table 1.2, otherwise we would only have 7 points to build our plot. Therefore, based on the temperature range

shown in Table 1.2, we can compute the luminosities of K dwarf stars thanks to the empirical relation $\log L(\log T_{eff})$ from Eq.(6) in [Boyajian et al., 2012]. Using this relation, we find a stellar luminosity ranging from 0.09 to 0.41 $L_{\odot}$ for an effective temperature ranging from 4000 K up to 5240 K (i.e. for the whole spectral class of K dwarfs), which is in relatively good coherence with the values of luminosity given on the website named in the caption of Table 1.2.

Therefore, making use of these luminosity and temperature values, as well as of Equations 1.1, 1.2 and of Table 1.3, we thus obtain the distance (in AU) of the inner and outer limits of the habitable zones of main-sequence K-type stars. We can also use Kepler's third law to obtain the orbital period of a planet located on the habitable zone boundaries:

$$P = \sqrt{\frac{4\pi^2 a^3}{G(m_p + m_*)}} \simeq \sqrt{\frac{4\pi^2 a^3}{G m_*}} \tag{1.3}$$

where $G = 6.674 \times 10^{-11}$ m^3 kg^{-1} s^{-2} is the universal gravitational constant, and a is the semi-major axis of the planet's orbit.

We therefore obtain the conservative and optimistic habitable zones expressed in orbital period (in days) with respect to the stellar effective temperature:

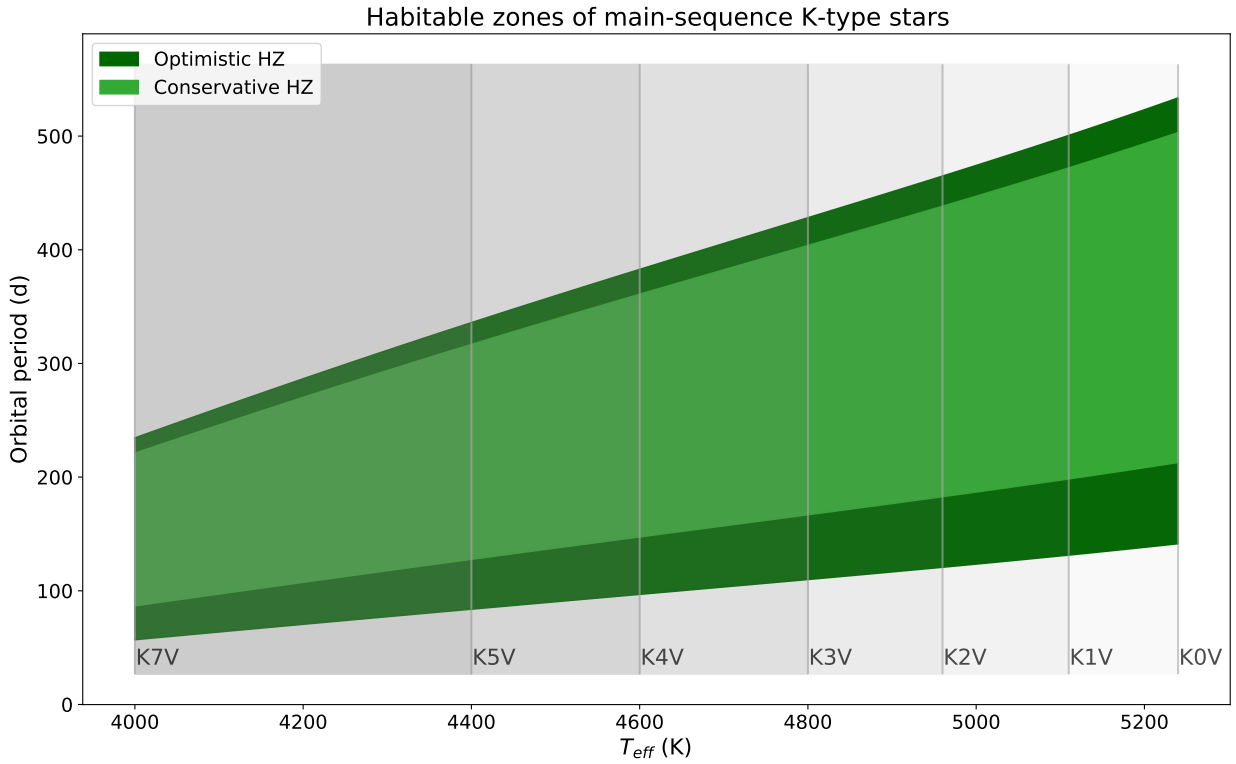

Figure 1.4: Conservative and optimistic habitable zones for the whole spectral class of K dwarfs.

The optimistic habitable zone being larger than the conservative one, we will work with the former in the next chapter to ensure ourselves, as much as we can, that we don't miss potentially habitable exoplanets in our investigations.

In the following, we will also need the mass and radius ranges of the main-sequence K-type stars. For the same reason as for the luminosity, it is preferable to obtain them from empirical relations. For the radius, we use Eq.(8) from [Boyajian et al., 2012]. This gives us values in the range 0.60 - 0.81 $R_{\odot}$. For the mass, the computation is based on the mass-luminosity relation for main-sequence stars ($L \sim M^4$). Using the luminosity values obtained above, we hence find masses in the range 0.54 - 0.80 $M_{\odot}$, which is quite close to the values on the website cited previously.

Wrapping all this up, the physical parameters of K dwarfs that we will use in the following chapter are listed in Table 1.4:

Parameters	T_{eff} (K)	L ($L_{\odot}$)	R ($R_{\odot}$)	M ($M_{\odot}$)
K7V	4000	0.09	0.60	0.54
K5V	4400	0.17	0.68	0.64
K4V	4600	0.21	0.71	0.68
K3V	4800	0.27	0.73	0.72
K2V	4960	0.31	0.75	0.75
K1V	5110	0.36	0.78	0.78
K0V	5240	0.41	0.81	0.80

Table 1.4: Physical parameters of the main-sequence K-type stars.

Chapter 2

Exoplanet detection methods

In this chapter, we will list some of the exoplanet detection methods that are used. We will explain how these methods work and, based on the expected characteristics of the superhabitable exoplanets taken from [Schulze-Makuch et al., 2020] and of the K dwarf stars given in Section 1.3, we will try to determine which of the methods are well suited to detect such exoplanets.

Detection methods

There exist several methods to detect exoplanets, some are easier to perform than others. As a consequence, most of the actually known exoplanets were discovered through transit, radial velocity, gravitational microlensing and, since quite recently, by direct imaging methods. This is further illustrated on Figure 2.1:

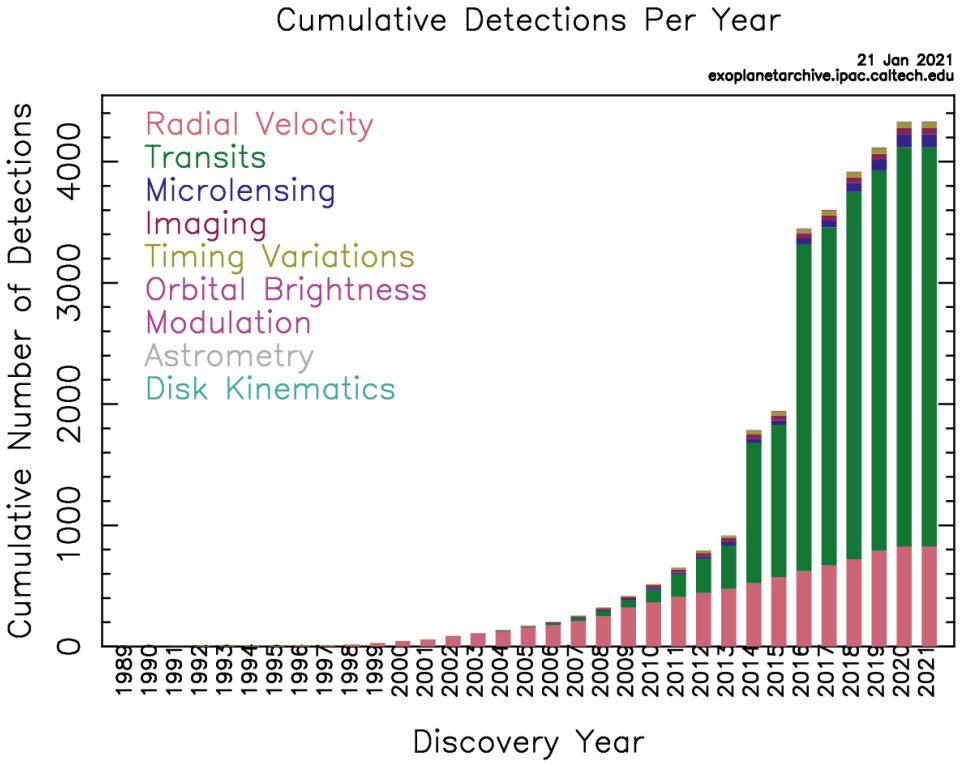

Figure 2.1: Cumulative detections of exoplanets per year, and per method. Taken from the website `https://exoplanetarchive.ipac.caltech.edu/exoplanetplots/`.

As we can see on Figure 2.1, transit and radial velocity methods have been and are still widely used to detect exoplanets. The first method to be applied was the radial velocity. It allowed Didier Queloz and Michel Mayor to discover Pegasi 51b, the first exoplanet orbiting a main-sequence star, in 1995. In 1999, the first transiting exoplanet, HD 209458b, was discovered by David Charbonneau and Greg Henry independently, and the use of this method exploded past 2009 with the launch of NASA's Kepler mission which led to the discovery of more than 2600 exoplanets. At the end of Kepler's lifetime in 2018, TESS took the relay and detected a whole bunch of new exoplanets via the transit method, making it the most used exoplanet detection method so far.[1] TESS, still working now, and its successor CHEOPS will continue to provide us with observations of transits for the next years. Other methods such as gravitational microlensing and direct imaging have made some discoveries too, but much less than the transit and radial velocity methods.

Let us now briefly explain how those different methods work (explanations mainly coming from The Exoplanet Handbook ([Perryman, 2018]) and from the course SPAT0063-1: *Introduction to exoplanetology* ([Gillon, 2020] and [Absil, 2020]), making the emphasize on their efficiency to detect potentially superhabitable exoplanets.

2.1 Transit

This method is one of the most used, and also the one that provided most of the discovered exoplanets so far. According to the NASA Exoplanet Archive[2], 3333 confirmed exoplanets have been discovered thanks to this method so far.

When a planet orbiting a star passes in between its host star and an observer, from the observer's point of view, the star's flux decreases. This situation is what we call a *transit*.

Let us first stress that the orbit of the exoplanet must be more or less perpendicular to the plane of the sky, i.e. to have an inclination $i \sim 90°$, in order to be able to notice a transit.

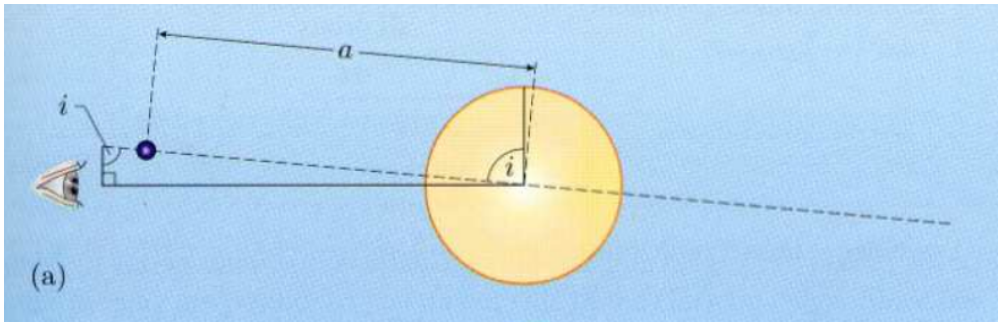

Figure 2.2: Representation of a planetary transit. If $i = 90°$, the orbital plane is perpendicular to the plane of the sky (the impact parameter $b = 0$). Taken from the course SPAT0063-1 : *Introduction to exoplanetology*, chapter *Transiting exoplanets* ([Gillon, 2020]).

Therefore, it is possible to determine the geometrical probability of a transit, for a given semi-major axis a of the planet and for a given stellar radius, as obtained by [Borucki and Summers, 1984]:

[1] Source: `https://exoplanets.nasa.gov/alien-worlds/historic-timeline`

[2] `https://exoplanetarchive.ipac.caltech.edu/docs/counts_detail.html` (consulted on the 29th of May 2021)

$$P = \frac{R_*}{a} = 0.005 \left(\frac{R_*}{R_\odot}\right) \left(\frac{a}{1 \text{ AU}}\right)^{-1} \tag{2.1}$$

where R_* is the radius of the star and a is the semi-major axis of the (circular) orbit of the transiting exoplanet.

Note that the last equality expresses the probability in terms of the Sun-Earth system, i.e. the probability to detect a transit from an Earth-like planet orbiting a Sun-like star on a circular orbit of radius $a = 1$ AU. The Sun-Earth system has a geometrical transit probability $P = 0.005 = 0.5\%$ only.

We can therefore see that for a star smaller than the Sun, a K dwarf star for instance, the geometrical transit probability for a planet orbiting that star at a distance of 1 AU is smaller than 0.5%. However, the goal here is to study the detectability of habitable zone rocky planets orbiting K dwarf stars. These stars being cooler than a G-type star like the Sun, their habitable zones are therefore closer, as shown in Figure 1.1. Indeed, while the Earth is in the HZ of the Sun (close to the moist greenhouse inner boundary) at a semi-major axis $a = 1$ AU, an exoplanet orbiting a K5V star with an orbital period of about 150 days, which corresponds, by virtue of Kepler's third law, to a semi-major axis:

$$a = \sqrt[3]{\frac{Gm_*P^2}{4\pi^2}} = 0.48 \text{ AU} \sim 0.5 \text{ AU} \tag{2.2}$$

is also in the HZ of its host star, as seen in Figure 1.4.

Let us try to estimate the geometrical transit probability in the case of a 150-day orbital period planet orbiting a K5V star (to take a late K dwarf). The stellar radius, as obtained in Section 1.3, is $R_* = 0.68\ R_\odot$. Therefore, the transit probability for such a star-planet system is:

$$P = 0.00708 = 0.708\% \simeq 0.7\% \tag{2.3}$$

This is just a bit larger than for the Sun-Earth system ($P = 0.5\%$). However, another element has to be taken into account, the probability of stars with respect to their masses (so to their spectral types). This is further shown in [Cuntz and Guinan, 2016], using the initial mass function (IMF):

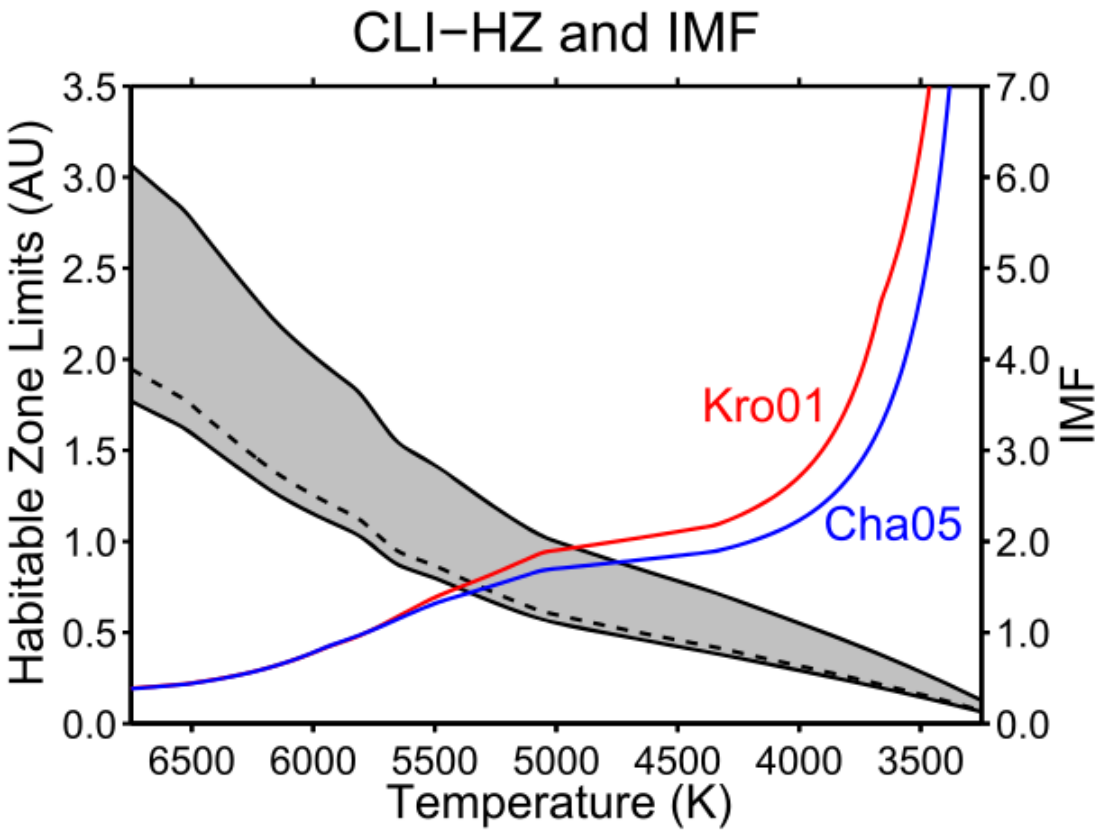

Figure 2.3: IMF derived from [Kroupa, 2001] (red) and [Chabrier et al., 2005] (blue). The grey shaded region represents the conservative HZ (defined by the runaway greenhouse limit and the first CO_2 condensation boundary), and the dashed line is the homeothermic distance, as explained in Section 1.1. Taken from [Cuntz and Guinan, 2016].

The IMF is represented with the blue line (given by [Chabrier et al., 2005]) and the red line (given by [Kroupa, 2001]), and normalized at unity for one solar mass. As we can see here, K dwarf stars are twice as more probable as Sun-like stars. As a consequence, even though the geometrical transit probability for superhabitable planets is still low, the increased number of K-type stars with respect to G-type stars makes transits a bit more likely for superhabitable planets than for Earth-twins (meaning Earth-like planets orbiting Sun-like stars at a distance of 1 AU).

Let us now imagine that we measure the flux of a star. During a transit, the flux will drop, as shown in Figure 2.4:

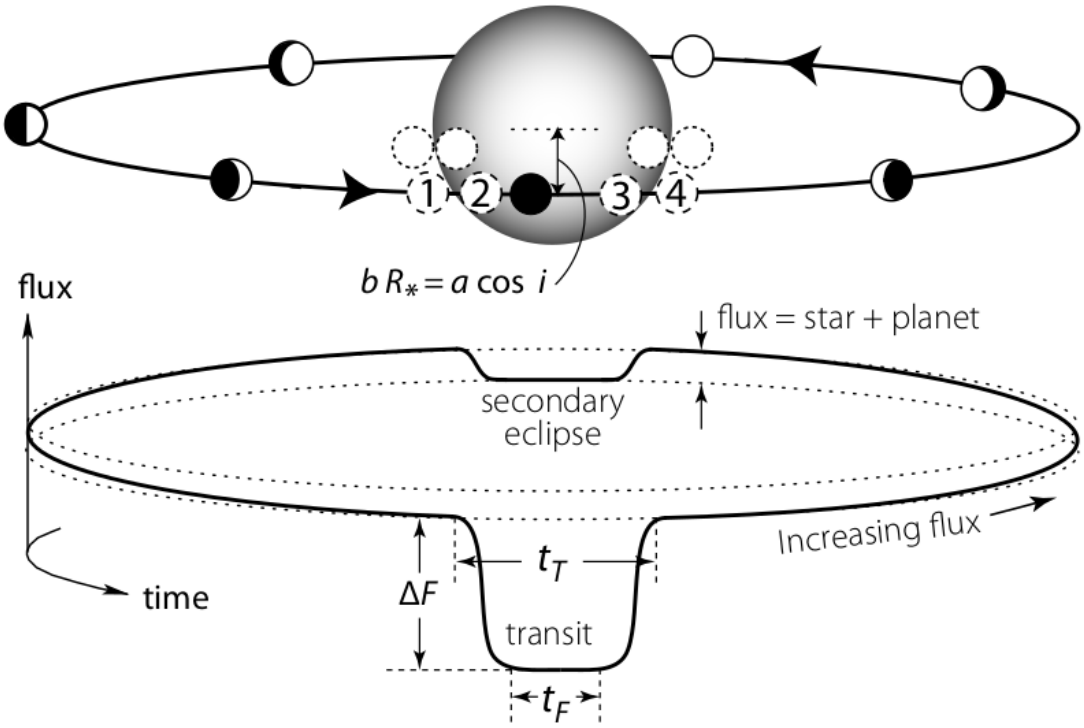

Figure 2.4: Overview of a planetary transit. ΔF is the transit depth, t_T is the total time of the transit event (between planet's positions 1 and 4 on the figure), t_F is the time interval during which the planetary disk completely overlaps the stellar disk. b is the impact parameter, i.e. the "distance" between the center of the stellar disk and the center of the planetary disk, when the planet is at the middle of the transit event ($b = 0$ if the planet passes right in front of the center of the stellar disk). Taken from [Perryman, 2018], p.200.

The flux curve with respect to time is called a light curve. The analysis of the light curve of a star during a transit event can furnish us with different physical quantities about the transiting planet and the star.

The transit depth ΔF can yield the ratio of the planetary radius and of the stellar radius:

$$\Delta F = \left(\frac{r_p}{R_*}\right)^2 \tag{2.4}$$

where r_p is the planetary radius, and R_* is the stellar radius. Therefore, using this relation in the case of our star-planet couple ($r_p = 1.1\ R_\oplus$ and $R_* = 0.68\ R_\odot$), we find a transit depth of:

$$\Delta F = 2.190 \times 10^{-4} \simeq 0.0219\% = 219 \text{ ppm} \tag{2.5}$$

As a comparison, the transit depth for the Sun-Earth system would be:

$$\Delta F_{Sun-Earth} = 8.371 \times 10^{-5} \simeq 0.0084\% = 84 \text{ ppm} \tag{2.6}$$

We can therefore notice that observing a transit of a superhabitable exoplanet is easier than for an Earth-like planet.

Using the ranges of physical parameters obtained from [Boyajian et al., 2012] and

[Kopparapu et al., 2013] in Section 1.3, we can also derive the geometrical transit probability and the transit depth for an exoplanet of mass $m_p = 1.25\ M_\oplus$ and radius $r_p = 1.1\ R_\oplus$ located in the optimistic habitable zone of its host, for the whole K spectral class. This is illustrated in Figure 2.5:

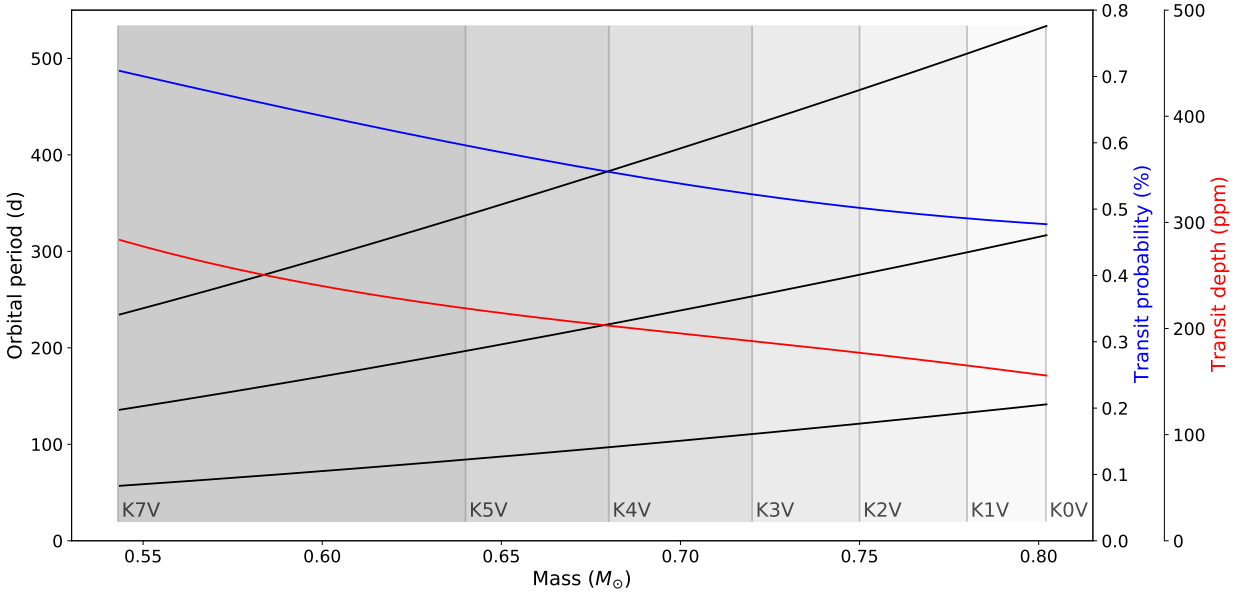

Figure 2.5: Orbital period (black), geometrical transit probability (blue) and transit depth (red) for superhabitable exoplanets located in the optimistic habitable zones of main-sequence K-type stars. Note that the transit probability and the transit depth are computed for planets located in the middle of the optimistic HZs of their host stars (on the middle black line).

In this plot is also represented the orbital period (in black) of a planet located in the habitable zone of its host star (inner edge, middle and outer edge). Planets orbiting late K dwarfs are therefore easier to detect via the transit method than planets around early K dwarf stars.

Such shallow decreases of the flux are hard to detect from current ground-based observatories, notably because of the photometric noise implied by atmospheric turbulence. This is one of the reasons why such detections should be done using space-based telescopes. Let us however note that this kind of photometric accuracy can already be achieved, at least for stars with G-mag < 14, with the CHEOPS mission which expected photometric precision can reach 20 ppm with a 6-hour integration. ([Benz et al., 2021])

A reason for which it is worth giving a shot to the transit method is because it can also allow, in addition to the detection of exoplanets, to perform spectroscopic studies of their atmospheres thanks to a method called *transit spectroscopy*. Indeed, as explained in [de Wit and Seager, 2013], due to the molecular absorption bands of its atmosphere, a transiting planet's effective radius will appear different depending on the observed wavelength. If the exoplanetary atmosphere contains molecules able to absorb light coming from its host star at a given wavelength, the transit depth for that wavelength will be larger than for a wavelength where no atmospheric absorption occurs, because a lesser amount of light arrives to us (the planet's effective radius is larger). This wavelength dependence of the transit light curve is further illustrated in Figure 2.6:

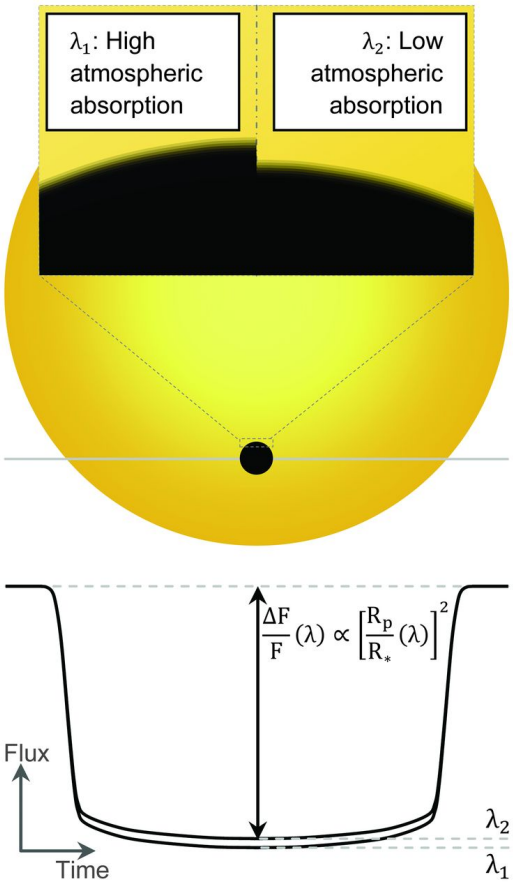

Figure 2.6: Illustration of the wavelength dependence of a transit light curve and of the effective radius of the planet. Taken from [de Wit and Seager, 2013].

We can therefore infer the chemical composition of an exoplanetary atmosphere by analyzing transits at multiple wavelengths at the same time. As a consequence of that spectroscopic application of the transit method, some future planned missions, as it will be described in the next chapter, will perform transit spectroscopy in order to study the atmospheric chemical compositions of some detected exoplanets of great interest.

Let us also insist on the fact that, even though it is possible to detect superhabitable planets using the transit method, it is important to note that the long orbital period of this kind of planet is inhibiting. Indeed, this would require a very long continuous observation time to be sure not to miss the transit, and this is only if we are sure that there is a transiting planet orbiting the star of interest. In general, we don't know it in advance, so it would be problematic to spend more than a hundred days observing a star without being sure that we will find what we are interested in. In some cases, the telescope will do a lot of observations in some regions of the sky, as it is the case for the TESS mission near the North and South poles of the ecliptic, where the cumulated observation time is 351 days[3], hence giving long enough observations to be able to find long-period transiting planets in the light curves. More details about the TESS mission will be given in chapter 4.

If a long-period transiting exoplanet has already been discovered around a given star via the transit method or even another technique such as the radial velocity method (discussed

[3]Source: `https://heasarc.gsfc.nasa.gov/docs/tess/operations.html`

hereafter), it is also possible to predict when future transits of the planet will occur. Therefore, it is possible to schedule an observation at those predicted transit times rather than monitoring continuously the stellar flux.

To conclude this section about the transit method, here is a list of current and past space-based telescopes that achieved most of the exoplanet detections using this technique:

- **Convection, Rotation et Transits planétaires (CoRoT)**: CoRoT was a CNES mission launched in 2006 on a low-Earth polar orbit, and it stopped working in 2012. It was the first space-based observatory dedicated to the detection of exoplanets via the transit method. It was carrying a 27-cm diameter telescope and a 4-CCD wide-field camera.[4] Designed to observe stars with apparent V-band magnitudes ranging from 11 to 16, it detected about a few dozens exoplanets during its lifetime.[5] According to The Exoplanet Handbook ([Perryman, 2018]), its photometric precision was reaching 75 ppm for a 1-hour integration time, for stars in its observed magnitude range.

- **Kepler**: NASA's mission[6] launched in 2009 on a heliocentric orbit and stopped in 2018. It observed only toward the Cygnus-Lyra region of the sky. To apply the transit method, it was equipped with a photometer able to reach, as said in The Exoplanet Handbook ([Perryman, 2018]), a combined differential photometric precision of about 30 - 40 ppm for stars with apparent V-band magnitudes $m_V \sim 12$, with a 6.5-hour integration time.

- **Transiting Exoplanet Survey Satellite (TESS)**: TESS is a NASA mission, launched in 2018 on an elliptical high-Earth orbit. It was dedicated to survey nearly 85% of the sky, looking at nearby stars, at maximum 200 light years away.[7] According to [Benz et al., 2021], it observes stars with m_V between 4 and 12 and its photometric precision is on the order of 60 ppm for a $m_V \sim 9$ star, with a 6-hour integration time. It is currently still working, and provides us with the most complete and accurate light curves database of nearby stars. More details about the TESS mission will be given in Chapter 4.

- **CHaracterising ExOPlanets Satellite (CHEOPS)**: CHEOPS is the most recent space-based observatory using the transit method to find exoplanets. This is an ESA space mission launched in 2019 on a Sun-synchronous low-Earth orbit. From [Benz et al., 2021], it is designed to observe stars with m_V in between 6 and 12, and it has a 6.5-hour integration photometric precision of 20 ppm for stars with m_V ranging from 6 to 9.

[4]Source: `https://sci.esa.int/web/corot`
[5]Source: `https://cheops.unibe.ch/science/corot-and-kepler-vs-cheops`
[6]Source: `https://www.nasa.gov/mission_pages/kepler/spacecraft/index.html`
[7]Source: `https://heasarc.gsfc.nasa.gov/docs/tess/objectives.html`

2.2 Radial velocity

The radial velocity method is the second most used technique to detect exoplanets. It has been used for the discovery of 842 confirmed exoplanets, as seen on the NASA Exoplanet Archive[8] website.

When a planet is orbiting a star, the star interacts with the planet through the gravitational attraction but the planet also does attract the star, by virtue of Newton's third law (action-reaction principle). This interaction will therefore imprint an orbital velocity to the star, in addition to its systemic velocity, i.e. the velocity of the whole system with respect to an absolute frame of reference. The resulting radial velocity (the velocity component aligned, or anti-aligned, with the observer's line of sight) of the star is expressed in Equation 2.7, as seen in the course SPAT0063-1: *Introduction to exoplanetology* ([Gillon, 2020]):

$$V_r = \gamma_r + K(\cos(\omega + f) + e\cos\omega) \tag{2.7}$$

where γ_r is the radial component of the systemic velocity, K is the radial velocity semi-amplitude, e is the eccentricity of the orbit, ω is the argument of the pericenter (the point of closest approach between the planet and the star), i.e. the angle between the line of nodes of the orbit and the direction to the pericenter, and f is the true anomaly (the angle between the direction to the pericenter and the direction to the planet). As we can see, the second term of the right-hand side of Equation 2.7, the radial component of the orbital velocity of the star, is a periodic term, as it will depend on the position of the planet on its orbit.

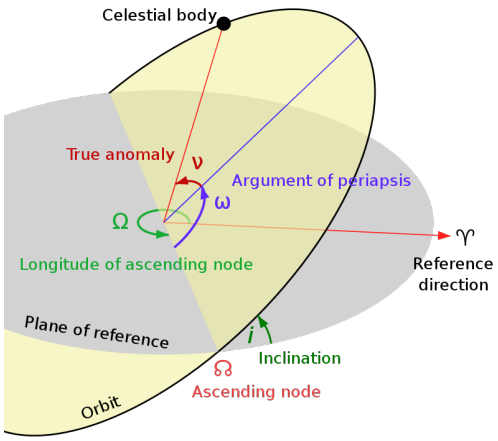

Figure 2.7: Representation of the orbital elements. Note that here the true anomaly is noted ν instead of f. Taken from the website `https://en.wikipedia.org/wiki/Orbital_elements`.

Due to that periodicity of the orbital velocity term, the radial velocity curve of a star under the effect of an orbiting planet looks like in Figure 2.8:

[8] `https://exoplanetarchive.ipac.caltech.edu/docs/counts_detail.html` (consulted on the 29th of May 2021)

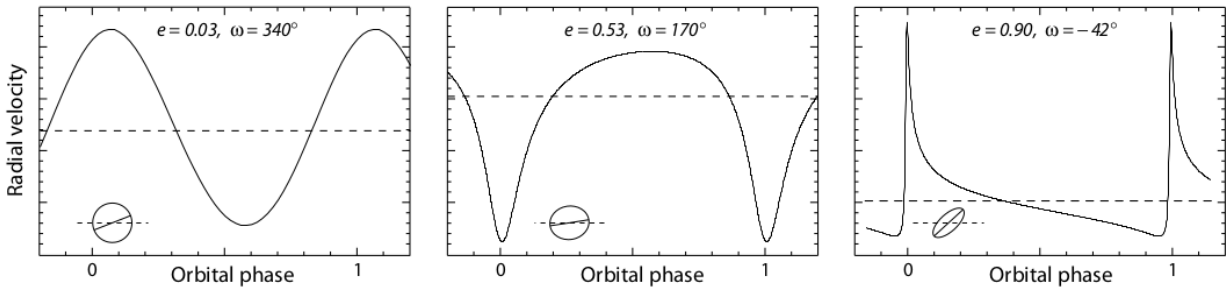

Figure 2.8: Radial velocity curves of a star due to an orbiting planet. The dependence on the eccentricity e and on the argument of the pericenter ω is illustrated. Taken from The Exoplanet Handbook ([Perryman, 2018]), p.21.

Without entering into many details, the radial velocity of a star can be measured, thanks to the relativistic Doppler effect, by analysis of spectral lines in the stellar spectrum. Indeed, due to the radial velocity of a star with respect to the observer, the spectral lines of the star's chemical compounds will be shifted in wavelength with respect to the lab reference spectrum for the same compounds. The lines of the stellar spectrum are blueshifted (resp. redshifted) with respect to the lines of the lab spectrum if the star moves toward (resp. away from) the observer:

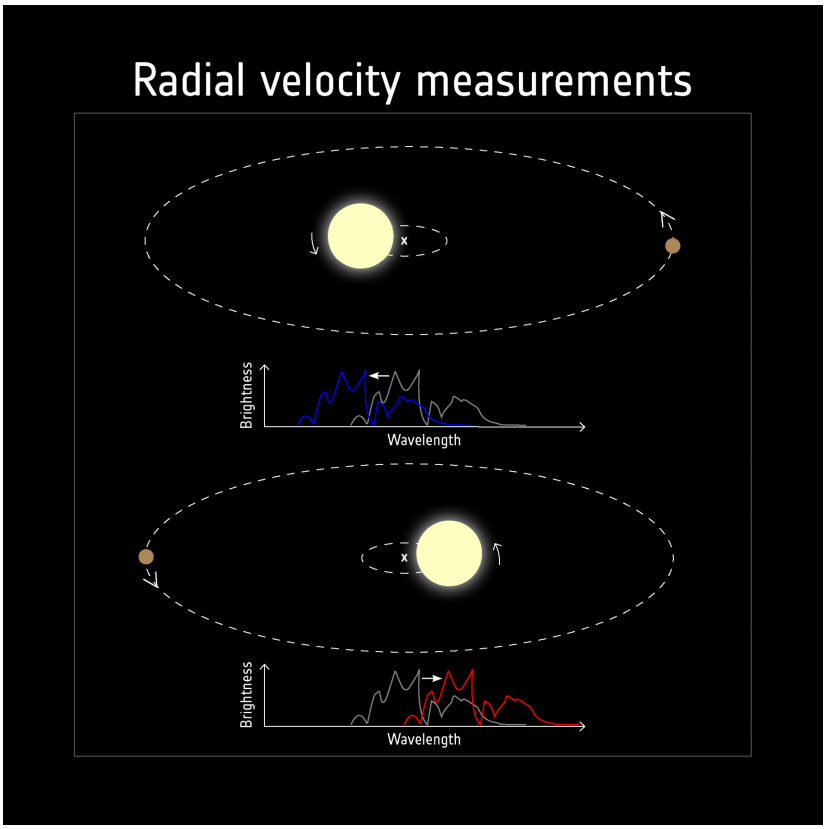

Figure 2.9: Illustration of the Doppler shift of a stellar spectrum due to the star's radial velocity. Taken from the website `https://www.esa.int/ESA_Multimedia/Images/2019/02/Detecting_exoplanets_with_radial_velocity`.

Therefore, if we are able to identify a chemical compound in a stellar spectrum and to measure its Doppler shift with respect to the reference spectrum, we have a mean to es-

timate the radial velocity of the star, thanks to the Doppler effect relation as derived in [Lindegren and Dravins, 2003]:

$$V_r = c\frac{\lambda - \lambda_0}{\lambda_0} \tag{2.8}$$

where c is the speed of light, λ is the wavelength at which the line is measured in the stellar spectrum and λ_0 is the wavelength of the same line in the reference spectrum.

The radial velocity semi-amplitude K is given by the relation seen in the course SPAT0063-1: *Introduction to exoplanetology*, chapter *Indirect methods for exoplanets detection* ([Gillon, 2020]):

$$K = \frac{28.4329}{\sqrt{1-e^2}} \frac{m_p \sin i}{M_{♃}} \left(\frac{m_p + m_*}{M_\odot}\right)^{-2/3} \left(\frac{P}{1 \text{ yr}}\right)^{-1/3} \text{ m s}^{-1} \tag{2.9}$$

$$= \frac{8.945 \times 10^{-2}}{\sqrt{1-e^2}} \frac{m_p \sin i}{M_\oplus} \left(\frac{m_p + m_*}{M_\odot}\right)^{-2/3} \left(\frac{P}{1 \text{ yr}}\right)^{-1/3} \text{ m s}^{-1} \tag{2.10}$$

where m_p, m_*, $M_\oplus$, $M_{♃}$ and $M_\odot$ stand for the masses of the orbiting planet, the star, the Earth, Jupiter and the Sun. i and e are the inclination and the eccentricity of the orbit, and P is the orbital period.

From Equation 2.10, we can see that K will be maximum if $i = 90°$ (same configuration as for a transit) and $e = 0$ (circular orbit). Moreover, K will be larger for a more massive, closer planet orbiting a low-mass star. We can also see that if we know K, e, P and $m_p + m_* \sim m_*$, it is possible to determine $m_p \sin i$. Therefore, $m_p \sin i$ being smaller or equal to m_p, the radial velocity method allows us to determine the minimal mass of the planet.

In order to determine whether or not the radial velocity method will be useful to detect small habitable zone rocky exoplanets orbiting K dwarf stars (the definition of superhabitable exoplanets), let us derive the value of K in this case. As a reminder from Section 1.3, a superhabitable planet and a K5V star may have the following characteristics:

- $m_p \sim 1.25\ M_\oplus$
- $P \sim 150$ d $= 0.41$ yr
- $m_* \sim 0.64\ M_\odot$

Let us determine K in the best possible case (to have its maximum value), so we take $i = 90°$ and $e = 0$. We also assume that $m_* \gg m_p$. Hence, Equation 2.10 can be written:

$$K = 8.945 \times 10^{-2} \left(\frac{m_p}{M_\oplus}\right) \left(\frac{m_*}{M_\odot}\right)^{-2/3} \left(\frac{P}{1 \text{ yr}}\right)^{-1/3} \text{ m s}^{-1} \tag{2.11}$$

$$= 2.027 \times 10^{-1} \text{ m s}^{-1} \tag{2.12}$$

$$\simeq 0.20 \text{ m s}^{-1} \tag{2.13}$$

So, for our superhabitable exoplanet, we therefore have:

$$K \simeq 20 \text{ cm s}^{-1} \quad \text{for } i = 90° \text{ and } e = 0 \tag{2.14}$$

As a comparison, the Sun-Earth system yields a radial velocity semi-amplitude $K \simeq 9$ cm s^{-1} and for Jupiter, it is $K \simeq 12.5$ m s^{-1}. The case of superhabitable exoplanets is further illustrated in Figure 2.10, where we plotted K, for the whole main-sequence K spectral class:

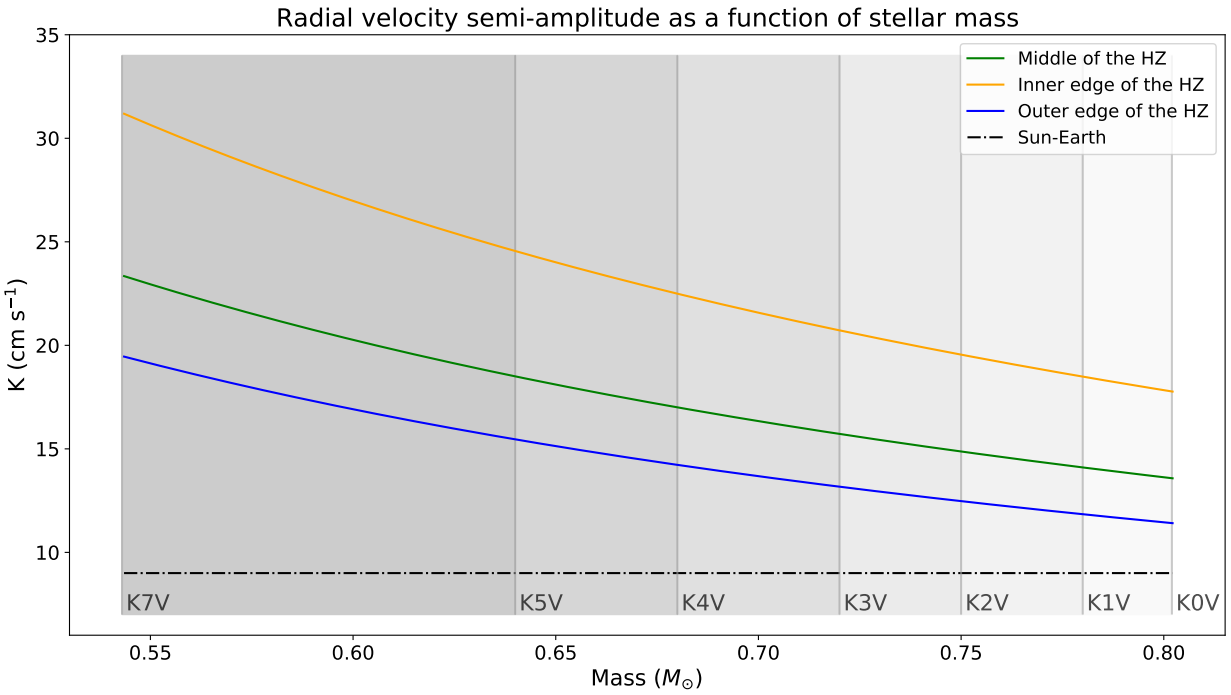

Figure 2.10: Radial velocity semi-amplitude K as a function of the stellar mass (for the whole K spectral class). K is computed for the inner edge, middle and outer edge of the optimistic habitable zone of each type of star. The case of the Sun-Earth system is also represented as a reference.

We see that for the whole K spectral type, the radial velocity semi-amplitude is larger than 9 cm s^{-1}, so the radial velocity detection of a superhabitable exoplanet seems easier than for an Earth twin ($K = 9$ cm s^{-1}).

As for the transit method, we will now enumerate current and past RV instruments, to check whether or not the detection of superhabitable exoplanets is/was already possible:

- **ESPRESSO**: The Echelle SPectrograph for Rocky Exoplanets and Stable Spectroscopic Observations (ESPRESSO) ([Pepe et al., 2021]), equipped on the Very Large Telescope (VLT) at the Cerro Paranal observatory, is so far the best spectrograph we have to detect exoplanets by the radial velocity method. It started its operations in October 2018. It can observe in the whole visible spectral range (380-788 nm). Its RV precision can reach 10 cm s^{-1}, [9] which is enough to detect superhabitable exoplanets, as we can see in Figure 2.10.
- **CARMENES**: Short for Calar Alto high-Resolution search for M dwarfs with Exoearths with Near-infrared and optical Echelle Spectrographs, CARMENES ([Quirrenbach et al., 2016]), as its name suggests, is installed at the Calar Alto observatory. It started working in November 2015. It is made of two spectrographs,

[9] Source: `https://www.eso.org/sci/facilities/paranal/instruments/espresso.html`

one mainly covering the visible wavelengths (520 - 960 nm), the other focusing on the near-infrared domain (960 - 1710 nm). Designed to search for Earth-like planets around late M dwarfs, its RV precision is on the order of 1 m s^{-1}, [10] so not enough for superhabitable exoplanets.

- **HARPS**: The High Accuracy Radial velocity Planet Searcher (HARPS) is an echelle spectrograph equipped on a 3.6-m telescope at the La Silla observatory in 2003. It measures light in the range 378 nm to 691 nm (visible), with a RV precision of 1 m s^{-1} ([Mayor et al., 2003]) [11], not enough for superhabitable exoplanets.

- **HARPS-North**: The HARPS-North echelle spectrograph ([Cosentino et al., 2012]) is mounted on the Telescopio Nazionale Galileo (TNG) at the La Palma observatory. Its first light was in March 2012. It covers nearly the same wavelengths as HARPS (383 - 693 nm), and its long-term RV precision is on the order of 0.6 m s^{-1}, [12] still not enough for superhabitable exoplanets.

- **SPIRou**: The SpectroPolarimètre InfraRouge (SPIRou), installed in 2018 on the Canada-France-Hawaii Telescope (CFHT) near Mauna Kea mountain in Hawaii, is notably dedicated to the detection of habitable Earth-like planets around M dwarfs. It observes in the near-infrared domain (0.98 - 2.40 μm), with a RV precision of about 1 m s^{-1}. ([Artigau et al., 2014])[13] This one is therefore not suited either to the detection of superhabitable exoplanets.

Advantages of using both radial velocity and transit methods:

The inclination i can't directly be obtained from the radial velocity method, hence we are limited to get $m_p \sin i$. However, combining radial velocity and transit methods can be very useful. Indeed, if we can observe a transit from a planet discovered via the radial velocity method, we know that the inclination i is close to 90°, so $\sin i \simeq 1$. Such a situation will therefore allow us to obtain directly the mass of the planet.

Since the transit method can furnish us the radii ratio of the transiting planet and of the star (thanks to the transit depth), we can also obtain the radius of the planet considering that we know the radius of the star (this can be done notably via interferometric studies, as explained in [Boyajian et al., 2012]).

In the end, combining results of both transit and radial velocity methods, we can even determine the density of the planet itself, which can be useful to find out its internal chemical composition, its planetary type (rocky or gaseous), etc.

Let us finally put stress on that, as it was the case for the transit method, the large orbital period of a superhabitable exoplanet is here also a problem since it is necessary to probe the radial velocity of the host star over a full orbital period before being able to precisely determine $m_p \sin i$, although it may be possible to fit the observations and to try to predict the radial velocity curve before the end of an orbital cycle.

[10] Source: `https://carmenes.caha.es/ext/instrument/index.html`
[11] Source: `http://www.eso.org/sci/facilities/lasilla/instruments/harps/overview.html`
[12] Source: `http://www.tng.iac.es/instruments/harps/`
[13] Source: `http://www.exoplanetes.umontreal.ca/spirou-spectrograph/?lang=en`

2.3 Astrometry

The astrometry detection method is quite difficult to apply. According to the Extrasolar Planet Encyclopaedia [14], only 14 confirmed exoplanets were discovered using the astrometry technique so far:

Planet	**Mass** (M_{Jup})	**Period** (day)	a (AU)	e	i (deg)	**Discovery**
DE0630-18 (bc)	53	-	-	-	-	2020
DE0630-18 a	58	-	-	-	-	2008
TVLM 513-46546 b	0.38	220	0.3	0	71	2020
SDSS J080531+481233 B	66.28	740.43	0.82	0.423	111.85	2016
2M1059-21 b	66.95	690	0.8	0.146	32.9	2020
WISE J0458+6434 A	57	15500	1	0.18	76.5	2019
WISE J0458+6434 B	14	15500	4	0.18	76.5	2019
2MASS J15344984-2952274 A	30.1	-	-	-	-	2008
2MASS J15344984-2952274 B	28.2	5550	2.3	0.24	84.3	2008
SDSS J080531+481233 A	60	-	-	-	-	2016
2MASS J0249-0557A	48	-	-	-	-	2018
2MASS J0249-0557 (AB) c	11.6	-	-	-	-	2018
2MASS J0249-0557B	44	-	-	-	-	2018
HD 176051 b	1.5	1016	1.76	0	-	2010

Table 2.1: The 14 confirmed exoplanets discovered using the astrometry technique. Taken from `http://exoplanet.eu`.

Several missions have been dedicated to perform astrometric studies, among which the High Precision Parallax Collecting Satellite (Hipparcos)[15] and Gaia[16], two ESA missions launched in 1989 and in 2013 respectively. Their goal was mainly to determine the parallax and the motion of stars in order to build an accurate stellar catalog.

In addition to the mapping of our galaxy, astrometry can also be used to indirectly detect the presence of planets orbiting stars. As in the case of the radial velocity technique, the star attracts gravitationally the orbiting planet, but the latter also implies a gravitational perturbation to the star, which makes the star and the planet orbiting around their common barycenter. Therefore, if we also take the systemic motion into account (the motion of the whole system in the galaxy) and the motion due to the rotating frame of reference in which is located the observer, the motion of the star projected on the plane of the sky can be seen as an ellipse:
Note that this can be much more complicated in the presence of multiple orbiting planets.

We can therefore define the *astrometric signature* θ, as seen in the course SPAT0063-1: *Introduction to exoplanetology*, chapter *Indirect methods for exoplanets detection* ([Gillon, 2020]):

[14] `http://exoplanet.eu` (consulted on the 29th of May 2021)
[15] Source: `https://www.cosmos.esa.int/web/hipparcos`
[16] Source: `https://www.esa.int/Science_Exploration/Space_Science/Gaia`

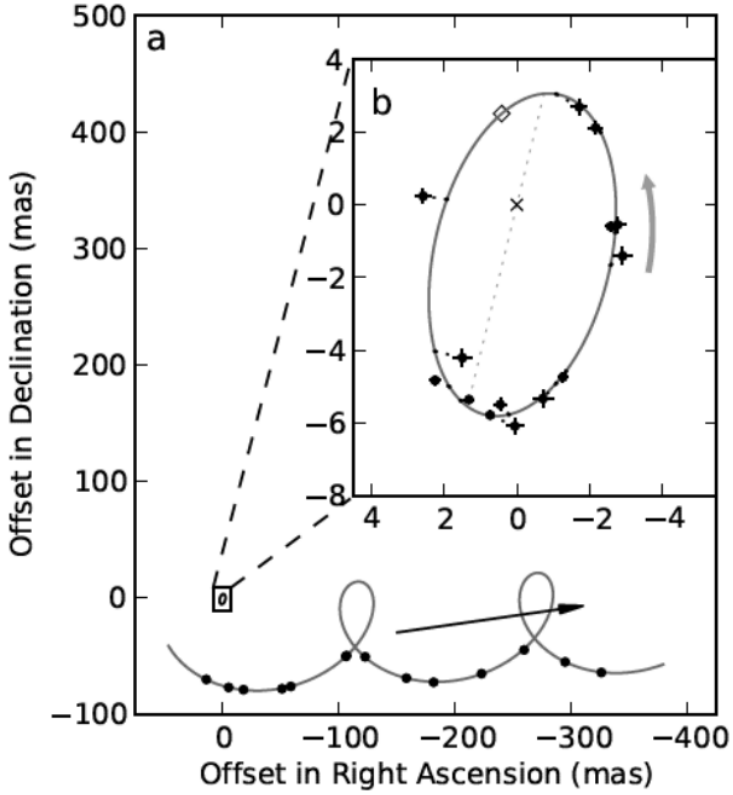

Figure 2.11: Representation of the orbital motion of a star caused by a planet, about the star-planet barycenter. Taken from the course SPAT0063-1: *Introduction to exoplanetology* ([Gillon, 2020]), chapter *Indirect methods for exoplanets detection*.

$$\theta = \frac{a}{d}\frac{m_p}{m_*} \tag{2.15}$$

$$= 3\left(\frac{m_p}{M_\oplus}\right)\left(\frac{m_*}{M_\odot}\right)^{-2/3}\left(\frac{P}{1\text{ yr}}\right)^{2/3}\left(\frac{d}{1\text{ pc}}\right)^{-1}\ \mu\text{as} \tag{2.16}$$

As explained in [Deeg and Belmonte, 2018] and in [Perryman, 2018], this corresponds to the semi-major axis of the elliptical orbit of the star around the star-planet barycenter.

As we can see, it is proportional to the mass of the planet m_p and to the semi-major axis a of the planetary orbit, and inversely proportional to the stellar distance d and to the stellar mass m_*. Therefore, this technique will be mainly sensitive for nearby systems, and especially for massive, long-period planets orbiting low-mass stars. This is in accordance with the 14 confirmed astrometric exoplanets listed on the Extrasolar Planets Encyclopaedia website and shown in Table 2.1.

Let us now compute the value of the astrometric signature θ, using Equation 2.16, in the case of our superhabitable exoplanet ($m_p = 1.25\ M_\oplus$, $m_* = 0.64\ M_\odot$ (K5V), $P = 150$ d). For distances d of 1, 10, 100 and 1000 pc, we have:

$$d = 1 \text{ pc} : \quad \theta = 2.787 \ \mu\text{as} \tag{2.17}$$
$$d = 10 \text{ pc} : \quad \theta = 0.2787 \ \mu\text{as} \tag{2.18}$$
$$d = 100 \text{ pc} : \quad \theta = 0.0279 \ \mu\text{as} \tag{2.19}$$
$$d = 1000 \text{ pc} : \quad \theta = 0.00279 \ \mu\text{as} \tag{2.20}$$

We are already below the μas regime at a distance of 10 pc. We can also apply Equation 2.16 to the different classes of K-type stars (K0V to K7V), using the stellar parameters and orbital periods obtained in Section 1.3 (and still with a planetary mass $m_p = 1.25 \ M_\oplus$). We take the distance between 1 and 10 pc only, because as we have seen above, θ decreases quickly with the distance. This is represented in Figure 2.12.

As a comparison, the astrometric signature of a Sun-like star under the influence of an Earth-like planet orbiting on a circular orbit of radius 1 AU, and observed at a distance of 1 pc is $\theta \simeq 3 \ \mu$as. The astrometric signature θ of the Sun-Earth system is also plotted in Figure 2.12, as a comparison with the superhabitable exoplanets orbiting K-type stars:

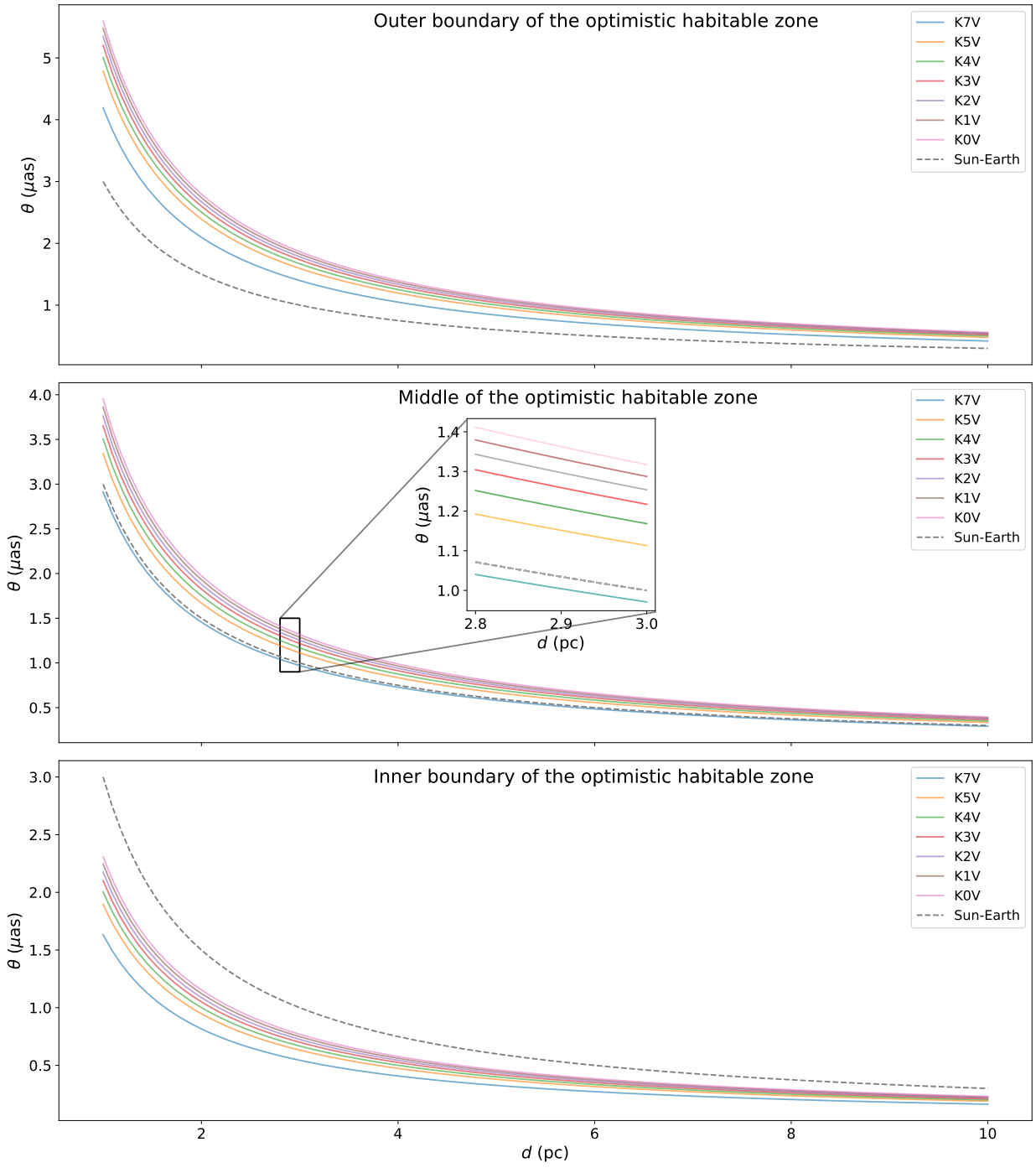

Figure 2.12: Astrometric signature for a superhabitable exoplanet of mass $m_p = 1.25\ M_\oplus$ orbiting in the optimistic habitable zone of a K-type star. The whole K spectral class is represented. The upper, middle and lower panels represent the situations where the planet is located on the outer edge, in the middle and on the inner edge of the optimistic HZ of its host star.

As we can see on Figure 2.12, depending on the position of the superhabitable exoplanet in the habitable zone of its host star, it may be slightly easier to detect its effect on the motion of the star. We can see that the astrometric signature for a superhabitable exoplanet is larger than that of the Sun-Earth system, whatever the class of the K-type star (except for the K7V star) when the exoplanet is located in between the middle of the optimistic habitable zone and the outer boundary. However, when the superhabitable exoplanet is

located on the inner edge of the optimistic habitable zone of its star, we see that for each K star, the astrometric signature is lower than for the Sun-Earth system.

Let us already stress that even Gaia, the current most accurate astrometric observatory, does not reach the 3 μas accuracy needed to detect an Earth-twin in a system located 1 pc away, and even though the astrometric signatures for superhabitable exoplanets can be larger than for the Sun-Earth system, Gaia's precision is still insufficient in this case. Indeed, Gaia's astrometric precision is, as seen in The Exoplanet Handbook ([Perryman, 2018]), about 10 μas for $V \sim 7 - 12$ (this was about 1 mas for Hipparcos). This is therefore not enough.

Moreover, the astrometric signature decreases with the distance ($\theta \propto d^{-1}$). Hence, since it is already not possible at 1 pc, there is no hope to discover superhabitable exoplanets with the astrometry detection method further away than 1 pc using current observatories. Indeed, the closest stellar neighbour of the Sun being Proxima Centauri[17], located at a distance of about 4.25 l.y. = 1.23 pc, we can conclude that the astrometry method can most likely not be used in the specific case of superhabitable exoplanets detection, at least for the current generation of telescopes.

However, as explained in [The LUVOIR Team, 2019], one of the instruments of the Large UV/Optical/IR Surveyor (LUVOIR) planned to be launched in the late 2030s, the High-Definition Imager (HDI), will be able to reach the sub-μas regime necessary to detect superhabitable exoplanets within 10 pc. More details on this mission are given in Subsection 3.2.3.

2.4 Gravitational microlensing

The microlensing exoplanets detection method is rather new. The first exoplanet discovery using this technique was made in 2003([Bond et al., 2004]). Since this first detection, 108 exoplanets were discovered with this method, according to the NASA Exoplanet Archive.[18]

The way this detection method works is based on General Relativity results. Due to the local curvature of spacetime as an effect of the presence of matter and energy, Einstein's theory predicts that the trajectory of a photon will be bended in the vicinity of a massive object. Considering an external observer, if the source of the photons and this massive object are aligned with its line of sight, instead of being blocked by the intermediate object, the photons will be deviated and reach the observer. Hence, the latter will see the background source as if it were misaligned with its line of sight:

[17] Source: `https://imagine.gsfc.nasa.gov/features/cosmic/nearest_star_info.html`

[18] `https://exoplanetarchive.ipac.caltech.edu/docs/counts_detail.html` (consulted on the 29th of May 2021)

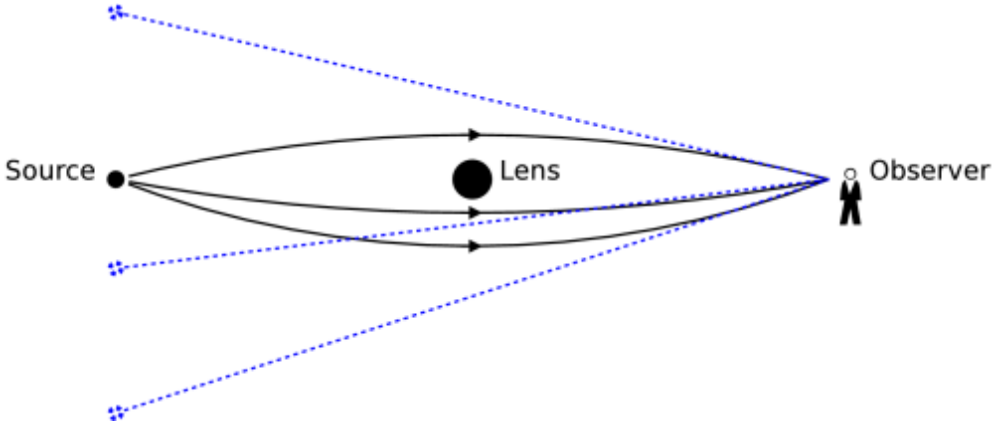

Figure 2.13: Sketch of a gravitational lensing event. Due to the bending of the photons trajectories, the source is seen at different locations than its real position by the observer. Taken from `https://en.citizendium.org/wiki/Gravitational_lens`.

If the observer-lens-source alignment is perfect (or nearly), and if the mass distribution of the lens is homogeneous and spherical, the observer will thus see the background source all around the lens as an annulus. This is called an *Einstein ring*:

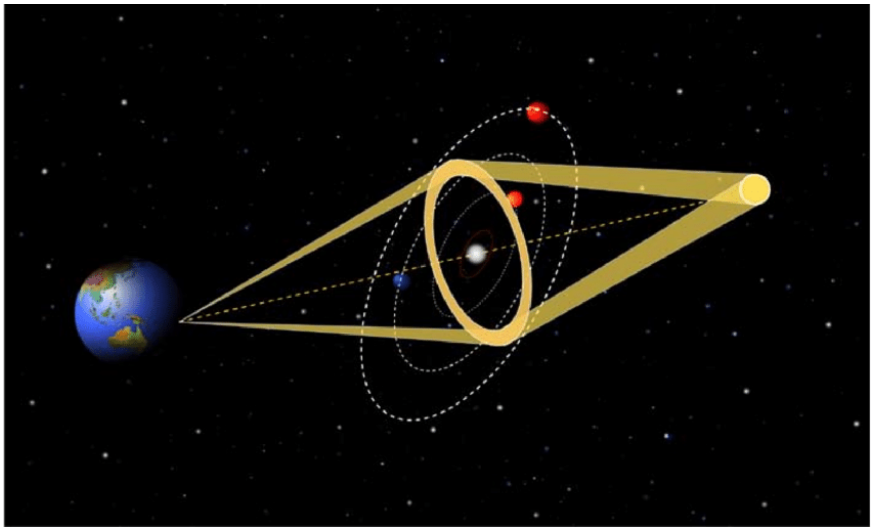

Figure 2.14: Bending of photons trajectories by a gravitational lens. If the observer, the lens and the source are perfectly aligned, and if the mass distribution of the lens is uniform and spherical, then the background source may be seen as a ring by the observer, a so-called "Einstein ring". Taken from the website `https://www.researchgate.net/figure/Formation-of-an-Einstein-ring-when-light-from-a-distant-source-star-is-bent-by-the_fig6_283118105`.

As derived in The Exoplanet Handbook ([Perryman, 2018]), p.121, the radius of this ring in the lens plane (perpendicular to the observer's line of sight), is given (both in angular distance and metric distance) by:

$$\theta_E = 1.0 \left(\frac{M_L}{M_\odot}\right)^{1/2} \left(\frac{D_L}{8 \text{ kpc}}\right)^{-1/2} \left(\frac{D_{LS}}{D_S}\right)^{1/2} \text{ mas} \tag{2.21}$$

$$R_E = 8.1 \left(\frac{M_L}{M_\odot}\right)^{1/2} \left(\frac{D_S}{8 \text{ kpc}}\right)^{-1/2} \left(\frac{D_L D_{LS}}{D_S^2}\right)^{1/2} \text{ AU} \tag{2.22}$$

where M_L and D_L are respectively the mass and the distance of the lens from the observer, D_S is the distance of the background source from the observer, and D_{LS} is the distance that separates the lens and the source.

When a telescope cannot distinguish the source images from the lens, i.e. when θ_E is smaller than its angular resolution, we talk about *gravitational microlensing*. This case notably happen when working with solar-mass lenses.

In addition to the bending of the trajectories of the photons emitted by the source, the light intensity of the source will also be increased. This light amplification, also called *magnification*, can be computed as it is done in [Tsapras, 2018] and shows, for a single lens crossing the observer's line of sight, a bell-like light curve. If the lens is a star around which is orbiting an exoplanet, this planet also being bending spacetime (but much less than its host star, due to its smaller mass), it will also act as a gravitational lens on the incident light. The duration of the magnification caused by an exoplanet when it crosses the line of sight of a telescope, due to its low mass, will be much shorter than its host star's effect.

The result of the star-planet microlensing event is a slight deviation from the single lens amplification curve. The magnification due to the star (broad peak) may last for a few months, while for a Jupiter-like planet, it reduces to several days, and only to a few hours for an Earth-like planet. The situations of a star acting as a microlens, without and with an orbiting exoplanet, are represented in Figure 2.15:

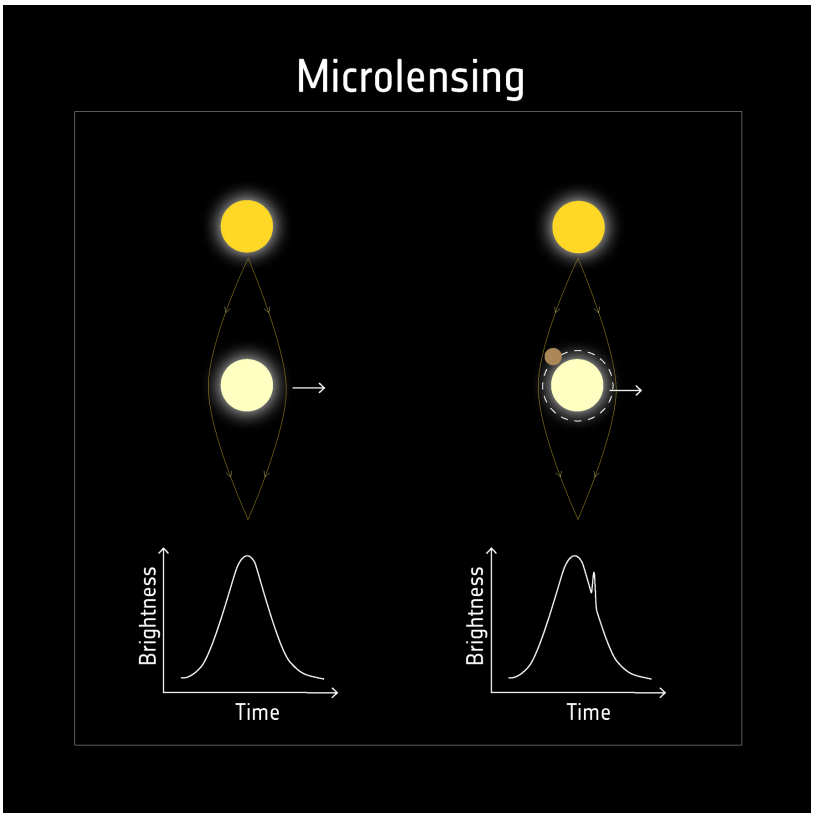

Figure 2.15: Left: microlensing event caused by a single star. Right: same situation, but with an exoplanet orbiting the lens. Taken from the website `https://www.esa.int/ESA_Multimedia/Images/2019/02/Detecting_exoplanets_with_microlensing`.

As we can see on Figure 2.15, when the exoplanet crosses the observer's line of sight, the observed brightness is slightly larger (a small, tight peak) than what it should be in the presence of the sole star acting as a lens. The careful analysis of such an event can therefore help constraining physical information about the exoplanet orbiting the stellar lens.

As explained in [Tsapras, 2018], as well as in The Exoplanet Handbook ([Perryman, 2018]), gravitational microlensing events are rare, being the fact that they need a nearly perfect alignment between the observer, the lens and the background source. Therefore, to witness such rare events, dedicated telescopes are turned toward dense stellar regions of our galaxy, and notably toward the galactic bulge.

The Milky Way's bulge is at a distance of about 8 kpc from the Earth. We can thus consider a typical source to be at a distance $D_S = 8$ kpc from the Earth, according to the references cited above. Assuming a typical lens-object to be located halfway this distance, $D_L = D_{LS} = 4$ kpc, we obtain, using Equations 2.21 and 2.22:

$$\theta_E = 0.8 \text{ mas}, \; R_E = 3.24 \text{ AU} \qquad \text{for } M_L = 0.64 \; M_\odot \text{ (a K5V star)} \tag{2.23}$$

Let us now do the same for the whole K spectral class:

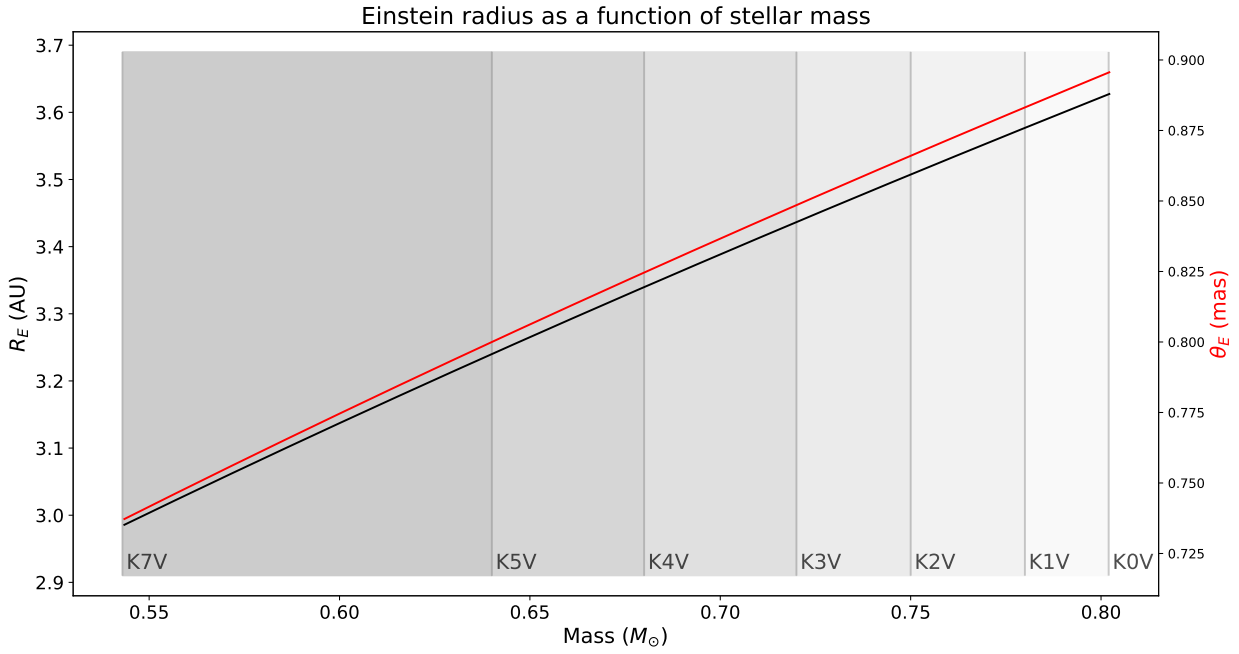

Figure 2.16: Einstein radius for a K dwarf lens located at 4 kpc and a background source at 8 kpc. The whole K spectral class is shown. Both R_E and θ_E are represented.

Such rings are too small to be imaged yet. Indeed, typical CCD imaging now have precisions of about 1 to 10 mas, as seen in the course *Introduction to exoplanetology*, chapter 3, p.37 ([Gillon, 2020]). We are therefore in the microlensing regime, as explained above.

In addition, as explained in [Barry et al., 2011], the microlensing method will be more efficient to detect planets located at a distance equal to the Einstein radius R_E from their stars, i.e. $a = 3 - 3.7$ AU for superhabitable exoplanets, as seen in Figure 2.16.
Indeed, a planetary signal appears on a microlensing light curve when one of the two images of the background source passes close to the planet, in the plane of the sky. Therefore, the magnification being the largest at R_E, the distortion caused by the planet will be larger if the planet is also at a distance R_E from its host star. From Figure 1.4 in Section 1.3, we know that superhabitable exoplanets in the optimistic habitable zones of their stars have orbital periods within 60 and 530 days, which corresponds to a semi-major axis in between 0.24 and 1.19 AU, well inside of the R_E of typical K dwarfs located at 4 kpc from the Earth. Hence, according to [Barry et al., 2011], superhabitable exoplanets should be difficult targets for gravitational microlensing surveys.

It is also worth noticing that the exoplanets discovered by the gravitational microlensing method are very far from the Earth, at distances of several kpc. Therefore, even if it is possible to detect habitable zone terrestrial planets, such as the superhabitable exoplanets we are interested in, these will probably not be the best candidates to perform further studies of their atmospheres using the next generation of observatories because they are too far away.

As it is also said in [Tsapras, 2018], if an exoplanetary candidate is discovered with this technique, there is no real possibility to observe it again later. Indeed, such gravitational microlensing events are in principle not expected before being observed, and there are poor chances to observe later another similar event implying the exact same exoplanet.

2.5 Direct imaging

The last exoplanet detection method we are going to discuss is the direct imaging method. Contrary to the previously reviewed techniques called *indirect detection methods*, this one will not detect exoplanets by analysis of some of their effects on their host stars, but rather by imaging them directly.

Up to now, 52 exoplanets were discovered, according to the Extrasolar Planet Encyclopaedia.[19]

The idea behind this technique is to try to detect the presence of a planet directly on an image. This is challenging because a star is much brighter than the light reflected by an orbiting planet. If we note F_p/F_* the ratio of the flux reflected by the planet and the flux of the star itself, from [Males et al., 2014], we can compute this ratio as

$$\frac{F_p}{F_*} = 1.818 \times 10^{-9} \left(\frac{R_p}{R_\oplus} \frac{1 \text{ AU}}{a} \right)^2 A_g \Phi(\alpha) \tag{2.24}$$

where A_g is the planet's geometric albedo and $\Phi(\alpha)$ is a function of the orbital phase angle α ($\alpha = 0$ corresponds to a full phase, a completely illuminated surface from the observer's point of view):

$$\Phi(\alpha) = \frac{\sin\alpha + (\pi - \alpha)\cos\alpha}{\pi} \tag{2.25}$$

If we assume an exoplanet to have the same geometric albedo as the Earth, $A_g = 0.3$ and if we further take the phase angle $\alpha = 90°$ (phase quadrature, half of the planet is illuminated from the observer's point of view), we therefore have $\Phi(\alpha) = \frac{1}{\pi}$, and

$$\frac{F_p}{F_*} = 1.736 \times 10^{-10} \left(\frac{R_p}{R_\oplus} \frac{1 \text{ AU}}{a} \right)^2 \tag{2.26}$$

For a superhabitable exoplanet ($R_p = 1.1\ R_\oplus$ and a corresponding to the radius of a circular orbit on the inner edge, outer edge or in the middle of the optimistic habitable zone of the host K dwarf, from Section 1.3), we thus have:

[19] `https://exoplanetarchive.ipac.caltech.edu/docs/counts_detail.html` (website consulted on the 29th of May 2021)

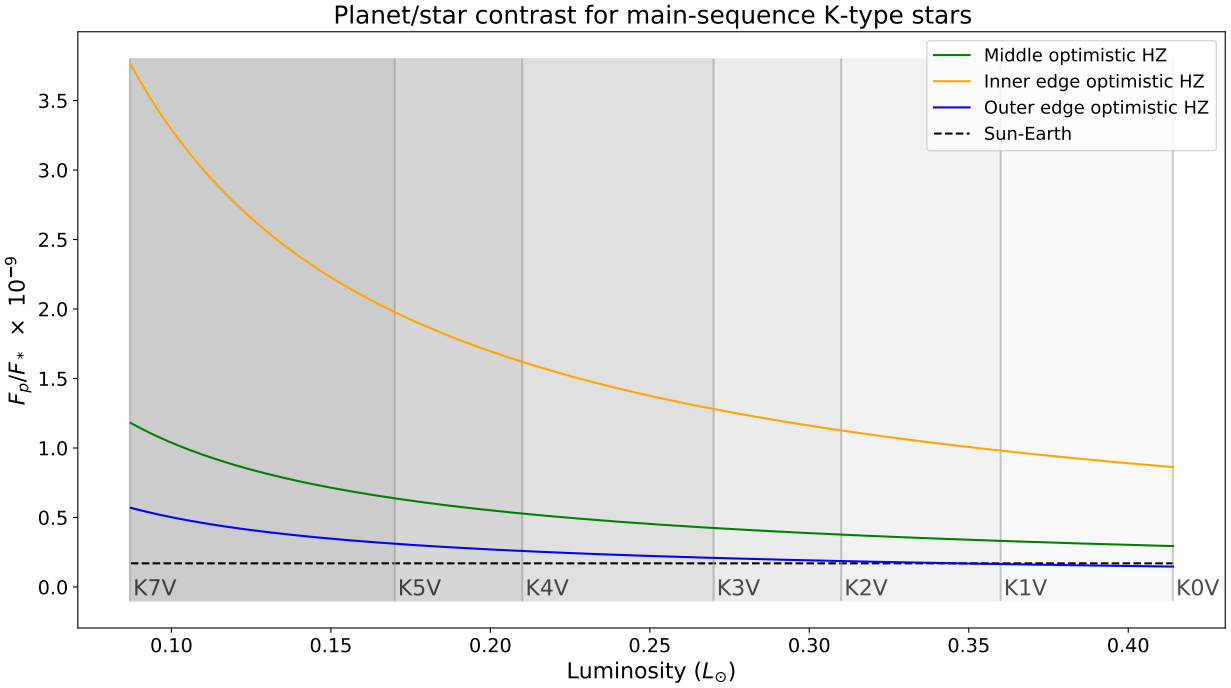

Figure 2.17: Planet/star contrast in the case of superhabitable exoplanets. The Sun-Earth case is also represented as a comparison.

As we can see in Figure 2.17, planets orbiting in the optimistic habitable zones of K dwarf stars seem easier to be detected in direct imaging than the Earth orbiting the Sun. This is in accordance with what is said in [Arney, 2019]. This is notably because K dwarfs are dimmer than G2V stars like the Sun. But even though it is in principle easier to detect a superhabitable exoplanet rather than an Earth-like one, it is important to note that the flux ratio is still tiny. The planets orbiting K dwarf stars remain faint with respect to their host stars.

Therefore, the planetary signal on an image will often be lost, flooded in the star's brightness. A good analogy to illustrate that is to try to see from a large distance a firefly flying around a bright lamp, without being able to turn off that lamp.

To increase the F_p/F_* ratio and to make the planets appear brighter on the image, the first solution is to block the stellar light by putting an opaque piece inside of the telescope. This method is called *coronagraphy*. This was first used by Bernard Lyot, a French astronomer, to study the solar corona, hence the name of the method ([Absil, 2020]). Coronagraphy is still used in today's best telescopes, along with other techniques, although it has largely evolved (they are no longer limited to opaque coronagraphs).

Another issue when trying to image exoplanets directly from ground-based telescopes is the atmospheric turbulence. It blurs the image, and creates "speckles" on it. The speckles are represented in Figure 2.18:

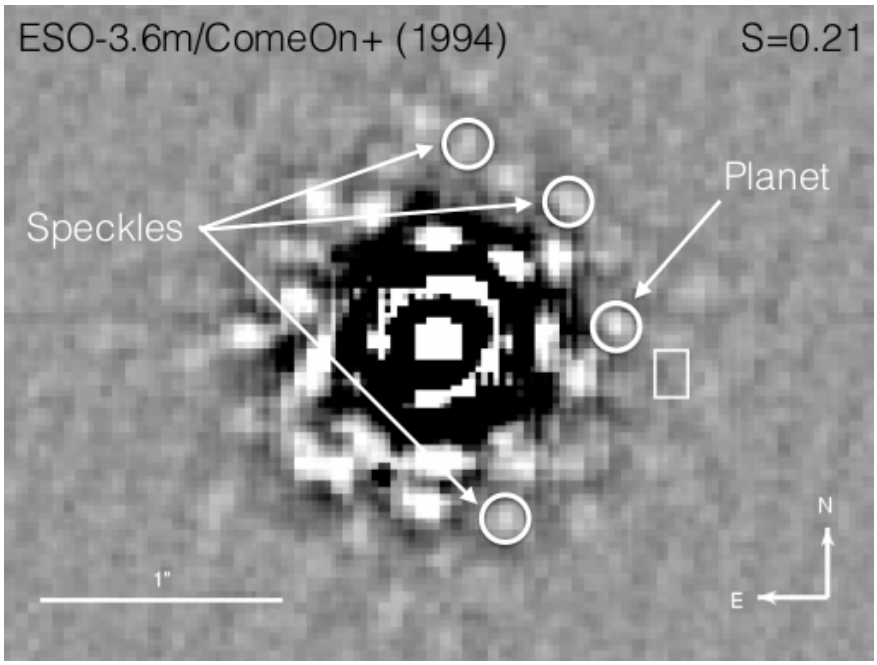

Figure 2.18: Image showing speckles and a planetary signal. We can see that both can be easily confused. Taken from Lecture 6 of the course SPAT0063-1: *Introduction to exoplanetology* ([Absil, 2020]).

These speckles can have the size of a typical exoplanet on an image, so they can lead to false detections. To enhance the quality of the images, today's ground-based telescopes are often using adaptive optics (AO) systems which basically correct the observed images for atmospheric turbulence by modifying the shapes of the mirrors of the telescope.

In addition to these challenging issues, we also have to take into account the angular separation of a planet and its host star:

$$\tan\beta \simeq \beta = \sin\alpha \frac{a}{d} \tag{2.27}$$

where a is the orbital distance of the planet, $d \gg a$ is the distance of the star from the Earth and α is the phase angle. Indeed, the presence of a coronagraph to extinguish the stellar light on an image will give the telescope a so-called inner working angle (IWA). It is defined as:

$$\text{IWA} = \frac{N\lambda}{D}$$

where D is the telescope diameter, λ is the wavelength of the observed light and N is an index that may vary for different instruments. The IWA roughly corresponds to the minimum angular separation at which the telescope can detect a planet. If the angular separation of the planet and its host star is smaller than the IWA of the telescope, the planet's signal on the image will therefore be lost, blocked like the stellar light by the action of the coronagraph. It won't therefore be possible to detect and confirm the presence of the exoplanet. So, first of all, to be detectable through the direct imaging method, exoplanets must have large enough angular separations with respect to their host stars.

Let us compute the angular separations in the case of superhabitable exoplanets (still using the orbital distances corresponding to the middle, inner and outer edges of the optimistic

habitable zone, for the whole class of K dwarf stars) for distances ranging between 1 and 10 pc, as in Section 2.3 concerning the astrometry detection method, and with a phase angle $\alpha = \pi/2$ corresponding to the maximum angular separation (at least in the same orbital configuration as for a transit, i.e. $i = 90°$ and $e = 0$):

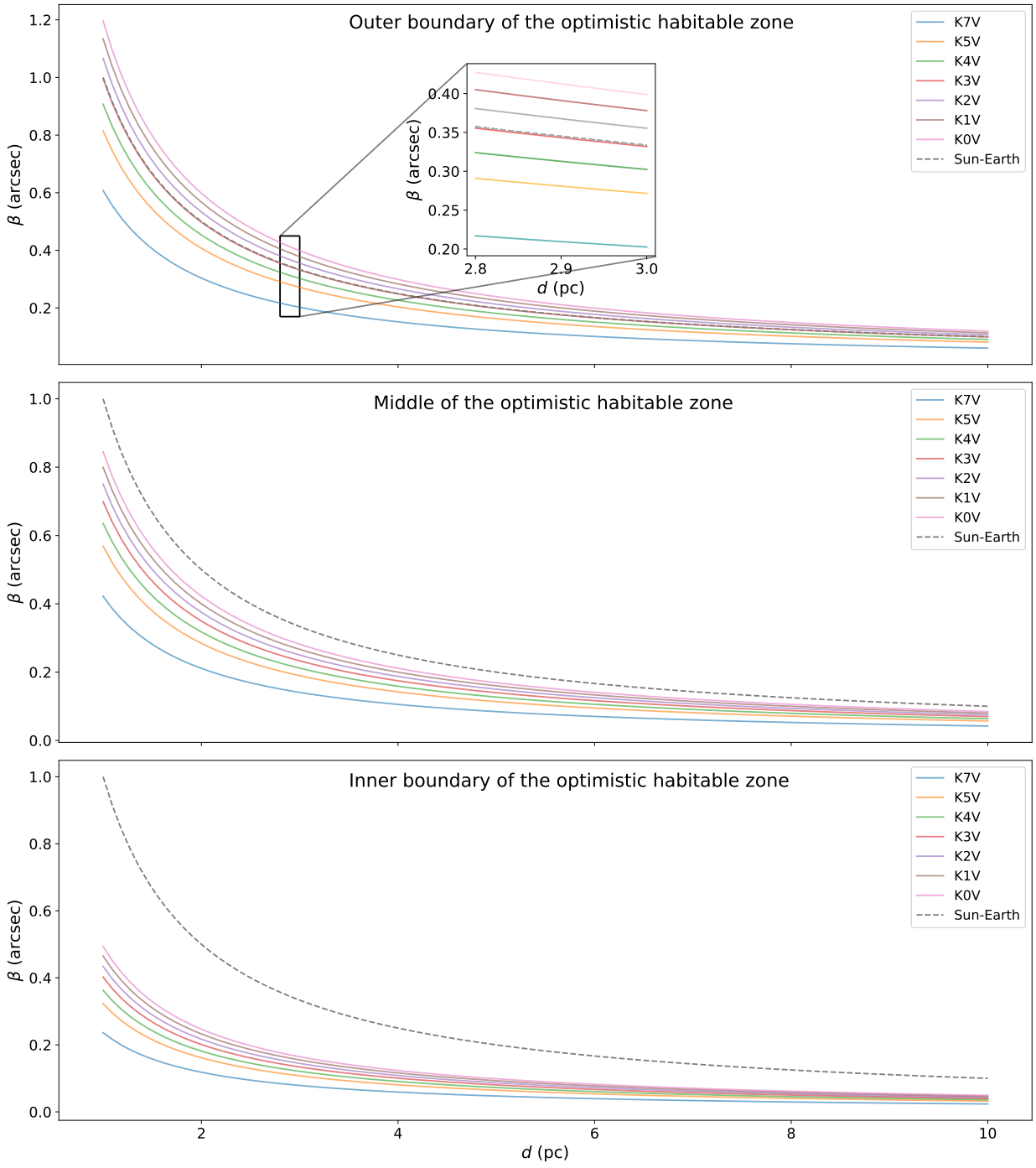

Figure 2.19: Angular separation of a superhabitable exoplanet located on the outer edge, in the middle or on the inner edge of the optimistic habitable zone of a K dwarf star. The whole K spectral class is represented. The Sun-Earth case is also shown as a comparison.

The effective temperatures of late K dwarfs being lower than that of early ones, their habitable zones are closer. Therefore, the angular separation between a habitable zone exoplanet and a K dwarf will be larger for a K0V than for a K7V star. We also see that the angular

separation for the Sun-Earth system is always larger than for superhabitable exoplanets, except for those orbiting on the outer edge of the optimistic habitable zone of a K0V - K2V star.

We can also combine both planet/star contrast and angular separation considerations in a single plot. This is done in Figure 2.20. Here the angular separation is computed for stars located at a distance of 10 pc:

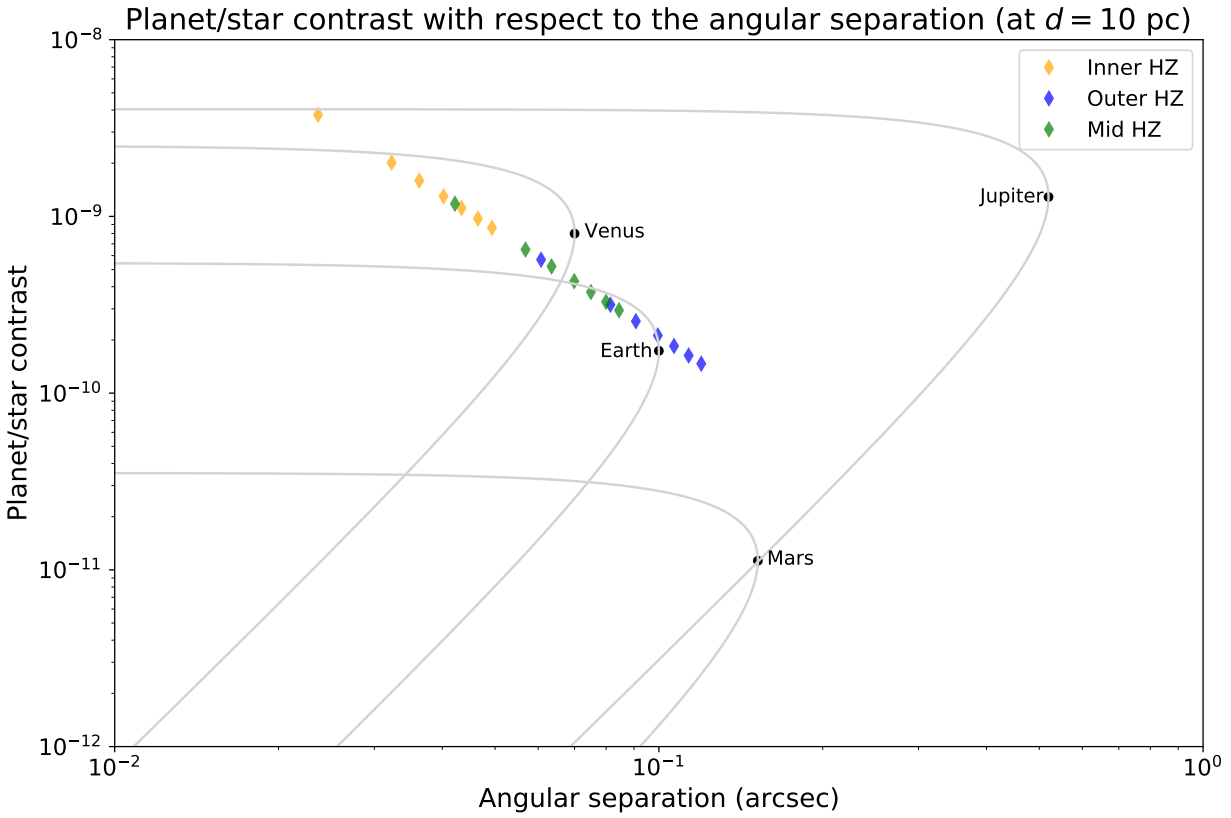

Figure 2.20: Planet/star contrast as a function of the angular separation (for stars at a distance of 10 pc). The orange, green and blue markers represent superhabitable exoplanets ($R_p = 1.1\ R_\oplus$) around K dwarf stars, on the inner edge, in the middle and on the outer edge of their optimistic habitable zones, respectively. The grey curves are showing the variation of the location of the Solar System's planets in the graph, depending on the phase angle α. The black dots correspond to a phase angle $\alpha = \frac{\pi}{2}$, i.e. a quadrature phase.

Some planets of the Solar System are also represented, to have comparison points. This figure can be compared with [Dalcanton et al., 2015]:

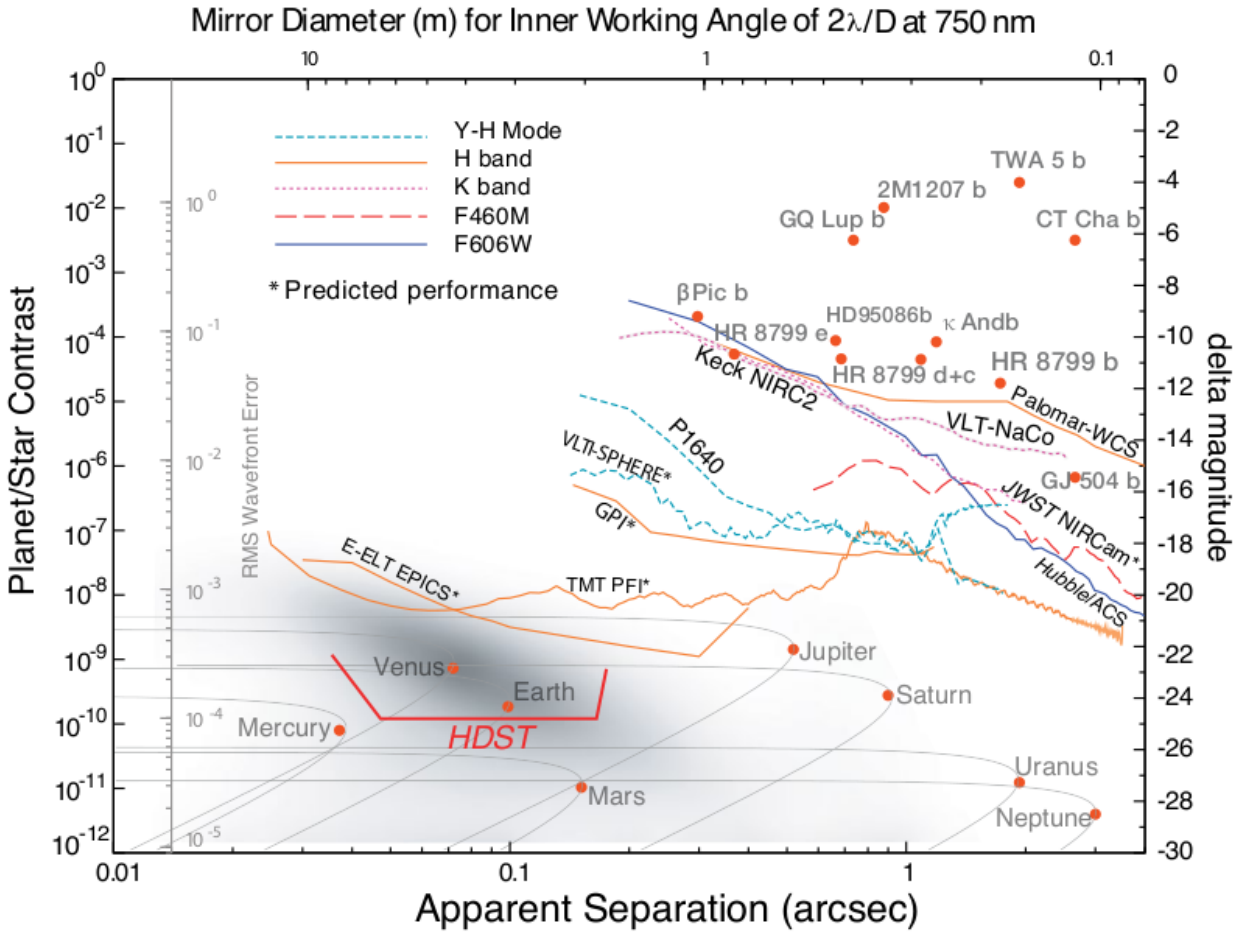

Figure 2.21: Planet/star contrast as a function of the angular separation, at a distance of 10 pc. They represented performance curves of several current and future instruments. HDST stands for High-Definition Space Telescopes, i.e. the next generation of space observatories that will perform high-definition direct imaging. Taken from [Dalcanton et al., 2015], p.18.

In Figure 2.21, they represented in the lower left corner a grey cloud that is the predicted planet/star contrasts and angular separations of habitable exoplanets orbiting around main-sequence F, G and K-type stars. As we can see, the superhabitable planets we represented in Figure 2.20 are within this grey cloud in Figure 2.21. In their plot, [Dalcanton et al., 2015] also represented the (predicted) performances of several (next generation) instruments, as well as some direct imaged exoplanets.

What we can directly infer from this is that current instruments are not able to perform direct imaging on habitable terrestrial exoplanets orbiting K dwarf stars. Not only their angular resolutions are insufficient to resolve a superhabitable planet on its orbit, but the minimum planet/star contrasts they can achieve are still too large. (a contrast threshold of 10^{-10} is required). However, we can notice that the Extremely Large Telescope (ELT) and Thirty Meter Telescope (TMT) will fulfil the angular resolution requirement, although the minimum contrasts they will achieve are still too high for our superhabitable exoplanets. This will be deeper discussed in the next chapter, as well as other future missions.

Although direct imaging of exoplanets is not possible at the time being, as we will see in Chapter 3 this will become more realistic with the next generations of space-based tele-

scopes and instruments which may be able to overcome the contrast limitation of 10^{-8} due to the atmosphere of the Earth, to reach the required contrast of 10^{-10}, as said in [The LUVOIR Team, 2019] (page 3-12, subsection 3.2.2).

However, this exoplanet detection method has several useful aspects:

- The shape of the orbit of a direct imaged exoplanet can be determined directly from follow-up observations. This can then be used to compute the mass of the host star, for instance.
- As for the transit method, direct imaging allows us to study the chemical compositions of exoplanetary atmospheres. Indeed, because we are able to directly see the exoplanets (by their reflected light), we can decide to analyze only the photons coming from the planets, regardless of the photons directly coming from the host stars. These spectroscopic observations can then give us exoplanetary spectra, in which we may find the presence of some spectral features related to different molecular species of the exoplanetary atmospheres.

so it would be a great opportunity for exoplanets investigations if we were able to use this method on habitable terrestrial planets.

Summary of the chapter

We have seen that some exoplanets detection methods are more promising than others to find superhabitable exoplanets.

First, the transit and direct imaging methods are special, and will be massively used in future observatories as we will see in the next chapter, because both can be used to study exoplanetary atmospheres. Therefore, for the goal of finding life elsewhere, both are quite important and useful. Nevertheless, these are not perfect either. Indeed, while transits of superhabitable exoplanets may already be detected now (for instance in TESS or CHEOPS light curves), the long orbital period of such a planet is quite problematic since more than one transit are needed to correctly characterize a system. Concerning direct imaging of superhabitable exoplanets, it is not achievable yet. However, if we were able to perform it, it would not be inhibited by the long orbital periods of these planets, so it seems better than the transit method in that sense, but it is more restricted in the range of distances in which it may study stars (angular separation inversely proportional to the distance), contrary to the transit method.

Then, the radial velocity detection of superhabitable exoplanets is already possible with the echelle spectrograph ESPRESSO mounted on the VLT, which used along with the transit method may constrain both the mass and the radius of an exoplanet, which is useful to characterize its density (type of planet: rocky, gaseous, icy giant, etc.). It could help to increase the length of the list of priority candidates for atmospheric studies with next generation telescopes.

Gravitational microlensing may in theory be possible. However, in the purpose of finding exoplanets to study their atmospheres and to possibly find life, this method will certainly not be the best. Indeed, exoplanets detected via this technique are very far from the Earth

(several kpc). And scheduling follow-up operations is additionally nearly impossible. Moreover, superhabitable exoplanets are well inside of the Einstein radii R_E of their host stars, hence making them difficult to detect with this method.

Finally, the astrometric method to detect superhabitable exoplanets is not feasible now and may still be tricky in the future, due to the tiny astrometric signatures, even at a few parsecs from the Earth, for such exoplanets.

Chapter 3

Future missions

As announced, we will now discuss some planned missions that will detect exoplanets, among other things. We will see that most of the missions will be performing both transit and direct spectroscopy in the purpose of studying exoplanetary atmospheres and finding, if possible, biosignatures suggesting the presence of life.

3.1 Near-future missions

In this first section, we are going to discuss some missions planned for this decade mainly, such as JWST, PLATO and Roman for space-based telescopes, and TMT, GMT and ELT for ground-based observatories.

3.1.1 James Webb Space Telescope (JWST)

The James Webb Space Telescope ([Gardner et al., 2006]) should be launched in Autumn 2021[1] on a halo orbit around the Lagrange point L2 of the Sun-Earth system, located at a distance of roughly 1.5×10^6 km in the nightside of the Earth. It is a 6.5-m diameter telescope made of 18 hexagonal tiles and cooled below 50 K that will essentially observe in the infrared domain. It will cover 100% of the sky in one year, with 30% observed for more than 197 contiguous days and a continuous observation around both ecliptic poles.

Among other things, it will study the formation and evolution of planets and their atmospheres. It will perform the transit method and notably transit spectroscopy, as described in Section 2.1, to characterize the structures and chemical compositions of exoplanetary atmospheres and eventually to detect traces of life in their spectra, the so-called biosignatures. It will also use the direct imaging method on nearby and bright stars, but only for giant planets, well separated from their host stars, since these are easier to detect via this method (their contrasts are higher as well as their angular separations).

Observing in the infrared is a good choice since this electromagnetic domain is where exoplanets exhibit most of their spectral features. Indeed, the kind of spectral features that could be observed in atmospheres of terrestrial exoplanets orbiting K dwarfs is represented in Figure 3.2:

[1]Source: `https://sci.esa.int/web/jwst/-/45759-fact-sheet`

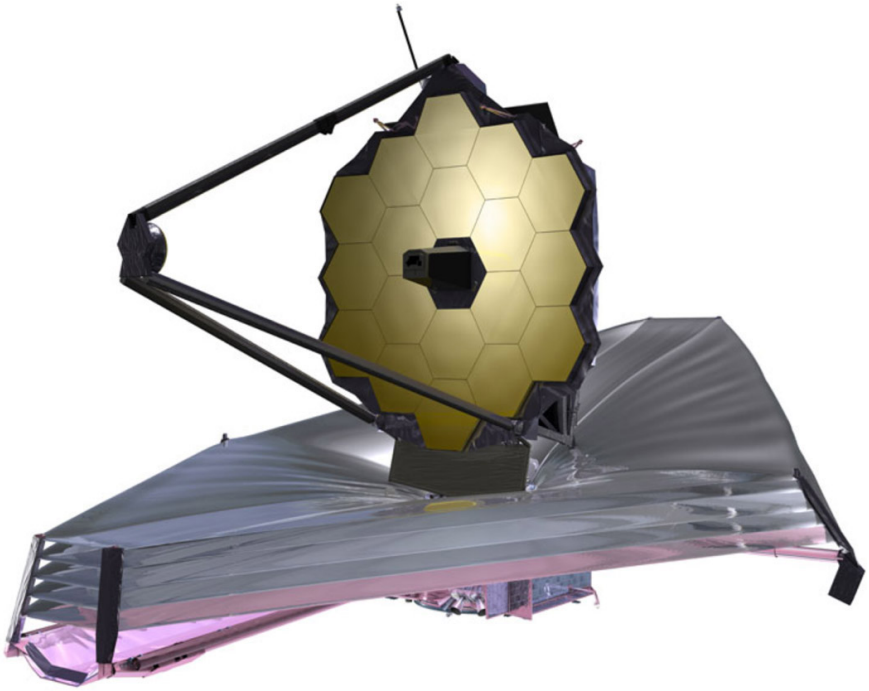

Figure 3.1: The James Webb Space Telescope. Taken from `https://spie.org/news/3570-optical-alignment-of-james-webb-space-telescope-breaks-new-ground?SSO=1`.

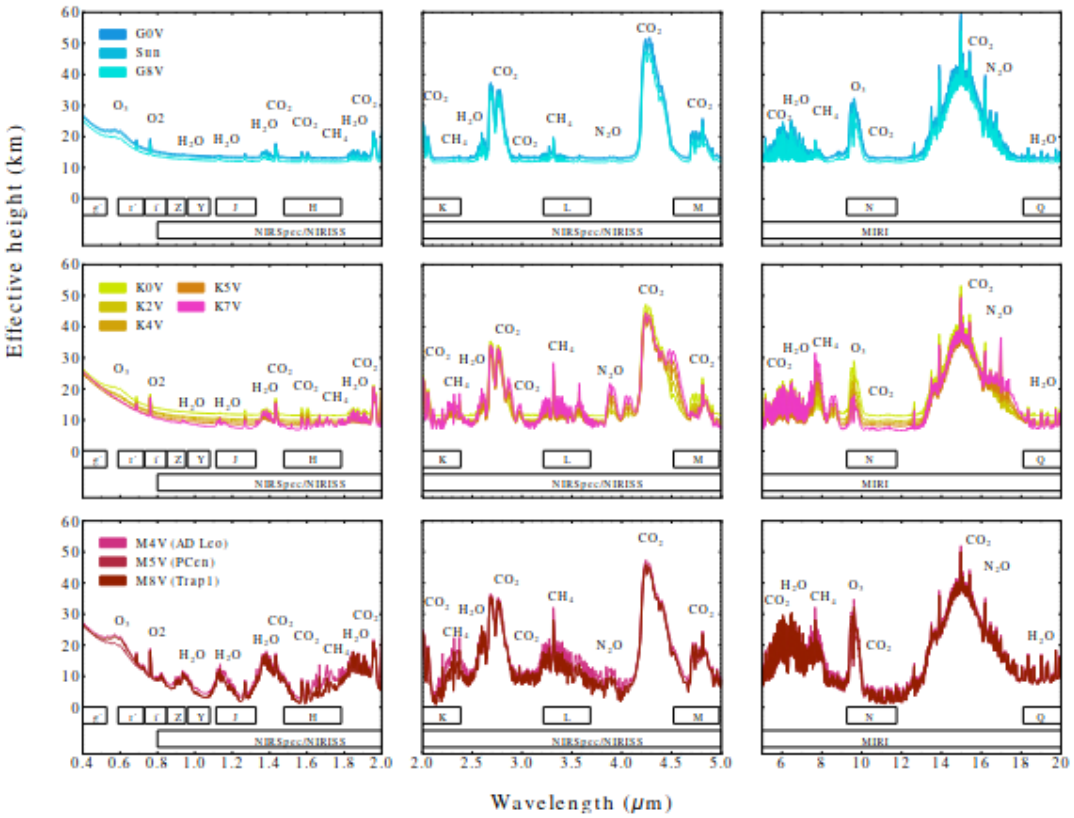

Figure 3.2: Simulated transmission spectra of an Earth-like planet orbiting around G, K and M dwarfs. The spectral resolution is $R = 700$. We can see the increase of spectral features for K and M dwarfs with respect to G-type stars. Taken from [Kaltenegger and Lin, 2021].

The JWST will be equipped with four science instruments[2]:

- **NIRSpec**: The Near-InfraRed Spectrograph is a multi-object spectrograph. It will cover wavelengths from 0.6 μm to 5.0 μm. It will have three spectroscopic observing modes with spectral resolutions $R \sim 100$, 1000 and 2700.
- **NIRCam**: The Near-InfraRed Camera is an instrument developed for imaging, coronagraphy and wide-field slitless spectroscopy. It will notably be used to align and phase correctly the tiles of the principal mirror of the telescope. It will cover wavelengths in between 0.6 μm and 5.0 μm.
- **FGS/NIRISS**: The Fine Guidance System and Near-InfraRed Imager and Slitless Spectrograph will provide imaging and spectroscopic capabilities. It has a spectroscopic wavelength range from 1.0 μm to 2.5 μm. Its spectral resolutions will be $R \sim 150$ and 700 at 1.4 μm for the wide-field and single object slitless spectroscopy modes respectively.
- **MIRI**: The Mid-InfraRed Instrument will make imaging, spectroscopic and coronagraphic observations for wavelengths from 5 μm up to 28.3 μm. Its spectral resolutions will be $R \sim 100$ and 3000.

As said in [Barstow et al., 2015], the JWST should be able to reach a photometric precision of 10 - 100 ppm, therefore enough to detect superhabitable exoplanets.

With the spectral resolutions of its instruments, the JWST should be able to detect absorption features of O_2, CO_2, CO, CH_4, H_2O, Na and K in exoplanetary spectra, hence opening the possibility to pinpoint biosignatures in their atmospheres. However, spectral features in transmission spectra of habitable zone Earth-like planets, such as the absorption bands visible in Figure 3.2, are tiny. This is shown in Figure 3.3:

[2]Sources: `https://sci.esa.int/web/jwst` and `https://jwst-docs.stsci.edu/`

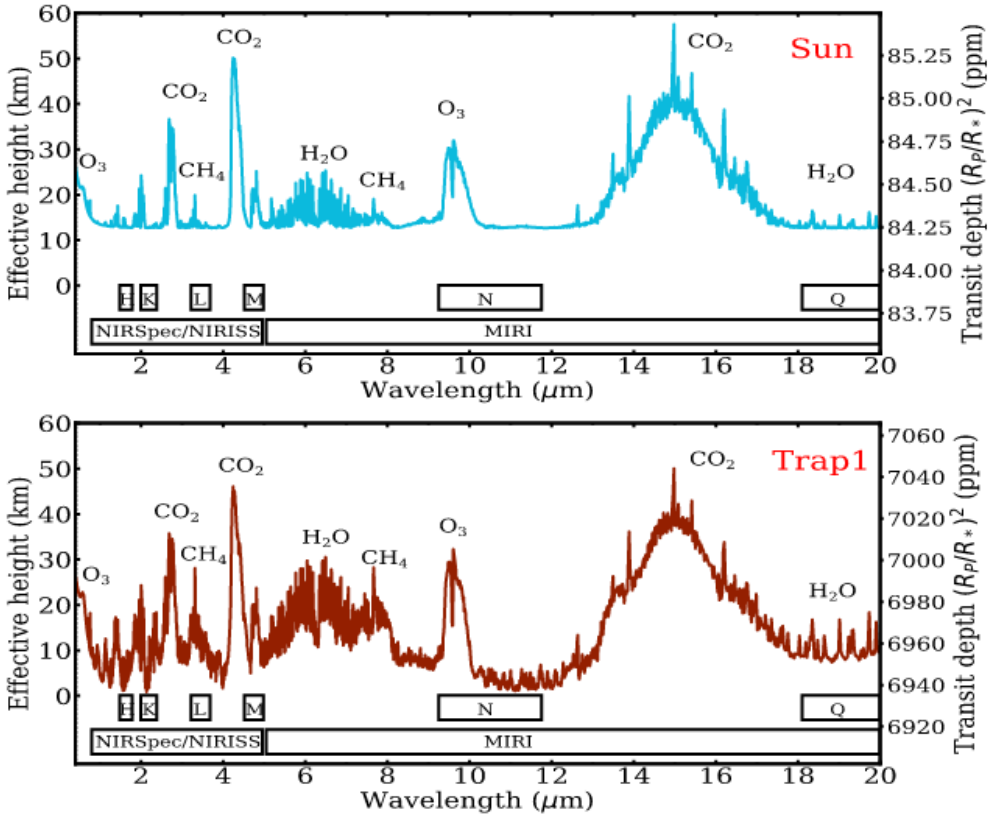

Figure 3.3: Transmission spectra of an HZ Earth-like planet orbiting a Sun-like star and a M8V star (TRAPPIST-1) respectively. The y-axis (right-hand scale) represents the transit depth. Taken from [Kaltenegger and Lin, 2021].

As explained in [Beichman and Greene, 2018], these spectral features would have, for HZ terrestrial planets around K dwarfs, relative transit depths of about 10 ppm or less. Therefore, a strong signal-to-noise ratio (SNR) is needed to be able to detect unambiguously such features. Nevertheless, for the latest M dwarfs (such as TRAPPIST-1), we can see in Figure 3.3 that the relative transit depths of the spectral features are larger. Some features such as NIR CH_4 bands can have relative transit depths of about 50 ppm, as said in [Gillon et al., 2020].

A comparison of some atmospheric spectral features of HZ terrestrial planets around the Sun, K or M dwarfs is shown in Figure 3.4:

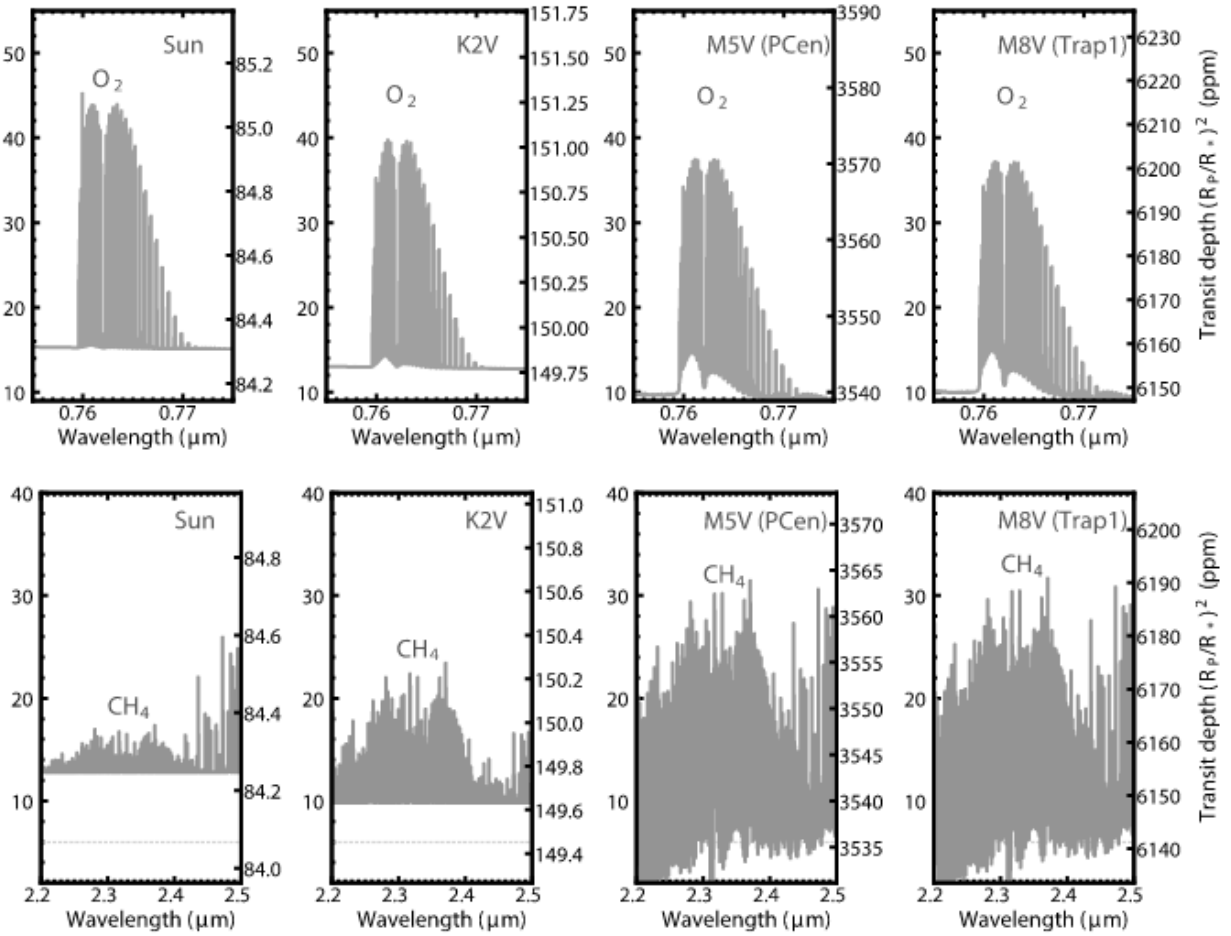

Figure 3.4: High-resolution transmission spectral features of HZ Earth-like planets orbiting around the Sun, a K2V, a M5V and a M8V star. For a same spectral feature, we can see the large increase of the relative transit depth for each M dwarf with respect to the Sun or the K2V star. Taken from [Kaltenegger and Lin, 2021].

We clearly see in Figure 3.4 that the relative transit depth of a same atmospheric spectral feature is much larger for planets orbiting late M dwarfs than around hotter stars.

In addition, as explained in [Gillon et al., 2020] HZ planets orbiting M dwarfs have much shorter orbital periods than HZ planets around K dwarfs, so it is also possible to stack more transit observations in order to increase the SNR.

Hence, the JWST may be able to detect biosignatures of habitable exoplanets around late M dwarfs, but this will be much more challenging as far as HZ planets orbiting K dwarfs (such as superhabitable exoplanets) are concerned.

Concerning the direct imaging method, as said above, it will only focus on giant planets around nearby bright stars. Indeed, superhabitable planets show contrasts on the order of 10^{-9}, while JWST will be able to reach contrasts of 10^{-6} at best.

3.1.2 PLAnetary Transits and Oscillations of stars (PLATO)

PLATO[3] is an ESA mission. It is planned to be launched in 2026, on a Lissajous orbit about the Lagrange point L2 of the Sun-Earth system, such as the JWST.

It will be equipped with 26 cameras, 2 said "fast" and the 24 others said "normal", and will perform high-precision photometric observations for 10% to 50% of the sky.

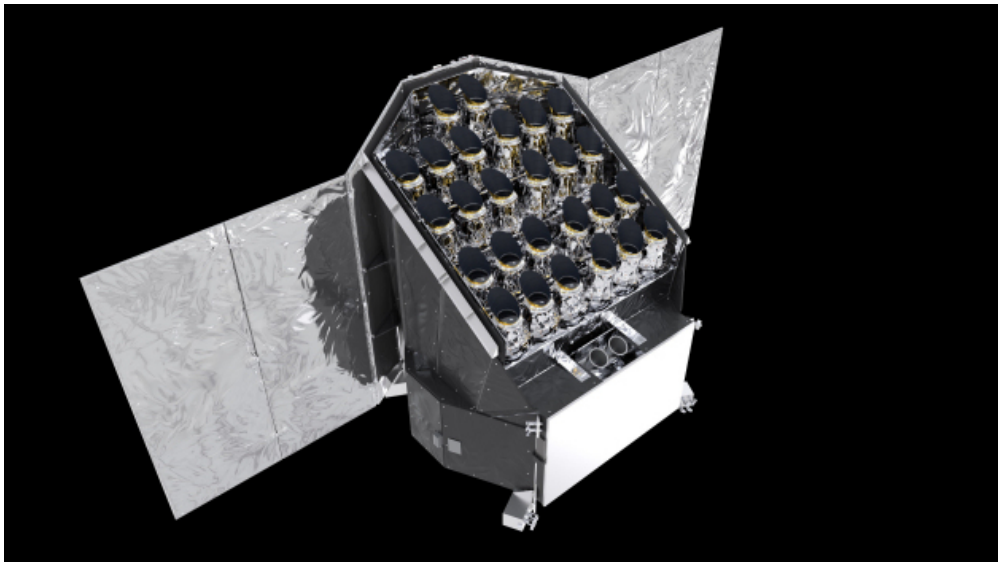

Figure 3.5: The PLATO telescope. Taken from `https://sci.esa.int/web/plato/display-page-cl-display-page-content-long/-/asset_publisher/33250/content/artist-s-impression-of-plato-1`.

Its main goal will be to detect and characterize terrestrial exoplanets orbiting bright Sun-like stars ($m_V \leq 11$), and notably to determine their radii. It will observe in the visible wavelengths, hence allowing ground-based follow-up operations of the discovered exoplanets, being the fact that the atmosphere of the Earth is mostly transparent to visible radiation. Its photometric precision should reach 34 ppm for solar-like stars with $m_V \leq 11$ in one hour. It will also perform asteroseismology to determine the radii, masses and ages of stars.

As seen in the Definition Study Report[4], it will be able to detect planets orbiting around M and K dwarf stars only beyond their snow lines, which is, by definition, outside of the optimistic habitable zone. So, it may not be that much useful in the specific case of superhabitable exoplanets, but it still promises to be very interesting.

3.1.3 Thirty Meter Telescope (TMT)

The Thirty Meter Telescope (TMT)[5] will be a 30-m diameter ground-based telescope. Its principal mirror will be composed of 492 hexagonal tiles of 1.44 m, and will have a collecting area of 644.2 m^2. In principle, it should be built at the Mauna Kea observatory in Hawaii, but it is not yet sure. If the construction in Hawaii is not allowed, the other plan will be the La Palma observatory in Spain. In any case, it will be a northern hemisphere telescope

[3]Sources: `https://sci.esa.int/web/plato` and `https://platomission.com/`
[4]Source: `https://platomission.files.wordpress.com/2018/05/plato2-rb.pdf`
[5]Source: `https://www.tmt.org/`

by opposition with the Extremely Large Telescope and Giant Magellan Telescope presented hereafter. It should start its operations in 2027, for an initial lifetime of about 50 years.

Figure 3.6: 3D representation of the Thirty Meter Telescope. Taken from `https://www.tmt.org/image/50`.

It will observe different kinds of objects in the sky, from galaxies to exoplanets, covering wavelengths from the optical to the mid-infrared domains. Concerning exoplanets, it will perform the radial velocity, transit and direct imaging detection methods.

At first light, it will be equipped with four instruments:

- **NFIRAOS**: The Narrow Field InfraRed Adaptive Optics System will provide adaptive optics to the telescope for better observations. Other instruments such as IRIS and MODHIS presented hereafter, will be connected to it to have better quality measurements.
- **IRIS**: The InfraRed Imager and Spectrograph will cover wavelengths from 0.8 μm up to 2.4 μm. It will be made of an integral field spectrograph with spectral resolutions $R \sim 4000$, 8000 and 10000 depending on the observing mode, and an imager with an absolute astrometric precision of 2 mas and a differential astrometric precision of 50 μas with an exposure of 100 seconds, far from enough to detect superhabitable exoplanets via the astrometry method, as it was discussed in Section 2.3.
- **WFOS**: The Wide Field Optical Spectrograph will provide imaging and spectroscopy in the range of wavelengths 0.31 - 1.0 μm (from near-UV to near-IR). Its spectral resolution will be $R \sim 1500$. It will mainly be used to study very distant objects in the Universe, such as quasars.
- **MODHIS**: The Multi-Object Diffraction-limited High-resolution Infrared Spectrograph will be able to obtain accurate spectra of up to 8 targets in a 5-arcsec field of view simultaneously, with a spectral resolution $R \sim 100000$. It will be used to detect exoplanets via the radial velocity method and to characterize their atmospheres with transit and direct spectroscopy. Its radial velocity precision will be below 1 m s^{-1} with a goal at 30 cm s^{-1}.

Another bunch of second generation instruments will arrive later. Among these, a currently conceptual one is the Planetary System Instrument (PSI). It would be an extreme adaptive optics (ExAO) instrument able to reach contrasts of 10^{-8} (10^{-9} maximum) with an inner working angle of 10^{-2} arcsec and an outer working angle of 1 arcsec. This could therefore nearly reach the field of superhabitable exoplanets, as seen in Figures 2.20 and 2.21.

3.1.4 Giant Magellan Telescope (GMT)

The Giant Magellan Telescope (GMT)[6], another of the giant ground-based telescopes of this decade, will start its operations in 2029 at the Las Campanas observatory in Chile for an initial lifespan of about 50 years. It will be a 24.5-m diameter telescope, with its principal mirror segmented in seven smaller 8.4-m diameter circular mirrors. The total collecting area will be 368 m^2.

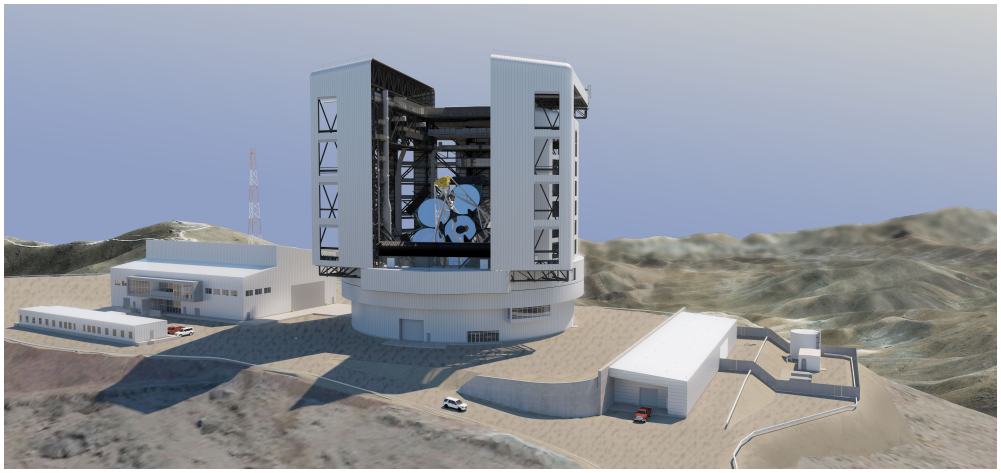

Figure 3.7: The Giant Magellan Telescope. Taken from `https://www.gmto.org/gallery/3d-renderings/#/lightbox&slide=4`.

Its secondary mirror will be equipped with many actuators, hence providing efficient adaptive optics to increase the quality of the observations.

To observe exoplanets, the GMT will perform photometry, radial velocity and direct imaging methods. For this purpose, different science instruments will be mounted on it:

- **G-CLEF**: The GMT Consortium Large Earth Finder is an echelle spectrograph with a high spectral resolution ($R \sim 25000 - 120000$) which will measure light in the optical domain, between 350 nm and 950 nm. It will be used for radial velocity measurements and should reach a RV precision of 10 cm s^{-1} for a $m_V \sim 9$ star in about 20 minutes (40 minutes for a $m_V \sim 10.5$ star).

  It will observe all the HZ Earth-sized exoplanets around main-sequence sun-like stars with $m_V < 11$ detected by PLATO.

- **GMACS**: The GMT Multi-object Astronomical and Cosmological Spectrograph will only focus on faint and far away objects such as galaxies, not exoplanets, in the wavelength range 320 - 1000 nm.

[6]Sources: `https://www.gmto.org/` and chapter 2 of the GMT Science Book 2018 `https://www.gmto.org/wp-content/uploads/GMTScienceBook2018.pdf`.

- **GMTIFS**: The GMT Integral Field Spectrograph will observe in the wavelength range 0.9 - 2.5 μm with spectral resolutions $R \sim 5000$ and $R \sim 10000$. Concerning exoplanets, it will study their formation processes, but not their atmospheres.
- **GMTNIRS**: The GMT Near-IR Spectrograph will analyze light in the range of wavelengths 1.1 - 5.4 μm. Its goal will notably be to study the atmospheric chemistry and internal structures of exoplanets with spectral resolutions $R \sim 50000 - 100000$.

With its spectral resolutions, the G-CLEF instrument should be able to detect the presence of biosignature molecules such as O_2 (strong absorption features in the visible domain) in atmospheres of close ($d \leq 8$ pc) Earth-sized habitable exoplanets around M3V or cooler main-sequence stars, as said in [Rodler and López-Morales, 2014]. As explained in Subsection 3.1.1 concerning the JWST, HZ planets orbiting earlier stars (K-type for instance) present tiny atmospheric spectral features (relative transit depths on the order of 1 to 10 ppm) and quite long orbital periods, so it takes a lot of time to stack enough transits to significantly increase the SNR in order to be able to detect the absorption bands in the transmission spectra. So here again, biosignatures in atmospheres of superhabitable exoplanets may be out of reach.

3.1.5 Extremely Large Telescope (ELT)

The Extremely Large Telescope (ELT)[7] is an ESO project. With its 39-m diameter principal mirror, it will be one of the three giant ground-based telescopes of the decade with TMT and GMT, and actually the largest one. Its main mirror will be made of 798 hexagonal segments, providing an enormous total light collecting area of 978 m^2. It is currently under construction at Cerro Armazones, in the Atacama desert in Chile, and should be ready for its first light in 2025. Hence, it should be the first of the three giant telescopes to be ready for observations. Its initial lifespan is set at more than 30 years.

Like TMT and GMT, it will observe different things in the Universe, and in particular exoplanets. Its observed wavelengths will be in the optical, near and mid-infrared domains. It will use radial velocity, transit and direct imaging methods to detect exoplanets, and also spectroscopy to analyze and characterize their atmospheres.

It should be able to detect habitable zone rocky exoplanets via radial velocity and transit methods, and then to direct image some of these planets, separating their reflected photons from those of their host stars, to determine their properties and to look for O_2, CO, CO_2, CH_4, H_2O and NH_3 spectral features in their spectra.

To achieve its science goals, the ELT will be equipped with several instruments. Four of them will be used immediately after first light (first generation instruments):

- **HARMONI**: The High Angular Resolution Monolithic Optical and Near-infrared Integral field spectrograph will provide measurements in the range 0.47 - 2.45 μm, with spectral resolutions $R \sim 3500$, 7500 and 18000 in the near-infrared, and $R \sim 3500$ in the optical domain. It will be able to characterize giant exoplanets on orbits with semi-major axes going from 1 to 40 AU.

[7]Source: `https://elt.eso.org/`

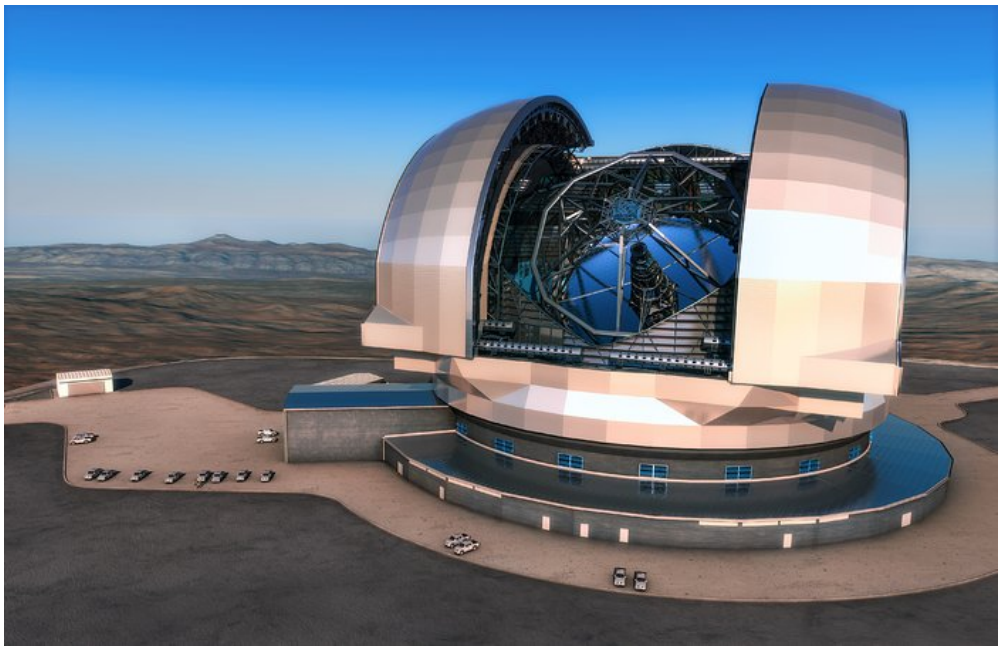

Figure 3.8: The Extremely Large Telescope. Taken from `https://www.eso.org/public/images/eso1440e/`.

- **MICADO**: The Multi-AO Imaging CAmera for Deep Observations will make high-resolution images in the range 0.8 - 2.4 μm. Its relative astrometric precision should be about 50 μas, with a 10 μas goal, as it was the case for the Gaia mission. The minimum contrasts MICADO should reach are 10^{-4} at 100 mas and 10^{-5} at 500 mas, clearly insufficient to detect superhabitable exoplanets. It will also provide wide-band spectroscopy with $R \sim 10000$ and 20000.
- **METIS**: The Mid-infrared ELT Imager and Spectrograph will be made of an integral field spectrograph and a high-contrast imager that will provide both coronagraphy and long-slit spectroscopy. It will cover wavelengths ranging from 3 to 13 μm for the imager, and 3 to 5 μm for the integral field spectrograph. The spectral resolutions of the imager will be $R \sim 400$, 1500 and 1900 for the L, M (3 - 5 μm) and N (7.5 - 13 μm) bands respectively, while it will reach $R \sim 100000$ for L and M bands with the integral field spectrograph. As seen in [Brandl et al., 2021], it should be able to reach contrasts of about 10^{-5} at $5\lambda/D$.
- **MAORY**: The Multi-conjugate Adaptive Optics RelaY will yield adaptive optics to other ELT instruments such as MICADO, to reach higher quality images. It will therefore only play the role of a support instrument, rather than an observing one.

Two second generation instruments are also proposed:

- **HIRES**: The HIgh REsolution Spectrograph will make observations in wavelengths ranging from 0.55 μm to 1.80 μm, with a goal in the range 0.33 - 2.44 μm. It will provide an exceptional spectral resolution $R \sim 100000 - 150000$, able to search for biosignatures in the atmospheres of Earth-sized exoplanets.
- **MOSAIC**: It will be a Multi-Object Spectrograph (MOS) working in the range of wavelengths 0.47 - 1.80 μm, with a spectral resolution in between $R \sim 5000$ and 20000,

depending on the adopted observing mode. It will observe the light from several types of objects simultaneously, but will mainly be used for very distant targets.

Another ELT instrument still to be confirmed is the Planetary Camera and Spectrograph (PCS), which was previously called Exo-Planet Imaging Camera and Spectrograph (EPICS). As explained in [Kasper et al., 2021], this instrument would be designed to reach contrasts of 10^{-8} at angular separations of 15 mas, and 10^{-9} at 100 mas. From Figures 2.20 and 2.21, we can see that this could be nearly enough to image superhabitable exoplanets. If this instrument is confirmed and reaches its goals, it would therefore be very interesting for superhabitable exoplanets surveys.

As for the GMT, we know from [Rodler and López-Morales, 2014] and [Lopez-Morales et al., 2019] that the ELT will be able to detect some biosignatures in the atmospheres of HZ Earth-like planets orbiting late M dwarfs (M3V or later) either through transit or direct spectroscopy, but not for K dwarfs and superhabitable exoplanets which show spectral features with too small amplitudes in their atmospheres.

3.1.6 Nancy Grace Roman Space Telescope

The Nancy Grace Roman Space Telescope[8] is a NASA mission, previously known as the Wide Field InfraRed Survey Telescope (WFIRST). It should be launched in 2025 on an orbit around the Lagrange point L2 of the Sun-Earth system, such as JWST and PLATO described above. It will have a 2.4-m diameter primary mirror. Its initial lifetime is set to 5 years, but it could obtain 5 more if needed and if its results are convincing.

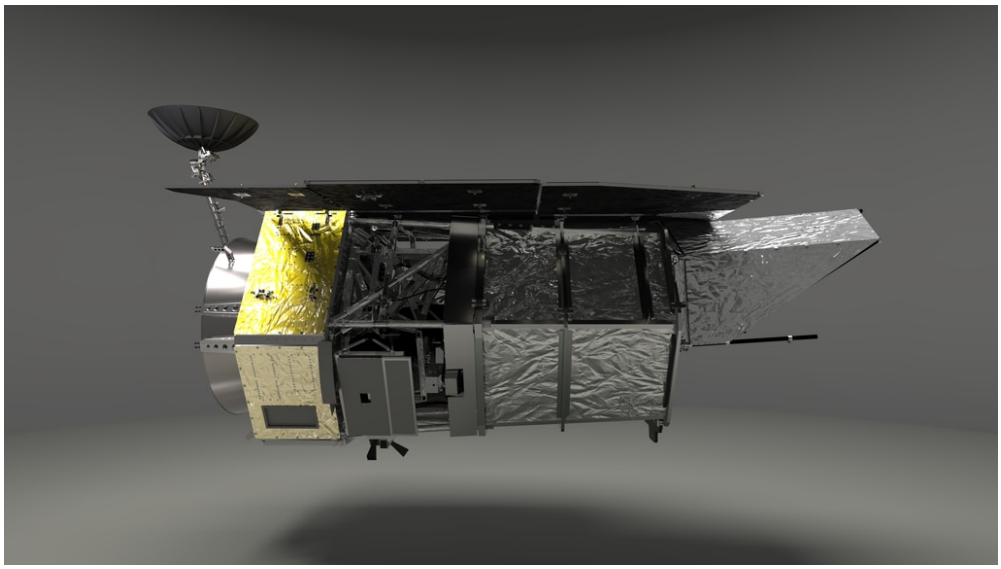

Figure 3.9: The Nancy Grace Roman Space Telescope. Taken from `https://roman.gsfc.nasa.gov/gallery-spacecraftillustrations.html`.

It will study galaxies, dark energy and exoplanets. About 2700 exoplanets are expected to be discovered toward the Milky Way's bulge by the Roman space telescope, either via gravitational microlensing and transit methods for the furthest planets, or via the direct imaging technique for nearby ones. In this purpose, it will carry two instruments:

[8]Sources: `https://roman.gsfc.nasa.gov/index.html` and `https://www.jpl.nasa.gov/missions/the-nancy-grace-roman-space-telescope`

- **WFI**: The Wide Field Instrument is a 300-megapixel camera that will observe the sky within a field of view 100 times larger than that of the Hubble Space Telescope, with a good quality and a lot of details in the images. It will survey over 10^8 stars and look for transits and microlensing events.
- **CGI**: The CoronaGraph Instrument is a high-contrast imager. It should be able, as explained on the official website of the mission, to reach a limiting contrast of about 10^{-9} for planets located around bright stars at apparent angular separations larger than 0.15 arcsec. Its inner and outer working angles will respectively be 0.15 arcsec and 0.66 arcsec.

As explained in Section 2.4 concerning the gravitational microlensing method, superhabitable exoplanets are well inside the Einstein radii R_E of their host K dwarf stars, so these are difficult to detect via the gravitational microlensing method since their magnifying effects on the background sources are small at such orbital separations. However, it could maybe still be possible to detect some of them. Concerning direct imaging, the CGI looks really efficient. The required planet-over-star contrasts for superhabitable exoplanets will be reached, but the angular separations for such planets at 10 pc are still a bit too small. Nevertheless, it could be able to detect such exoplanets around stars closer than 10 pc from the Earth.

3.1.7 The Terra Hunting Experiment (THE) and HARPS3

The Terra Hunting Experiment (THE)[9] is not a telescope as it was the case for all the other subsections in this chapter, but a survey program. Its goal will be to detect exoplanets orbiting G and K dwarf stars using the radial velocity method. The program should start in 2022 and last for at least 10 years.

The exoplanets that will be targeted are Earth-mass planets orbiting around their stars with orbital periods ranging from 60 to 300 days. Therefore, it seems that superhabitable exoplanets are right in the scope of the Terra Hunting Experiment.

To achieve this goal, a new instrument is being built, the High Accuracy Radial-velocity Planet Searcher 3 (HARPS3) and will be equipped on the refurbished 2.5-m diameter Isaac Newton Telescope at the observatory of La Palma. This instrument will be the successor of the HARPS and HARPS-North spectrographs, as discussed in Section 2.2. It will be an echelle spectrograph monitoring light in the optical wavelengths (380 - 690 nm) with a high spectral resolution $R = 115000$ and with a radial velocity precision of 10 cm s^{-1} to be able to detect Earth-mass planets. Hence, it should be able to detect superhabitable exoplanets, as seen in Section 2.2. It will also perform spectropolarimetric observations, as SPIRou does, but this time in the visible domain.

3.2 Far-future missions

Here, we will go one step further and take a look at what is planned for the far future, namely ARIEL, HabEx and LUVOIR which promise, among others, to be very interesting for the search of life on habitable exoplanets.

[9]Sources: `http://www.terrahunting.org/index.html` and `https://www.youtube.com/watch?v=VBt3jaqRAxo`

3.2.1 Atmospheric Remote-sensing Infrared Exoplanet Large-survey (ARIEL)

ARIEL[10] is an ESA mission ([Pascale et al., 2018]). It will be a small space telescope with a total collecting area of 0.64 m^2. It should be launched in 2029 and placed on a halo orbit around the Lagrange point L2 of the Sun-Earth system (like all the other space telescopes seen in Section 3.1). Its initial lifetime is 4 years, with possibly 2 more.

Figure 3.10: The ARIEL space telescope. Taken from the website `https://arielmission.space/`.

It will observe rocky and gas giant exoplanets around F to M-type stars. It will perform transit and eclipse spectroscopy in the infrared domain, and photometry in the visible wavelengths to detect exoplanets and characterize their atmospheres (chemical composition, structure, etc.).

As seen in the Definition Study Report[11], ARIEL's photometric accuracy should be on the order of 50 ppm (with a goal at 10 ppm) for $m_V \leq 11$ over an integration time of one transit duration (several hours). Its spectral resolutions will be $R \sim 30$ and 100. Its photometric precision would therefore allow to detect transiting superhabitable exoplanets. However, as for the JWST, it should be too challenging to detect biosignatures (transit depths of 10 ppm or less) in their atmospheric spectra. As said in [The LUVOIR Team, 2019], ARIEL will therefore focus on the atmospheres of giant exoplanets and Earth-like orbiting M dwarfs.

[10]Source: `https://sci.esa.int/web/ariel/`

[11]Source: `https://sci.esa.int/documents/34022/36216/Ariel_Definition_Study_Report_2020.pdf`, p.124

3.2.2 Habitable Exoplanet Observatory (HabEx)

HabEx[12] ([Gaudi et al., 2020]) is a space telescope planned to be launched in the late 2030s on a halo orbit around the Sun-Earth Lagrange point L2. It will carry a 4-m diameter monolithic primary mirror and will cover wavelengths in the ultraviolet, visible and infrared domains. Its initial lifetime is set to 5 years, but could be extended up to 10 years with its quantity of consumables.

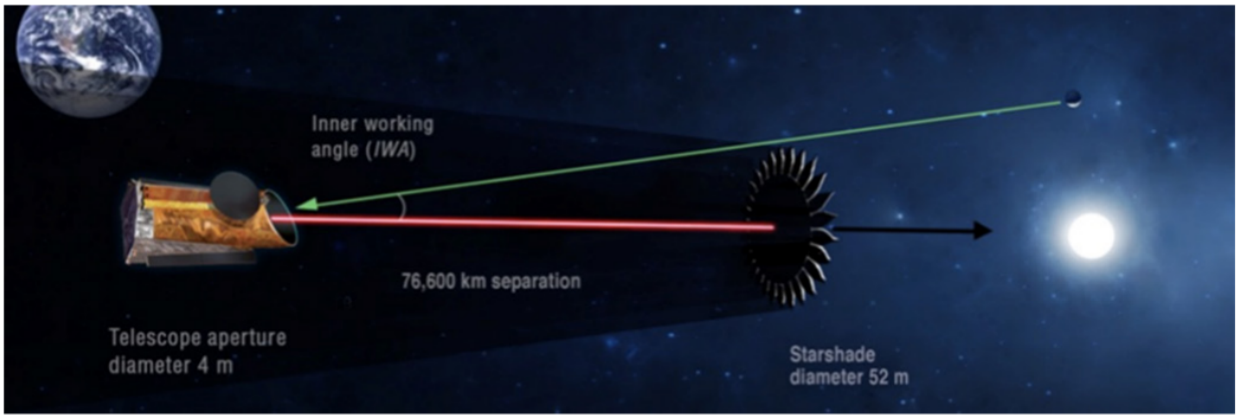

Figure 3.11: HabEx and the Starshade instrument in formation flight. Taken from [Gaudi et al., 2020].

The telescope will have several scientific goals to reach, among which the detection and characterization of HZ Earth-like planets orbiting Sun-like stars. It will also focus on all other types of exoplanets, not only rocky ones.

Out of its instruments, two of them will be designed for exoplanetary science:

- **HCG**: The HabEx CoronaGraph instrument will be used for detection of exoplanets and characterization of their orbits via direct imaging. Its inner and outer working angles should respectively be 62 mas at 0.5 μm (2.4 λ/D) and 0.74 arcsec at 0.5 μm. It may reach contrasts of 10^{-10} for all angular separations between its IWA and OWA.
- **Starshade**: The Starshade instrument will be in formation flight with the telescope itself, as illustrated in Figure 3.11. Its purpose will be to block the starlight just like a coronagraph, but also to provide a constant IWA of 60 mas for all wavelengths between 0.3 μm and 1.0 μm.

Once direct imaging of an exoplanet would be done, direct spectroscopy will then be performed by HabEx to analyze the atmosphere of the planet, with hope of finding relevant features for life in the spectrum.

From the performances of the HCG instrument, we can therefore tell that HabEx should be totally able to direct image superhabitable exoplanets as seen in Figures 2.20 and 2.21. Indeed, both the required contrasts and angular separations, at least for stars 10 pc away from the Earth, should be met by the HCG. This mission will be very interesting, although it will mainly focus on Sun-like stars. Since it would, in theory, be able to direct image superhabitable exoplanets, it would also likely be possible for HabEx to detect biosignatures in the atmospheres of these planets using direct spectroscopy.

[12]Source: `https://www.jpl.nasa.gov/habex/`

3.2.3 Large UV/Optical/Infrared Surveyor (LUVOIR)

LUVOIR[13] ([The LUVOIR Team, 2019]) is a space-based observatory planned to be launched in 2039 on a halo orbit around the Sun-Earth Lagrange point L2.

Two concepts, namely LUVOIR-A and LUVOIR-B, are proposed. LUVOIR-A will have a 15-m diameter principal mirror, while LUVOIR-B would be smaller with a 8-m diameter mirror. The initial lifetime of LUVOIR would be 5 years, but as for HabEx, it could be extended up to 10 years due to the amount of consumables it would carry.

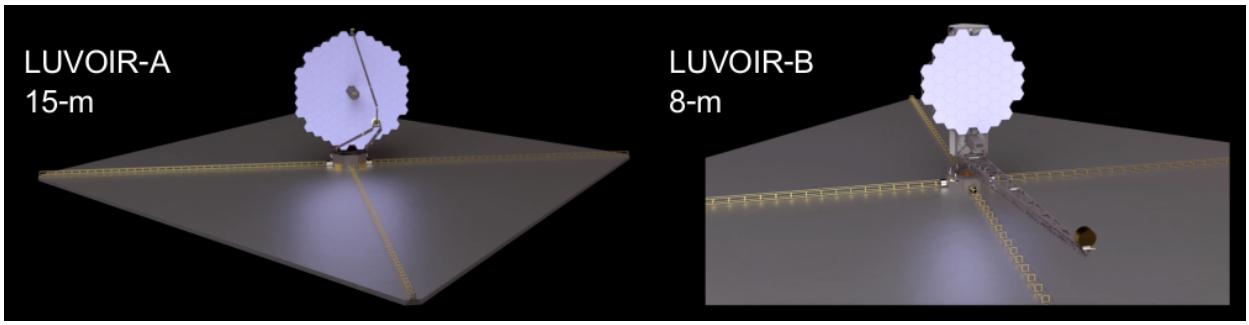

Figure 3.12: The two concepts of the LUVOIR space telescope. Taken from [The LUVOIR Team, 2019].

LUVOIR will study many things, just like HabEx: galaxies, cosmology, evolution of stars and planetary systems, and also planets of the Solar System and exoplanets.
Regarding exoplanet-related goals, it will look for all kinds of exoplanets, but notably for habitable zone rocky exoplanets. It will also study their atmospheres via transit and direct spectroscopy to find biosignatures in their spectra (H_2O, O_2, O_3, CO_2, CH_4, etc.). However, let us note that transit spectroscopy will also only be performed on planets orbiting M dwarfs, as explained in [The LUVOIR Team, 2019], since HZ Earth-like exoplanets orbiting K dwarfs or hotter stars have spectral features with too small transit depths and long orbital periods.

Currently, four instruments have been proposed to be equipped on LUVOIR:

- **HDI**: The High-Definition Imager will be a wide-field imaging camera covering wavelengths in the range 0.2 - 2.5 μm. This instrument will also perform high-precision astrometry. Indeed, equipped on LUVOIR-A (resp. B), its astrometric precision would reach at least 0.34 μas (resp. 0.65 μas), which is enough to detect superhabitable exoplanets within a distance from the Earth smaller than 10 pc, as seen in Section 2.3.
- **ECLIPS**: The Extreme Coronagraph for LIving Planetary Systems will be used to direct image exoplanets in the wavelength range 0.2 - 2.0 μm. This instrument should make LUVOIR able to reach a planet/star contrast of 10^{-10}. Its IWA will be $4\lambda/D$ in the near-UV and $3.5\lambda/D$ in the visible and the near-IR. For the OWA, it will be $40\lambda/D$ in the near-UV and $64\lambda/D$ in the visible and the near-IR. For a wavelength of 0.5 μm, this corresponds to:

[13]Source: `https://asd.gsfc.nasa.gov/luvoir/`

	IWA (arcsec)	**OWA** (arcsec)
LUVOIR-A	2.4×10^{-2}	4.4×10^{-1}
LUVOIR-B	4.5×10^{-2}	8.2×10^{-1}

which is definitely enough for superhabitable exoplanets 10 pc away from the Earth, as seen in Figures 2.20 and 2.21.

- **LUMOS**: The LUVOIR UV Multi-Object Spectrograph will cover wavelengths from 0.1 μm up to 1.0 μm and will be able to observe many targets at the same time. Its main purpose will be to study gases in the range of temperatures 10 - 10^5 K with spectral resolutions from $R = 583$ to $R = 47000$ for LUVOIR-A and $R = 537$ to $R = 52000$ for LUVOIR-B, depending on the observed wavelength range.
- **POLLUX**: This instrument will be a UV spectropolarimeter with a high spectral resolution $R \sim 120000$ in the range of wavelengths 100 - 400 nm.

From the expected performances of LUVOIR and its instruments, the realm of superhabitable exoplanets should be easily reached via astrometry or direct imaging methods. So, like HabEx, LUVOIR should be able to detect biosignatures in the atmospheres of superhabitable exoplanets via direct spectroscopy. Nevertheless, the launch of this telescope is quite far away from now. We, therefore, have to be patient before having the opportunity to use it.

Chapter 4

The TESS mission

At the time being, we still don't have these missions operating. Therefore, what we can do for the moment is to detect new exoplanets in order to enrich the list of interesting exoplanetary candidates.

We have seen in the previous chapters that direct imaging and astrometry methods are not achievable yet, but will be in the future. Gravitational microlensing, on the other hand, generally discovers far exoplanets, too far for being good candidates for future atmospheric studies. For the moment, we therefore have to detect superhabitable exoplanets using the transit and the radial velocity methods. The latter method will for instance be used in the Terra Hunting Experiment as described in Subsection 3.1.7 or with already existing echelle spectrographs such as ESPRESSO@VLT, whilst for the transit method, we can already analyze light curves from space missions like the Transiting Exoplanet Survey Satellite (TESS) or Kepler.

The goal being to study the atmospheres of these planets with the next generation of telescopes and instruments, notably using the direct imaging method, it is preferential to focus on nearby exoplanets. For this reason, the TESS mission is the most interesting one. Indeed, it yields the largest and most accurate light curves database of stars within approximately 60 pc from the Earth, in all directions.

In what follows, we will give an overview of the TESS mission and we will then estimate where to look, based on TESS data, to find superhabitable exoplanet candidates. We will also briefly see how to retrieve a list of suitable stars observed by TESS to be analyzed by external softwares.

4.1 TESS

As explained in Section 2.1, TESS[1] is on a high-Earth elliptical orbit. It completes one turn on its orbit in 13.7 days.
It is made of four aligned CCD cameras, each having a field of view of 24 $\times$ 24 degrees. Hence, the total field of view of TESS is 96 $\times$ 24 degrees. The four cameras are configured as represented in Figure 4.1:

[1]Source: `https://heasarc.gsfc.nasa.gov/docs/tess/`

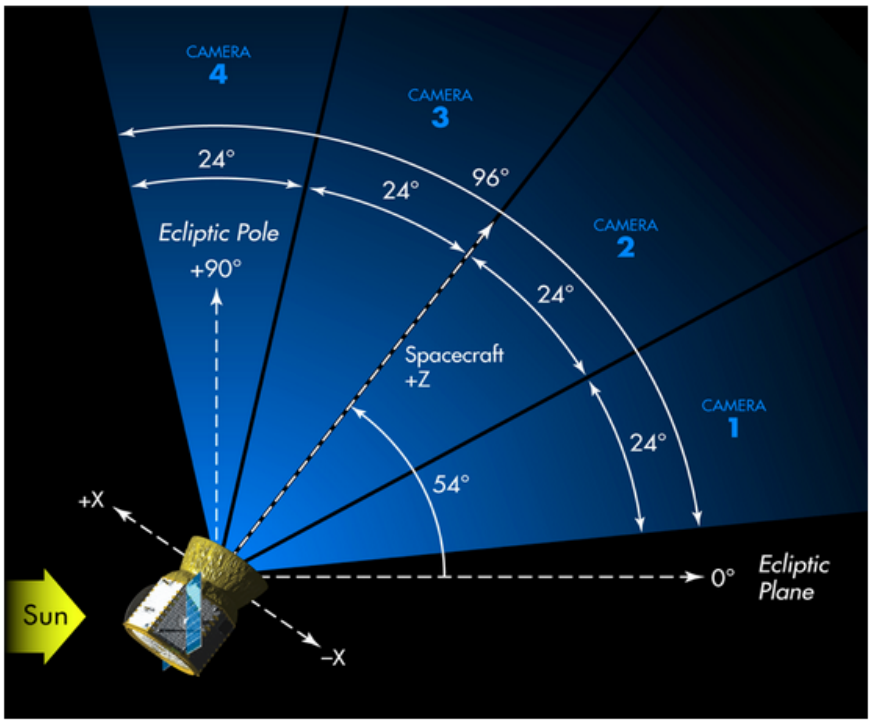

Figure 4.1: Representation of the field of view of TESS. Taken from the website `https://heasarc.gsfc.nasa.gov/docs/tess/operations.html`.

TESS observes the sky in 26 different sectors of 96 × 24 degrees, 13 in each hemisphere of the ecliptic. Each sector is observed during two continuous orbits, i.e. for about 27 days. Once the 13 sectors of an hemisphere have been observed, TESS flips over its axis to start observing the other hemisphere of the ecliptic.

Since the field of view of the 4th camera (see Figure 4.1) is aligned with the ecliptic pole of the considered hemisphere, the sectors are overlapping more and more while going toward the poles. Hence, some regions of the sky are being observed for more than 27 days, i.e. the number of sectors in which they are simultaneously present *times* 27 days. The most extreme case is for targets located in the field of view of camera 4. Indeed, some of these targets are observed in all 13 sectors of the given hemisphere, which corresponds to 351 contiguous days of observation. This is further illustrated in Figure 4.2:

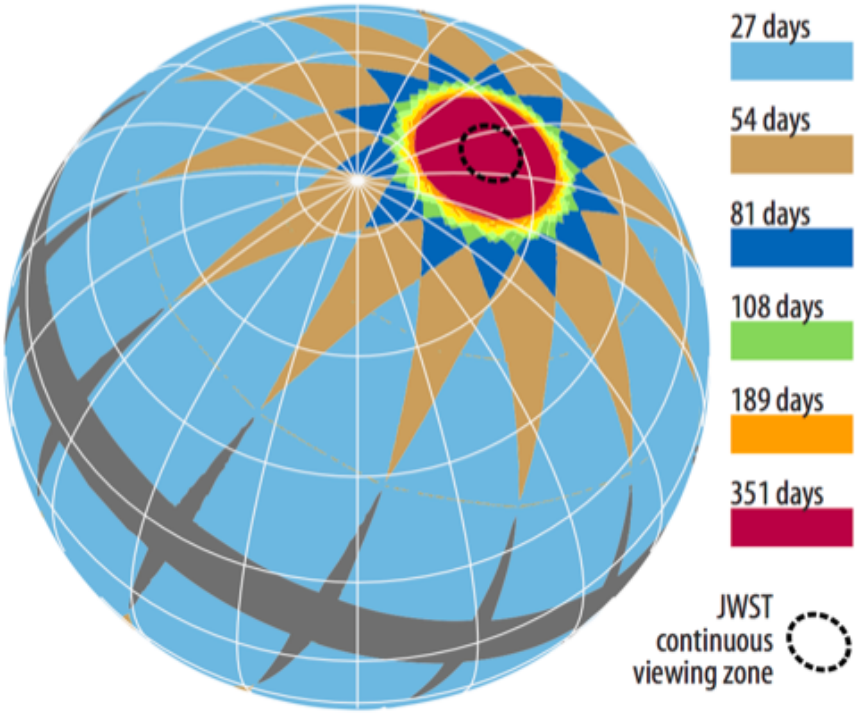

Figure 4.2: Representation of the overlapping between the sectors observed by TESS. More overlaps are occurring toward the ecliptic poles. Taken from the website `https://heasarc.gsfc.nasa.gov/docs/tess/operations.html`.

It is also interesting to note that the JWST will have a continuous observation zone in a small circle centered on the ecliptic poles (see Figure 4.2) as explained in Subsection 3.1.1, in correlation with the field of view of the 4th camera of TESS.

Most of the superhabitable exoplanets having orbital periods of about 100 days or more, we need light curves of at least more than this. Therefore, we will have more chance to detect these planets using the transit method (what TESS does) if they are in regions of the sky where at least five TESS sectors are overlapping (135 days of continuous observation). Indeed, to know whether we are dealing with a periodic event, e.g. a transiting exoplanet, or with something else, we need a minimum of two transits. This is also required in order to determine the orbital period of the planet. To have five overlapping sectors or more, we can thus focus on stars in the field of view of the 4th camera.

This 4th camera being centered on the ecliptic pole, and the sides of its field of view being 24° (diagonal of the field of view equal to 33.94°), it is therefore better to focus on stars with ecliptic latitudes $|\lambda| > 73°$ (circles centered on the poles and with a "diameter" of 33.94°).

4.2 Gaia archive and MAST portal

Now that we have introduced the TESS observation plan and figured out that stars around the ecliptic poles have long enough light curves to allow the detection of superhabitable exoplanets, let us explain how to find these interesting stars and to retrieve their TIC IDs (TESS Input Catalog IDs) in order to obtain their light curves.

First, using the Gaia Archive website[2], we can apply a query to obtain a list of stars from the Gaia DR2 catalog having the desired characteristics. In our case, we want to retrieve K dwarf stars (T in between 4000 and 5240 K and L in the range 0.09 and 0.41 $L_{\odot}$) within a distance of 30 pc.

Then, we may use the MAST portal website[3]. This portal allows us to input a list of stars and to cross-match it with other stellar catalogs. Our goal being to know which stars of the Gaia DR2 catalog have been observed by TESS, we will cross-match our list with the TESS Input Catalog. This will also allow us to obtain the TIC IDs of the targets in our list. These stars are represented in Figure 4.3:

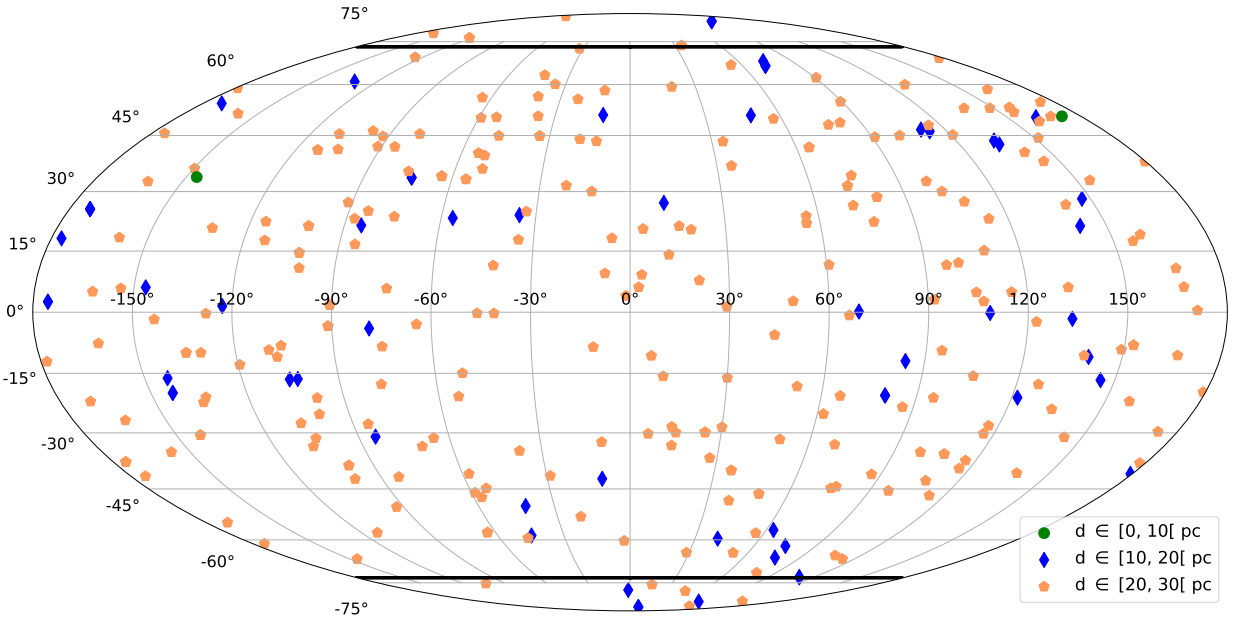

Figure 4.3: Mollweide projection of the K dwarf stars observed by TESS within a distance of 30 pc. Stars within 10 pc are in green, in between 10 and 20 pc in blue, and in between 20 and 30 pc in orange. The coordinates used are the ecliptic latitude and longitude. The ecliptic polar circles at latitudes ± 73° (thick black lines) are also represented.

As we can see, only a few K dwarfs are located within 10 pc from the Earth (green dots). There are also a few stars within the ecliptic polar circles at latitudes ± 73° delimited by the black straight lines. These stars are listed in Table 4.1:

[2] `https://gea.esac.esa.int/archive/`
[3] `https://mast.stsci.edu/portal/Mashup/Clients/Mast/Portal.html`

TIC ID	d **(pc)**	T_{eff} **(K)**	L $(L_\odot)$	**Opt. HZ limits (days)**	**#TOIs**	**#Confirmed planets**
38462407	19.72	4000	0.07	60 - 234	0	0
1201208237	27.77	4858	0.23	114 - 441	0	0
374859347	12.94	4893	0.26	116 - 449	0	5
375058105	22.24	4170	0.11	68 - 279	0	0
220473309	26.90	4033	0.16	59 - 243	0	0
219792161	27.30	4985	0.35	122 - 471	0	0
233192934	19.06	4541	0.18	93 - 369	0	0
198381445	21.24	4210	0.14	71 - 289	0	0
198381449	21.25	4503	0.18	90 - 360	0	0
358289822	27.33	4377	0.15	82 - 330	0	0
149248196	15.31	5117	0.40	132 - 502	0	0
387809195	26.79	4602	0.18	97 - 383	0	0
278199697	29.97	4205	0.15	71 - 288	0	0
150098542	28.32	4682	0.18	102 - 401	0	0

Table 4.1: List of the stars within the ecliptic polar circles represented in Figure 4.3. The values delimiting the optimistic habitable zone of a star are derived from the results of Section 1.3. The other columns are coming either from the Gaia DR2 archive or from the MAST portal.

No TESS Objects of Interest (TOIs) have been reported for these stars yet. We also see in Table 4.1 that the star TIC 374859347 has 5 confirmed exoplanets. One of them, HD 40307 g[4], is inside of the optimistic habitable zone of its host star with an orbital period of nearly 200 days. However, its computed minimal mass is $m_p \sin i = 7.2 \pm 2.6\ M_\oplus$. This is therefore much more than the expected mass of a superhabitable exoplanet, as seen in Section 1.2.

The light curves of these stars located in the polar circles (and listed in Table 4.1) could be analyzed in a further study, notably using a software such as the SHERLOCK pipeline[5], to look for transits of superhabitable exoplanets.

[4]Sources: `https://exofop.ipac.caltech.edu/tess/target.php?id=374859347` and `https://exoplanetarchive.ipac.caltech.edu/overview/HD%2040307%20g#planet_HD-40307-g_collapsible`

[5]Link to the official GitHub page: `https://github.com/franpoz/SHERLOCK`

Conclusion

In this Master thesis, we have studied the detectability of habitable zone Earth-like exoplanets orbiting around K dwarf stars. We have first determined that these superhabitable exoplanets are very interesting for studies aiming to search for life elsewhere in the Universe, since K dwarfs are good compromises in terms of lifetimes and high-energy photon fluxes. We also found the expected parameters of these planets from [Schulze-Makuch et al., 2020], i.e. planets slightly older, bigger, hotter and more massive than the Earth with a surface partially covered with shallow oceans instead of deep ones.

Then, we found out that such planets may already be discovered thanks to the radial velocity and transit methods, but not through astrometry, gravitational microlensing or direct imaging. However, our investigations about upcoming space-based and ground-based telescopes have shown that astrometry and direct imaging of superhabitable exoplanets may be achievable in the late 2030s by the HabEx and LUVOIR space missions. However, the Roman space telescope and the second generation instruments planned to be equipped on the ELT (PCS) and TMT (PSI) may perhaps be able to direct image some superhabitable exoplanets during this decade, although this would probably be quite challenging. Nevertheless, near-future missions such as JWST, PLATO, Roman or the ELTs (TMT, GMT and ELT), will have the required precisions to detect such exoplanets using the transit or the radial velocity methods.

In addition, most of these missions will be dedicated to characterize exoplanetary atmospheres. Although they will be able to study the atmospheres of gas giants or habitable zone terrestrial planets orbiting mid to late M dwarfs, the characterization of the atmospheres of superhabitable exoplanets won't be reached, either via transit or direct spectroscopy, until the advent of far-future LUVOIR and HabEx missions, these missions expected to be able to direct image the superhabitable exoplanets.

Therefore, what we can do before having these missions able to characterize the atmospheres of superhabitable exoplanets is to discover new potential candidates to enrich the priority list for further studies. This could notably be done by analyzing TESS light curves for stars near the ecliptic poles, i.e. for stars having more than 100 days of continuous observation. This could be investigated in future studies.

In conclusion, the search for exoplanets and biosignatures in their atmospheres in the coming years promises to be very exciting with all the upcoming telescopes and instruments. However, although it might be possible to increase the length of the list of potential superhabitable candidates, we will most likely have to wait for the next decade before having the opportunity to verify their superhabitable (or even habitable) characteristics through studies of their atmospheres.

Bibliography

[Absil, 2020] Absil, O. (2020). *SPAT0063-1: Introduction to exoplanetology - Lectures 6 and 7 - Direct exoplanet detection methods*.

[Armstrong et al., 2014] Armstrong, J. C., Barnes, R., Domagal-Goldman, S., Breiner, J., Quinn, T. R., and Meadows, V. S. (2014). Effects of Extreme Obliquity Variations on the Habitability of Exoplanets. *Astrobiology*, 14(4):277–291.

[Arney, 2019] Arney, G. N. (2019). The K Dwarf Advantage for Biosignatures on Directly Imaged Exoplanets. *The Astrophysical Journal Letters*, 873(1):L7.

[Artigau et al., 2014] Artigau, É., Kouach, D., Donati, J.-F., Doyon, R., Delfosse, X., Baratchart, S., Lacombe, M., Moutou, C., Rabou, P., Parès, L. P., Micheau, Y., Thibault, S., Reshetov, V. A., Dubois, B., and others (2014). SPIRou: the near-infrared spectropolarimeter/high-precision velocimeter for the Canada-France-Hawaii telescope. In Ramsay, S. K., McLean, I. S., and Takami, H., editors, *Ground-based and Airborne Instrumentation for Astronomy V*, volume 9147 of *Society of Photo-Optical Instrumentation Engineers (SPIE) Conference Series*, page 914715.

[Barry et al., 2011] Barry, R., Kruk, J., Anderson, J., Beaulieu, J.-P., Bennett, D. P., Catanzarite, J., Cheng, E., Gaudi, S., Gehrels, N., Kane, S., Lunine, J., Sumi, T., Tanner, A., and Traub, W. (2011). The exoplanet microlensing survey by the proposed WFIRST Observatory. In Shaklan, S., editor, *Techniques and Instrumentation for Detection of Exoplanets V*, volume 8151 of *Society of Photo-Optical Instrumentation Engineers (SPIE) Conference Series*, page 81510L.

[Barstow et al., 2015] Barstow, J. K., Aigrain, S., Irwin, P. G. J., Kendrew, S., and Fletcher, L. N. (2015). Transit spectroscopy with James Webb Space Telescope: systematics, starspots and stitching. *Monthly Notices of the Royal Astronomical Society*, 448(3):2546–2561.

[Beichman and Greene, 2018] Beichman, C. A. and Greene, T. P. (2018). *Observing Exoplanets with the James Webb Space Telescope*, page 85.

[Benz et al., 2021] Benz, W., Broeg, C., Fortier, A., Rando, N., Beck, T., Beck, M., Queloz, D., Ehrenreich, D., Maxted, P. F. L., Isaak, K. G., and others (2021). The CHEOPS mission. *Experimental Astronomy*, 51(1):109–151.

[Bond et al., 2004] Bond, I. A., Udalski, A., Jaroszyński, M., Rattenbury, N. J., Paczyński, B., Soszyński, I., and others (2004). OGLE 2003-BLG-235/MOA 2003-BLG-53: A Planetary Microlensing Event. *The Astrophysical Journal*, 606(2):L155–L158.

[Borucki and Summers, 1984] Borucki, W. J. and Summers, A. L. (1984). The photometric method of detecting other planetary systems. *Icarus*, 58(1):121–134.

[Boyajian et al., 2012] Boyajian, T. S., von Braun, K., van Belle, G., McAlister, H. A., and others (2012). Stellar Diameters and Temperatures. II. Main-sequence K- and M-stars. *The Astrophysical Journal*, 757(2):112.

[Brandl et al., 2021] Brandl, B., Bettonvil, F., van Boekel, R., Glauser, A., Quanz, S., Absil, O., Amorim, A., Feldt, M., Glasse, A., Güdel, M., Ho, P., Labadie, L., Meyer, M., Pantin, E., van Winckel, H., and METIS Consortium (2021). METIS: The Mid-infrared ELT Imager and Spectrograph. *The Messenger*, 182:22–26.

[Chabrier et al., 2005] Chabrier, G., Baraffe, I., Allard, F., and Hauschildt, P. H. (2005). Review on low-mass stars and brown dwarfs. *arXiv e-prints*, pages astro–ph/0509798.

[Cosentino et al., 2012] Cosentino, R., Lovis, C., Pepe, F., Collier Cameron, A., Latham, D. W., Molinari, E., Udry, S., Bezawada, N., Black, M., Born, A., Buchschacher, N., Charbonneau, D., Figueira, P., Fleury, M., Galli, A., and others (2012). Harps-N: the new planet hunter at TNG. In McLean, I. S., Ramsay, S. K., and Takami, H., editors, *Ground-based and Airborne Instrumentation for Astronomy IV*, volume 8446 of *Society of Photo-Optical Instrumentation Engineers (SPIE) Conference Series*, page 84461V.

[Cuntz and Guinan, 2016] Cuntz, M. and Guinan, E. F. (2016). About Exobiology: The Case for Dwarf K Stars. *The Astrophysical Journal*, 827(1):79.

[Dalcanton et al., 2015] Dalcanton, J., Seager, S., Aigrain, S., Battel, S., Brandt, N., Conroy, C., Feinberg, L., Gezari, S., Guyon, O., Harris, W., Hirata, C., Mather, J., Postman, M., Redding, D., Schiminovich, D., Stahl, H. P., and Tumlinson, J. (2015). From Cosmic Birth to Living Earths: The Future of UVOIR Space Astronomy. *arXiv e-prints*, page arXiv:1507.04779.

[de Wit and Seager, 2013] de Wit, J. and Seager, S. (2013). Constraining Exoplanet Mass from Transmission Spectroscopy. *Science*, 342(6165):1473–1477.

[Deeg and Belmonte, 2018] Deeg, H. J. and Belmonte, J. A. (2018). *Handbook of Exoplanets*.

[Gardner et al., 2006] Gardner, J. P., Mather, J. C., Clampin, M., and others (2006). The James Webb Space Telescope. *Space Science Reviews*, 123(4):485–606.

[Gaudi et al., 2020] Gaudi, B. S., Seager, S., Mennesson, B., and others (2020). The Habitable Exoplanet Observatory (HabEx) Mission Concept Study Final Report. *arXiv e-prints*, page arXiv:2001.06683.

[Gillon, 2020] Gillon, M. (2020). *SPAT0063-1: Introduction to exoplanetology - All but Lectures 6 and 7*.

[Gillon et al., 2020] Gillon, M., Meadows, V., Agol, E., Burgasser, A. J., Deming, D., Doyon, R., Fortney, J., Kreidberg, L., Owen, J., Selsis, F., de Wit, J., Lustig-Yaeger, J., and Rackham, B. V. (2020). The TRAPPIST-1 JWST Community Initiative. In *Bulletin of the American Astronomical Society*, volume 52, page 0208.

[Heller, 2015] Heller, R. (2015). Better Than Earth. *Scientific American*, 312(1):32–39.

[Heller and Armstrong, 2014] Heller, R. and Armstrong, J. (2014). Superhabitable Worlds. *Astrobiology*, 14(1):50–66.

[Heller et al., 2020] Heller, R., Duda, J.-P., Winkler, M., Reitner, J., and Gizon, L. (2020). Habitability of the early Earth: Liquid water under a faint young Sun facilitated by strong tidal heating due to a nearby Moon. *arXiv e-prints*, page arXiv:2007.03423.

[Kaltenegger and Lin, 2021] Kaltenegger, L. and Lin, Z. (2021). Finding Signs of Life in Transits: High-resolution Transmission Spectra of Earth-line Planets around FGKM Host Stars. *The Astrophysical Journal Letters*, 909(1):L2.

[Kasper et al., 2021] Kasper, M., Cerpa Urra, N., Pathak, P., Bonse, M., Nousiainen, J., Engler, B., Heritier, C. T., Kammerer, J., Leveratto, S., Rajani, C., Bristow, P., Le Louarn, M., Madec, P. Y., Ströbele, S., Verinaud, C., Glauser, A., Quanz, S. P., Helin, T., Keller, C., Snik, F., Boccaletti, A., Chauvin, G., Mouillet, D., Kulcsár, C., and Raynaud, H. F. (2021). PCS — A Roadmap for Exoearth Imaging with the ELT. *The Messenger*, 182:38–43.

[Kopparapu et al., 2013] Kopparapu, R. K., Ramirez, R., Kasting, J. F., Eymet, V., Robinson, T. D., Mahadevan, S., Terrien, R. C., Domagal-Goldman, S., Meadows, V., and Deshpande, R. (2013). Habitable Zones around Main-sequence Stars: New Estimates. *The Astrophysical Journal*, 765(2):131.

[Kroupa, 2001] Kroupa, P. (2001). On the variation of the initial mass function. *Monthly Notices of the Royal Astronomical Society*, 322(2):231–246.

[Lindegren and Dravins, 2003] Lindegren, L. and Dravins, D. (2003). The fundamental definition of "radial velocity". *Astronomy and Astrophysics*, 401:1185–1201.

[Lissauer et al., 2012] Lissauer, J. J., Barnes, J. W., and Chambers, J. E. (2012). Obliquity variations of a moonless Earth. *Icarus*, 217(1):77–87.

[Lopez-Morales et al., 2019] Lopez-Morales, M., Currie, T., Teske, J., Gaidos, E., Kempton, E., Males, J., Lewis, N., Rackham, B. V., Ben-Ami, S., Birkby, J., Charbonneau, D., Close, L., Crane, J., Dressing, C., Froning, C., Hasegawa, Y., Konopacky, Q., Kopparapu, R. K., Mawet, D., Mennesson, B., Ramirez, R., Stelter, D., Szentgyorgyi, A., Wang, J., Alam, M., Collins, K., Dupree, A., Karovska, M., Kirk, J., Levi, A., McGruder, C., Packman, C., Rugheimer, S., and Rukdee, S. (2019). Detecting Earth-like Biosignatures on Rocky Exoplanets around Nearby Stars with Ground-based Extremely Large Telescopes. *Bulletin of the American Astronomical Society*, 51(3):162.

[Males et al., 2014] Males, J. R., Close, L. M., Guyon, O., Morzinski, K., Puglisi, A., Hinz, P., Follette, K. B., Monnier, J. D., Tolls, V., Rodigas, T. J., Weinberger, A., Boss, A., Kopon, D., Wu, Y.-l., Esposito, S., Riccardi, A., Xompero, M., Briguglio, R., and Pinna, E. (2014). Direct imaging of exoplanets in the habitable zone with adaptive optics. In Marchetti, E., Close, L. M., and Vran, J.-P., editors, *Adaptive Optics Systems IV*, volume 9148 of *Society of Photo-Optical Instrumentation Engineers (SPIE) Conference Series*, page 914820.

[Mayor et al., 2003] Mayor, M., Pepe, F., Queloz, D., Bouchy, F., Rupprecht, G., Lo Curto, G., Avila, G., Benz, W., Bertaux, J. L., Bonfils, X., Dall, T., Dekker, H., Delabre, B., Eckert, W., Fleury, M., Gilliotte, A., Gojak, D., Guzman, J. C., Kohler, D., Lizon, J. L., Longinotti, A., Lovis, C., Megevand, D., Pasquini, L., Reyes, J., Sivan, J. P., Sosnowska, D., Soto, R., Udry, S., van Kesteren, A., Weber, L., and Weilenmann, U. (2003). Setting New Standards with HARPS. *The Messenger*, 114:20–24.

[Pascale et al., 2018] Pascale, E., Bezawada, N., Barstow, J., Beaulieu, J.-P., Bowles, N., Coudé du Foresto, V., Coustenis, A., Decin, L., Drossart, P., Eccleston, P., Encrenaz, T., Forget, F., Griffin, M., Güdel, M., Hartogh, P., Heske, A., Lagage, P.-O., and others (2018). The ARIEL space mission. In Lystrup, M., MacEwen, H. A., Fazio, G. G., Batalha, N., Siegler, N., and Tong, E. C., editors, *Space Telescopes and Instrumentation 2018: Optical, Infrared, and Millimeter Wave*, volume 10698 of *Society of Photo-Optical Instrumentation Engineers (SPIE) Conference Series*, page 106980H.

[Pepe et al., 2021] Pepe, F., Cristiani, S., Rebolo, R., Santos, N. C., Dekker, H., and others (2021). ESPRESSO at VLT. On-sky performance and first results. *Astronomy and Astrophysics*, 645:A96.

[Perryman, 2018] Perryman, M. (2018). *The Exoplanet Handbook*.

[Pozuelos et al., 2020] Pozuelos, F. J., Suárez, J. C., de Elía, G. C., Berdiñas, Z. M., Bonfanti, A., Dugaro, A., Gillon, M., Jehin, E., Günther, M. N., Van Grootel, V., Garcia, L. J., Thuillier, A., Delrez, L., and Rodón, J. R. (2020). GJ 273: on the formation, dynamical evolution, and habitability of a planetary system hosted by an M dwarf at 3.75 parsec. *Astronomy and Astrophysics*, 641:A23.

[Quirrenbach et al., 2016] Quirrenbach, A., Amado, P. J., Caballero, J. A., Mundt, R., Reiners, A., Ribas, I., Seifert, W., Abril, M., Aceituno, J., Alonso-Floriano, F. J., Anwand-Heerwart, H., Azzaro, M., Bauer, F., Barrado, D., and others (2016). CARMENES: an overview six months after first light. In Evans, C. J., Simard, L., and Takami, H., editors, *Ground-based and Airborne Instrumentation for Astronomy VI*, volume 9908 of *Society of Photo-Optical Instrumentation Engineers (SPIE) Conference Series*, page 990812.

[Ramirez, 2014] Ramirez, R. (2014). *Terrestrial Planets Under Extreme Radiative Forcings: Applications to Habitable Zones, Early Mars, and a High-Carbon Dioxide Earth*. PhD thesis.

[Rodler and López-Morales, 2014] Rodler, F. and López-Morales, M. (2014). Feasibility Studies for the Detection of O_2 in an Earth-like Exoplanet. *The Astrophysical Journal*, 781(1):54.

[Schulze-Makuch et al., 2020] Schulze-Makuch, D., Heller, R., and Guinan, E. (2020). In search for a planet better than earth: Top contenders for a superhabitable world. *Astrobiology*, 20(12):1394–1404. PMID: 32955925.

[The LUVOIR Team, 2019] The LUVOIR Team (2019). The LUVOIR Mission Concept Study Final Report. *arXiv e-prints*, page arXiv:1912.06219.

[Tsapras, 2018] Tsapras, Y. (2018). Microlensing Searches for Exoplanets. *Geosciences*, 8(10):365.